

NANOELECTRONICS AND QUANTUM TRANSPORT OF DIRAC PARTICLES

by

SABER ROSTAMZADEH

Submitted to the Graduate School of Engineering and Natural Sciences
in partial fulfillment of
the requirements for the degree of
Doctor of Philosophy


Sabanci University

2019

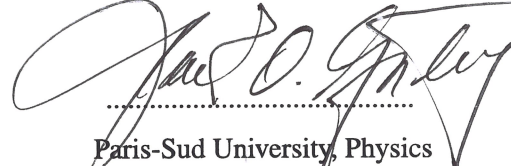
NANOELECTRONICS AND QUANTUM TRANSPORT OF DIRAC PARTICLES

APPROVED BY

Assoc. Prof. İnanç Adagideli
(Thesis Supervisor)


.....
Sabanci University, Physics

Prof. Mark Oliver Goerbig
(Promoter)


.....
Paris-Sud University, Physics


Prof. Ceyhun Bulutay


.....
Bilkent University, Physics

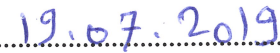
Prof. Zafer Gedik


.....
Sabanci University, Physics

Prof. Selmiye Alkan Gursel


.....
Sabanci University, Material Science

DATE OF APPROVAL


.....

© SABER ROSTAMZADEH

All Rights Reserved

ABSTRACT

NANOELECTRONICS AND QUANTUM TRANSPORT OF DIRAC PARTICLES

SABER ROSTAMZADEH

Ph.D. Thesis, 2019

Thesis Supervisor: Assoc. Prof. İnanç Adagideli

Keywords: Mesoscopic and nanoscale systems, topological phase, spintronics, diffusion, quantum Boltzmann equation, relativity, Kubo formula, Keldysh formalism

In this thesis, we concentrate on the charge and spin transport in Dirac materials and discuss their implications in future electronic technologies. These materials are known for their peculiar band structures, which, unlike the conventional semiconductors, is effectively described by the massless Dirac equation, and their spectrum possesses Dirac nodes. We particularly consider two members of this class of materials: graphene and Weyl semimetals. We first investigate the manipulation of the electronic properties of graphene via adatom engineering. We demonstrate that adatom deposition induces a strong spin-orbit interaction in graphene and, furthermore, couples the spin and valley degrees of freedom, which, in turn, allows for the realization of the valley assisted spin transport and vice versa using a spin-valley device. We also show that the coupled degrees of freedom of graphene due to the presence of disorder causes the intrinsic accumulation of pseudospin charge and pseudospin polarization, which, as we demonstrate, can be used to construct a pseudospin switch device built from a graphene nanoribbon. We next study the Weyl semimetals, as the three-dimensional version of graphene, which has attracted strong interest from the fundamental viewpoint, where they constitute a low energy framework to study the quantum anomalies of the field theory. The electronic structure of these materials is also interesting owing to the fact that the tilting of the band crossing point causes giant electronic conduction and hence a more favorable feature for the electronics industry. We then study the quantum kinetic theory of anomalous transport in these systems to analyze the origin of the chiral anomaly and chiral magnetic effect in Weyl semimetals. Finally, we study the electronic response of tilted Weyl semimetals by associating a relativistic feature to the tilted Weyl cones and then compare our results with the standard linear response approach. Our calculations show that both the covariant transport equation and Kubo formula methods offer correct and equivalent results which strongly agree with the experimental findings.

ÖZET

SABER ROSTAMZADEH

Doktora Tezi, 2019

Tez Danışmanı: Doç. Dr. İnanç Adagideli

Anahtar kelimeler: Meso ve nanoölçekli sistemler, topolojik yalıtkan ve üstüniletkenler, rastlantısal matrisler, spintronik, kuantum termodinamiği

Bu tez çalışmasında, Dirac malzemelerindeki yük ve spin taşınımı üzerinde duruyoruz ve bunların elektronik teknolojiler üzerindeki etkilerini tartışıyoruz. Bu malzemeler, sıradan yarı iletkenlerin ve geleneksel malzemelerin aksine, etkin olarak Dirac denklemine benzer bir denklem ile tarif edilen, ve spektrumları Dirac düğümlerine sahip olan tuhaf bant yapıları ile bilinir. Özellikle bu malzeme sınıfının iki üyesini, grafeni ve Weyl yarımetallerini gözönüne alıyoruz. İlk önce grafenin elektronik özelliklerinin adatom mühendisliği ile değiştirilmesini araştırıyoruz. Adatom birikiminin grafende kuvvetli bir spin-yörünge etkileşimi yarattığını, ayrıca spin ve vadi serbestlik derecelerini ilişkilendirdiğini, bunun da bir spin-vadi cihazı kullanımıyla vadi destekli spin taşınımını (veya tersini) sağladığını gösteriyoruz. Ayrıca, düzensizlikten dolayı grafen serbestlik derecelerinin ilişkilendirilmesinin içsel psödospin yükü birikimine ve psödospin polarizasyonununa neden olduğunu, bunun da grafen nanokurdeleden oluşan bir psödospin anahtar cihazı yapımında kullanılabildiğini gösteriyoruz. Weyl yarımetalleri, ilk başlarda grafenin üç boyutlu versiyonu olarak alan teorisinin önerdiği kuantum anomalilerini düşük enerjili bir çerçevede incelemek için temel bakış açısından büyük ilgi görmüştür. Ayrıca, bu malzemelerin elektronik yapısı, bant geçiş noktasının eğilmesinin dev elektronik iletme neden olması ve dolayısıyla gelecekteki elektronik endüstrisi için daha elverişli olması nedeniyle de ilginçtir. Weyl yarımetallerinde kiral anomalinin kökenini ve kiral manyetik etkisini analiz etmek için bu sistemlerde aykırı taşınımın kuantum kinetik teorisini inceliyoruz. Sonunda, eğik Weyl yarımetallerinin elektronik tepkisini, Weyl konilerine göreli bir özellik ilişkilendirerek araştırıyor ve ardından sonuçlarımızı standart doğrusal tepki yöntemi ile karşılaştırıyoruz. Hesaplamalarımız, hem kovaryant taşıma denkleminin hem de Kubo formül yöntemlerinin, deneysel bulgularla kuvvetle uyuşan doğru ve eşdeğer sonuçlar sunduğunu göstermektedir.

ACKNOWLEDGEMENTS

Undertaking this work has been a truly life-changing experience for me that filled me with a melange of fury and finally content at the end. It would not have been possible to pull it off without the support and guidance that I received from many people.

My deep appreciation foremost goes out to my academic advisors, Prof. İnanç Adagideli at Sabanci University for all the support and encouragement he gave me during this work, and then to Prof. Mark-Oliver Goerbig at Paris-Sud university for his support and unbounded kindness that I experienced during my visit in his group. I appreciate all your contributions of time, ideas, and funding to make my Ph.D. experience productive.

My thanks also go out to the support I received from my friends and collaborators Vahid Sazgari, Ali Asgharpour and Hadi Khaksaran. I also owe special thanks to Baris Pekerten for proofreading this thesis. I am especially grateful to our secretary Mrs. Sinem Aydin for her helps throughout my Ph.D.

I would also like to say a heartfelt thank you to my family for supporting me. I can't thank you enough for encouraging me throughout this experience and believing in me.

Contents

1	INTRODUCTION	1
2	SPIN, VALLEY AND PSEUDOSPIN DYNAMICS IN GRAPHENE	3
2.1	Introduction	3
2.2	Tight binding model	5
2.2.1	Spin-valley coupling from adatoms	7
2.2.2	Intervalley scattering	10
2.3	Spin scattering rates: Fermi's golden rule	13
2.4	Quantum transport equation	14
2.4.1	Collision kernel: Disorder scattering	18
2.4.2	Magnetotransport	20
2.5	Diffusion model	21
2.6	Pseudospin Edelstein effect	24
2.7	Conclusion	28
3	ANOMALOUS TRANSPORT IN WEYL SEMIMETALS	29
3.1	Introduction	29
3.2	Nonabelian Boltzmann equation and $U(1)$ gauge fields	30
3.3	Non-abelian $SU(2)$ gauge, band projection and Berry curvature	32
3.4	Anomalous equations of motion	37
3.5	Conclusion	40
4	COVARIANT TRANSPORT IN TILTED CONES: PSEUDO-RELATIVITY AND LINEAR RESPONSE	41
4.1	Introduction	41
4.2	Covariant Boltzmann equation	43
4.3	Hamiltonian for 2D anisotropic tilted Dirac cones	49
4.3.1	Conductivity from the Boltzmann equation	50
4.3.2	Kubo formula	52

4.4	Type-I Weyl Semimetal	58
4.4.1	Boltzmann equation	58
4.4.2	Kubo formalism	59
4.4.3	Density of states as a function of the tilt parameter	64
4.5	Conclusion	67
BIBLIOGRAPHY		86
APPENDIX		86
A	COHERENT DYNAMICS OF DIRAC PARTICLES IN GRAPHENE	87
A.1	Tightbinding of the Dirac Hamiltonian	87
A.2	Keldysh formalism	89
A.3	Derivation of the diffusion equations	91
A.4	Charge-spin coupling	94
B	LORENTZ TRANSFORMATION OF THE DIRAC HAMILTONIAN	97
C	RENORMALIZATION OF EINSTEIN RELATION	99

List of Figures and Tables

2.1	(Color online) Hexagonal lattice of Graphene where the two sublattices that give rise to the pseudospin index are shown in red and blue colors. The infinitesimal displacement vectors $\delta_{1,2,3}$ between the neighboring atoms that are given in (2.3) are presented as bold arrows.	6
2.2	(Color online) The schematics of a finite width graphene nanoribbon with randomly deposited adatoms on atomic sites. The spin-orbit interaction (2.11) in this system induces the spin-valley locking (2.18) that can be utilized to generate spin current I_s from an injected valley current I_v	10
2.3	(Color online) The spin scattering rates for the adatom engineered graphene that induces SOC given in (2.17) and (2.18). During the intravalley scattering the suppression of back scattering happens while for in the valley mixed spin flips the backscattering is allowed.	14
2.4	(Color online) Diffusion of the pseudospin accumulation (2.122) inside a graphene conductor along the x -direction plotted with the different degrees of polarization η . The decay rate follows a Gaussian pattern with spread peak as one expects from diffusion equation.	27
2.5	(Color online) Pseudospin accumulation in the right (2.124) and left (2.123) interface of a graphene nanoribbon with polarization degree $\eta = 0.3$. There is a critical length where the accumulation in both the interfaces are identical. Eventually the accumulation at the interfaces leak to the bulk and reach a constant value.	28
3.1	(Color online) The energy separation between the left and right Weyl nodes is due to the monopole fields \mathbf{b} (Berry curvature) where $\mu_5 = \frac{e\Delta}{4}(\mathbf{b} \cdot \mathbf{B})$ as given in the anomalous equations of motion. This generates the chemical imbalance between the two chiral fermions giving rise to the chiral anomaly.	37

4.1	(Color online) Comparison between the conductivity of the tilted Graphene in directions perpendicular and parallel to the tilt as a function of the tilt parameter η for values of the normalized energy as $z = 1, 5$ and 10 . Around zero tilt both the parallel and perpendicular conductivities, calculated from the Kubo formula, correspond to the isotropic value; while increasing the tilt develops an anisotropy such that the perpendicular conductivity diverges, while the parallel one continues to grow up to a finite value.	55
4.2	(Color online) Comparison between the conductivities $\sigma_{\text{tilt}}/\sigma_0$ and $\sigma_{\text{perp}}/\sigma_0$ of the tilted Graphene in terms of the tilt parameter for energies at $z = 1, 5$ and 10 . Conductivity Calculated from the Kubo formula (dashed) agree with the covariant Boltzmann approach (solid) in (4.31), (4.30). While the perpendicular conductivity diverges in critical limit; the conductivity parallel to tilt direction saturates at finite value.	57
4.3	The conical spectrum of a tilted Weyl crossing.	60
4.4	(Color online) Isotropic conductivity $\sigma_w = \sigma_0 \frac{\Gamma}{4\pi v_F}$ of Weyl semimetals with zero tilt ($\eta = 0$) as a function of the normalized energy z . The results calculated from the Boltzmann and Kubo approaches agree except for a small offset. This nonzero residual conductivity is due to the band coherence contributions.	61
4.5	(Color online) Comparison between the parallel-perpendicular conductivity of type-I WSM computed from the Kubo formula in terms of the tilt parameter, for different values of the normalized energies. The conductivity in both directions diverge for $\eta \rightarrow 1$, but the divergence is more pronounced in the direction perpendicular to the tilt. In the zero-tilt limit, both conductivities match restoring the isotropic value.	63
4.6	(Color online) Conductivity of the tilted type-I WSM perpendicular and parallel to the tilt direction computed from the covariant Boltzmann equation (solid) and Kubo formula (dashed). The conductivities are expressed as a function of the tilt parameter for different values of the normalized energy z . The perpendicular conductivity enhances and diverges at critical value $\eta = 1$ while the parallel increases but stays finite in the critical limit.	65
4.7	(Color online) Density plot of the normalized perpendicular conductivity in terms of the tilt degree and chemical energy.	66

4.8	Increasing pattern of the normalized Density of states $g(z)/g_0$ of type-I WSM by the degree of tilting, $g_0 = \frac{\Gamma^2}{2\pi^2 v_F^3}$	69
4.9	Renormalization of the Fermi velocity of type-I WSM with the tilted cone is a clear indication of the Lorentz violation.	69

Chapter 1

INTRODUCTION

In this thesis, we consider various aspects of transport in Dirac materials. Specifically, we consider (i) the effect of adatoms in spin-valley scattering in graphene, (ii) generalized Boltzmann equation in Dirac materials with broken time-reversal symmetry, (iii) anomalous transport in Weyl semimetals and (iv) covariant transport in Dirac materials and Weyl semimetals with tilted cones.

Dirac materials are a wide range of newly discovered solid state systems that share certain similarities: their low energy electronic dispersion obeys the Dirac equation and fermionic excitations behave like massless Dirac fermions. Graphene, topological insulators, Dirac semimetals and Weyl semimetals are among the most notable examples of Dirac matter, and all possess Dirac cones in their spectrum. These materials offer interesting transport qualities which have motivated extensive studies oriented towards the technological exploitation of these materials in spintronics and valleytronics applications.

The advent of new technological tools in the fabrication of nanodevices allows the study of transport in the length scales where the quantum effects are important. These technological achievements, along with the electronic properties of the Dirac materials suggest that the Dirac material nanostructures have the potential to be a preferred avenue for certain device physics applications compared to traditional materials and systems used in electronics. These novel materials can be engineered to boost their transport qualities.

The presence of adatoms forces both intravalley and intervalley scattering of electrons as well as producing a spin-orbit coupling. To understand this effect, we first describe a tight-binding model of graphene with impurities and show how the impurities affect the spin transitions in graphene. We demonstrate that adatom deposition on graphene causes coupling between the spin and valley degrees of freedom, rendering graphene with adatoms a suitable playground for valleytronics and quantum computing applications. We next construct the quantum kinetic equation using density matrix formalism and Keldysh Green's function approaches. We use the diffusion model to study the coupled dynamics of charge and pseudospin inside a graphene conductor. We find that in graphene the

coherent transport of charge and pseudospin induces intrinsic pseudospin polarization due to the charge current with applications in pseudo-spintronics.

We next consider the transport theory of Weyl semimetals from the kinetic equation point of view in the presence of adatoms and electric and magnetic fields. Weyl semimetals are significant for the realization of the chiral fermions and the quantum anomalies associated with them. We use the transport equation approach since it provides a lucid microscopic description of anomalous transport and the quantum anomalies. We first present a systematic derivation of the anomalous equations of motion by projecting the two band model of Weyl semimetals into an effective one band model. We next focus on the electronic transport in tilted Weyl semimetals (type I), which violate the Lorentz invariance, by adopting a relativistic approach and then compare our results with the Kubo linear response formalism. We show that these two methods agree in describing the dc conductivity of tilted Weyl semimetals and its monotonically increasing pattern as a function of the tilt parameter.

This thesis is organized as follows: In Chapter 2, we study the importance of adatoms on the electronic properties of graphene. Within our tight-binding model with impurities, we show spin transitions are affected in graphene. We demonstrate that adatom deposition on graphene causes its degrees of freedom such as spin and valley to couple which makes it a suitable playground for valleytronics and quantum computing applications.

In Chapter 3, we present the transport theory of graphene by first constructing the quantum kinetic equation. We arrive at the kinetic equation from the density matrix and the Keldysh approaches. We then use the diffusion model to study the coupled dynamics of charge and pseudospin inside a graphene conductor.

In Chapter 4, we deal with the transport theory of Weyl semimetals from the kinetic equation point of view. We first present a systematic derivation of the anomalous equations of motion by projecting the two band model of Weyl semimetals into an effective one band model. We then apply this effective single band kinetic equation to study the microscopic origin of the chiral anomaly and chiral magnetic effect.

In Chapter 5, we focus on the electronic transport of the Lorentz violating tilted Weyl semimetals (type I) by adopting a relativistic approach and then compare our results with the Kubo linear response formalism.

Chapter 2

SPIN, VALLEY AND PSEUDOSPIN DYNAMICS IN GRAPHENE

2.1. Introduction

In this chapter, we investigate the coherent transport of extra degrees of freedom of Dirac particles in graphene. The spin and the valley, associated with the number of the band crossing point in the Brillouin zone, are two of the additional binary quantum degrees of freedom that make graphene attractive for nanoelectronic applications. Moreover, a quantum state constructed from the entangling of the spin and valley degrees of freedom is appealing as it can be used to write spin information into the valley and vice versa via a simultaneous flip of spin and valley. Such a coupled basis state also finds various applications in quantum computation [1]. Most importantly this coupling opens an interface to join the emergent field of valleytronics which aims to use the valley degrees of freedom in electronic transport with the well established field of spintronics. The valley degrees of freedom in silicon, graphene, and TMDs due to their unique lattice band structure can grant these materials essential roles to play in the realization of valleytronics technology [2, 3]. Here, we propose an adatom impurity model to generate strong spin orbit coupling (SOC) on graphene and then study the transport of charge carriers as well as a spin-valley coupling in graphene. We then investigate these features and the coherent coupling of charge and pseudospin giving rise to the pseudospin Edelstein effect from a quantum transport equation point of view.

With the advent of graphene as a two dimensional material hosting massless Dirac fermions, there is a growing interest in utilizing the graphene as a next generation material that can find applications in valleytronics and spintronics. Other than graphene, the transition metal dichalcogenides (TMDs) which are among the recently developed two dimensional materials serve as the candidates for such device realization due to the presence of valley degrees of freedom in the band structure of the carriers [4–6]. SOC is already known to be essential in the realization of novel spintronic devices in which the information exchange happens not only by charge but with the spin degrees of free-

dom as well [7, 8]. In graphene, due to its weak SOC, the engineering of its properties via external methods appears to be promising for spintronics applications[9–13]. Here, we demonstrate that the spin-valley coupling, which is induced by the adatoms deposition of graphene’s surface, offers further functionalities using yet another degree of freedom associated with the carriers, namely, the valley index [14, 15].

When engineering a valleytronic device, in addition to the intrinsic properties such as the presence of degenerate multivalleys as well as induced coupling of these valleys to applied external fields, impurities have the potential to offer additional functionality by modulating the valley dependent properties [14, 16, 17]. Hence, disorder engineering aims to control the electronics properties to obtain useful effects for device applications. The presence of adatoms influences the electronic transport via inducing spin orbit interaction [18–20]. One of the important features of the spin-valley coupling is that it allows for the conversion of the spin current into polarized valley current and vice versa. The manipulation of spin via the valley degrees of freedom resolves a long sought challenge of spintronics, which is the generation of polarized spin current without external fields, so in this sense, the valley engineering in systems possessing multivalleys is crucial [21–23].

In the following, we first present a method of achieving the spin-valley coupling as well as strong SOC by means of the adatom impurities. We employ a tight binding model of graphene with randomly distributed impurities and find that, in addition to the standard Rashba SOC, there is a local spin-valley coupling in graphene lattice which was not taken into account in the previous studies. We investigate this additional local spin dependent interaction and compute the spin flip transition rates.

Next, in order to study the coherent transport of spin and valley degrees of freedom for valleytronic applications, we focus on the derivation of the generalized quantum Boltzmann equation[24–28]. The reason for this derivation is that quantum transport equation in the low dimensional systems, [29, 30], to capture the quantum coherence, tunneling effects and discreteness of the electronic energy bands[31, 32].

Our construction is based on a dynamical equation and we start from the quantum Liouville’s equation. We, then, reduce this equation into a balance equation of Boltzmann type by noting that the observables are quantum mechanical operators and commutators are respected. This operator approach naturally takes into account the quantum coherence effects. We also provide alternative approaches to transport by using nonequilibrium Green’s function methods (see the Appendix.B) and semiclassical diffusion approximation. We then apply the results from the kinetic equation to study the coherent pseudospin-charge and spin-charge transport in graphene.

2.2. Tight binding model

In the tight binding model, [33], we obtain the effective description of the electronic band structure near the Fermi energy, by projecting our Hamiltonian to a space spanned by a suitable minimal basis set [34–36]. The choice of this minimal basis set, however, is non-unique, and, as the observables are basis independent, they can be represented via different basis sets in a different space [37–40]. The electronic structure of graphene has been studied extensively using the two atomic basis of a single Dirac cone in the tight binding [41–45]. However, using a two Dirac cone tight binding model can result in new interaction terms in the Hamiltonian especially when there is intervalley coupling [38]. Motivated by this, we ask the question of whether there will be novel corrections to spin dependent interaction if one uses a different representation for the localized wave functions in the tight binding model.

We start our calculations by choosing a suitable Wannier function that is spread over the two inequivalent valleys in graphene:

$$\psi(\mathbf{r}_i) = \sum_{\tau=\pm} \psi_{\tau}(\mathbf{r}_i) e^{-i\mathbf{K}_{\tau} \cdot \mathbf{r}_i}, \quad (2.1)$$

where τ stands for the valley index. To justify our ansatz, we first show that the dispersion of graphene carriers by using these plane waves, which are written in the Hilbert space $\mathcal{H}_{\nu} \otimes \mathcal{H}_{\sigma} \otimes \mathcal{H}_s$ that indeed gives the Dirac dispersion (see the Appendix.A). Note that the indices ν, σ and s stand for the valley, sublattice (pseudospin) and real spin degrees of freedom, respectively. The tight binding Hamiltonian in the second quantized form reads

$$H_0 = t \sum_{\mathbf{r}_i, \delta_j} \left(\psi_{\text{A}}^{\dagger}(\mathbf{r}_i) \psi_{\text{B}}(\mathbf{r}_i + \delta_j) + \text{h.c.} \right), \quad (2.2)$$

where $\psi_{\text{A/B}}^{\dagger}(\psi_{\text{A/B}})$ are the operators creating (annihilating) particles at the corresponding position of the atomic sites A and B. The parameter t is the nearest neighbor hopping which for graphene is about $t = 3 \text{ meV}$ [45]. The carbon atoms are localized in graphene lattice around $\mathbf{r}_i = n_1 \mathbf{a}_1 + n_2 \mathbf{a}_2$ where \mathbf{a}_1 and \mathbf{a}_2 are the primitive cell vectors. The unit vectors connecting the triangular lattice points are given by, Fig.2.1,

$$\delta_1 = a \left(0, \frac{1}{\sqrt{3}} \right), \quad \delta_2 = \frac{a}{2} \left(1, -\frac{1}{\sqrt{3}} \right), \quad \delta_3 = \frac{a}{2} \left(-1, -\frac{1}{\sqrt{3}} \right), \quad (2.3)$$

where the lattice spacing is about $a = 1.42 \text{ \AA}$. The conduction and valence bands cross at two time reversal momenta $\mathbf{K}_{\tau} = \tau \left(\frac{4\pi}{3a}, 0 \right)$, so-called valleys in graphene, where $\tau = \pm$ is the valley index and $\mathbf{K}_{\pm} = \pm \mathbf{K}$. It is straightforward to show that the tight binding model in Eq. (2.2) reproduces the standard Dirac Hamiltonian for graphene using the Taylor

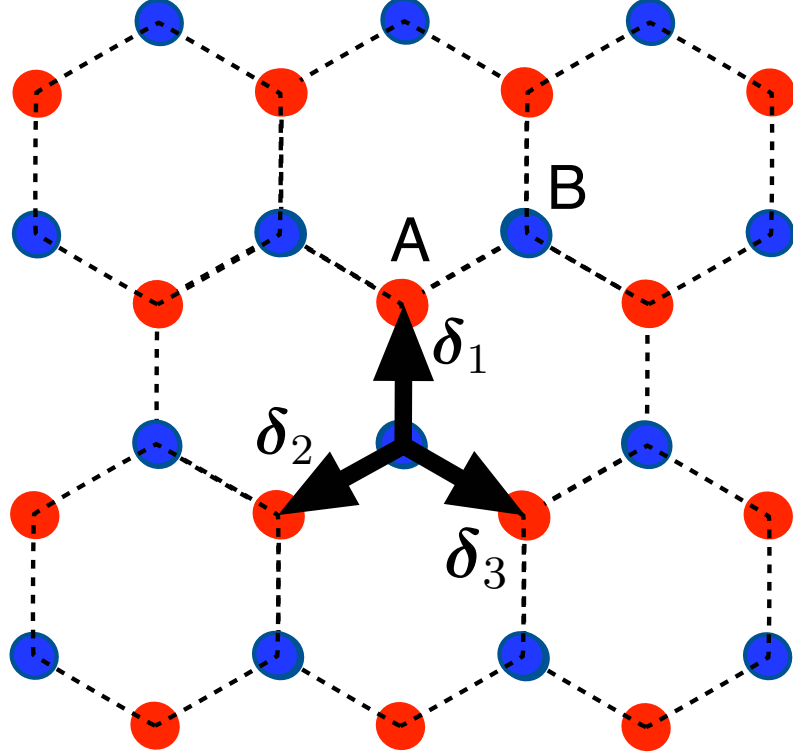


Figure 2.1: (Color online) Hexagonal lattice of Graphene where the two sublattices that give rise to the pseudospin index are shown in red and blue colors. The infinitesimal displacement vectors $\delta_{1,2,3}$ between the neighboring atoms that are given in (2.3) are presented as bold arrows.

expansion for the field operator for the sublattice B as

$$\psi_{\pm B}(\mathbf{r}_i + \boldsymbol{\delta}_j) = \psi_{\pm B}(\mathbf{r}_i) + \boldsymbol{\delta}_j \cdot \nabla \psi_{\pm B}(\mathbf{r}_i) + O(|\boldsymbol{\delta}|^2), \quad (2.4)$$

and in light of the relations

$$\sum_{j=1}^3 e^{\pm i \mathbf{K} \cdot \boldsymbol{\delta}_j} = 0, \quad \sum_{j=1}^3 \boldsymbol{\delta}_j e^{\pm i \mathbf{K} \cdot \boldsymbol{\delta}_j} = \frac{a\sqrt{3}}{2} (\pm i, 1). \quad (2.5)$$

Having checked that the introduced field operator (2.1) indeed gives the correct Dirac Hamiltonian [45] in the valley isotropic basis, [46],

$$\Psi^\dagger = \begin{pmatrix} \psi_{+A}^\dagger & \psi_{+B}^\dagger & -\psi_{-B}^\dagger & \psi_{-A}^\dagger \end{pmatrix}, \quad (2.6)$$

we now focus on obtaining an effective spin-orbit interaction model to investigate the effect of the valley dof on spin states. We anticipate that the effective description for the SOC using the ansatz (2.1) can reveal new interaction terms indicating the interplay between spin and valley degrees of freedom.

2.2.1. Spin-valley coupling from adatoms

The theoretical calculations show that in graphene the spin relaxation time is large and is about $1\mu s$ [47, 48] yielding a large spin diffusion length, very suitable for spintronics applications. However, reported experimental results of spin relaxation time are about $100ps$, much shorter than what is expected [49, 50]. The main source of this strong spin relaxation in graphene has been suggested to be the extrinsic effects such as impurity scattering, spin scattering by magnetic moments and the effect of substrate [9, 47, 48, 51]. Therefore the effect of the disorder in inducing SOC is vital in understanding the spin relaxation mechanisms in graphene [47, 52, 53]. The intrinsic SOC in pristine graphene is due to the deep $\sigma - \pi$ bonds, whereas the Rashba interaction is due to the nearby $\pi - \pi$ bonds [45]. The first principle calculations show that the intrinsic SOC is roughly about $10^{-3}meV$ and the Rashba effect is of the order of $10^{-2}meV$ [47, 54]. A comparison of these two SOC suggests that the Rashba SOC is the dominant effect that possibly governs the relaxation [55].

Apart from the investigations on the spin relaxation in graphene, it turns out that the enhancement of SOC in graphene is interesting for observation of the quantum spin Hall effect [56]. Moreover, SOC tuning in graphene is a promising step towards spintronics applications, where effective manipulation of spins (by only using electric field) needs sizable SOC [7, 8]. To that end, it has been proposed that the impurity adsorption in graphene can significantly improve the SOC where spin splitting of Rashba type and about $200meV$ has been reported for Au adsorbed graphene [57]—mainly due to the lattice distortions generated by the adatoms [9–11, 13, 18, 58, 59]. Furthermore, engineering of graphene surface using metallic adatoms can magnetize graphene by inducing magnetic moments [60], which can be an additional source of spin flip scattering and spin relaxation.

Here we show that the impurity adsorption can also play an essential role in improving the valleytronics properties of graphene by generating spin-valley coupling which will be important for valleytronics applications [19, 21, 22, 61]. To derive the effective SOC in graphene, we start with the tight binding description where we consider dilute impurity adsorption and neglect the correlation between these neighbor impurity centers.

We, first, note that using the hexagonal lattice of graphene, the position operator in the two atomic site basis can be given as

$$\hat{\mathbf{x}} = \sum_{i \in A} \sum_{j \in B} |\mathbf{r}_i\rangle \langle \mathbf{r}_i | \hat{\mathbf{x}} | \mathbf{r}_j \rangle \langle \mathbf{r}_j |$$

$$= \sum_{\mathbf{r}_i} \mathbf{r}_i |\mathbf{r}_i\rangle\langle\mathbf{r}_i| + \sum_{\mathbf{r}_i, \boldsymbol{\delta}_j} (\mathbf{r}_i + \boldsymbol{\delta}_j) |\mathbf{r}_i + \boldsymbol{\delta}_j\rangle\langle\mathbf{r}_i + \boldsymbol{\delta}_j|, \quad (2.7)$$

where $|\mathbf{r}_i\rangle$ and $|\mathbf{r}_i + \boldsymbol{\delta}_j\rangle$ are the single electronic π -orbitals in sites A and B. Likewise, using the Heisenberg's equation of motion, $\hat{\mathbf{v}} = -i[\hat{\mathbf{x}}, H]$ the velocity operator has the representation

$$\begin{aligned} \hat{\mathbf{v}} &= \sum_{i \in A} \sum_{j \in B} |\mathbf{r}_i\rangle\langle\mathbf{r}_i| \hat{\mathbf{v}} |\mathbf{r}_j\rangle\langle\mathbf{r}_j|, \\ &= \sum_{\mathbf{r}_i, \boldsymbol{\delta}_j} |\mathbf{r}_i\rangle\langle\mathbf{r}_i| \hat{\mathbf{v}} |\mathbf{r}_i + \boldsymbol{\delta}_j\rangle\langle\mathbf{r}_i + \boldsymbol{\delta}_j|, \\ &= it \sum_{\mathbf{r}_i, \boldsymbol{\delta}_j} \boldsymbol{\delta}_j |\mathbf{r}_i\rangle\langle\mathbf{r}_i + \boldsymbol{\delta}_j|. \end{aligned} \quad (2.8)$$

We note that the matrix elements now are

$$\langle\mathbf{r}_i|\hat{\mathbf{v}}|\mathbf{r}_i + \boldsymbol{\delta}_i\rangle = -i \left(\langle\mathbf{r}_i|\hat{\mathbf{x}} H |\mathbf{r}_i + \boldsymbol{\delta}_i\rangle - \langle\mathbf{r}_i|H \hat{\mathbf{x}} |\mathbf{r}_i + \boldsymbol{\delta}_i\rangle \right) = i \boldsymbol{\delta}_i \langle\mathbf{r}_i|H|\mathbf{r}_i + \boldsymbol{\delta}_i\rangle. \quad (2.9)$$

We recall that the matrix elements of the bare Hamiltonian $\langle\mathbf{r}_i|H|\mathbf{r}_i + \boldsymbol{\delta}_i\rangle = t$ is the hopping parameter defined in (2.2). It is also worth mentioning that the expansion of velocity operator up to first order will give the pseudospin vector, which we expected to be the case in the low energy description of graphene.

Using these preliminaries and the representation of the velocity operator, and considering the Rashba Hamiltonian in terms of the velocity operator [54]

$$H_{\text{soc}} = \alpha (\hat{\mathbf{z}} \times \mathbf{s}) \cdot \hat{\mathbf{v}}, \quad (2.10)$$

where $\hat{\mathbf{z}} = (0, 0, 1)$ is the unit vector and $\mathbf{s} = (s_x, s_y, s_z)$ is the vector of the Pauli spin matrices, we construct the tight binding form of the Rashba interaction induced by the random adatom impurities as follows

$$H_{\text{soc}} = it \sum_{\mathbf{r}_i, \boldsymbol{\delta}_i} \sum_{\mathbf{r}_a} \alpha(\mathbf{r}_a) (\hat{\mathbf{z}} \times \mathbf{s} \cdot \boldsymbol{\delta}_i) |\mathbf{r}_i\rangle\langle\mathbf{r}_i + \boldsymbol{\delta}_i| + h.c. \quad (2.11)$$

Here $\alpha(\mathbf{r}_a) = \alpha \delta(\mathbf{r}_a - \mathbf{r}_i)$, is the strength of the uncorrelated adatom impurities. We assume that adatoms are deposited right on top of the sublattice points \mathbf{r}_i in random fashion in the hexagonal lattice. Now defining $t_{\text{so}} = t\alpha$, then the effective second quantized Hamiltonian by defining

$$\boldsymbol{\eta} = \hat{\mathbf{z}} \times \mathbf{s} = (-s_y, s_x, 0), \quad (2.12)$$

and substituting (2.1) reads

$$\begin{aligned}
H_{\text{soc}} &= it_{\text{so}} \sum_{\mathbf{r}_i, \boldsymbol{\delta}_j} \boldsymbol{\eta} \cdot \boldsymbol{\delta}_j \left(\left[\psi_{+A}^\dagger(\mathbf{r}_i) e^{i\mathbf{K} \cdot \mathbf{r}_i} + \psi_{-A}^\dagger(\mathbf{r}_i) e^{-i\mathbf{K} \cdot \mathbf{r}_i} \right] \times \right. \\
&\quad \left. \left[\psi_{+B}(\mathbf{r}_i + \boldsymbol{\delta}_j) e^{-i\mathbf{K} \cdot (\mathbf{r}_i + \boldsymbol{\delta}_j)} + \psi_{-B}(\mathbf{r}_i + \boldsymbol{\delta}_j) e^{i\mathbf{K} \cdot (\mathbf{r}_i + \boldsymbol{\delta}_j)} \right] \right) + \text{h.c.}, \\
&= it_{\text{so}} \sum_{\mathbf{r}_i, \boldsymbol{\delta}_j} \boldsymbol{\eta} \cdot \boldsymbol{\delta}_j \left(\psi_{+A}^\dagger(\mathbf{r}_i) \psi_{+B}(\mathbf{r}_i + \boldsymbol{\delta}_j) e^{-i\mathbf{K} \cdot \boldsymbol{\delta}_j} + \psi_{+A}^\dagger(\mathbf{r}_i) \psi_{-B}(\mathbf{r}_i + \boldsymbol{\delta}_j) e^{i\mathbf{K} \cdot \boldsymbol{\delta}_j} e^{i\zeta(\mathbf{r}_i)} \right. \\
&\quad \left. + \psi_{-A}^\dagger(\mathbf{r}_i) \psi_{+B}(\mathbf{r}_i + \boldsymbol{\delta}_j) e^{-i\mathbf{K} \cdot \boldsymbol{\delta}_j} e^{-i\zeta(\mathbf{r}_i)} + \psi_{-A}^\dagger(\mathbf{r}_i) \psi_{-B}(\mathbf{r}_i + \boldsymbol{\delta}_j) e^{i\mathbf{K} \cdot \boldsymbol{\delta}_j} \right) + \text{h.c.},
\end{aligned} \tag{2.13}$$

where $\zeta(\mathbf{r}_i) = \Delta\mathbf{K} \cdot \mathbf{r}_i$, and $\Delta\mathbf{K} = \mathbf{K}_+ - \mathbf{K}_- = 2\mathbf{K}$ is the momentum distance between the two valleys. Next, keeping only the linear terms in the Taylor expansion for the field operator in Eq. 2.4 and in lights of the relations relations (2.3) and (2.12) and noting that

$$\boldsymbol{\eta} \cdot \sum_{j=1}^3 \boldsymbol{\delta}_j e^{\pm i\mathbf{K} \cdot \boldsymbol{\delta}_j} = \frac{a\sqrt{3}}{2} s_{\mp}, \tag{2.14}$$

where $s_{\pm} = s_x \pm is_y$, we finally arrive at the effective Hamiltonian for the SOC as

$$\begin{aligned}
H_{\text{soc}} &= t_{\text{so}} \sum_{\mathbf{r}_i} \left(i \boldsymbol{\eta} \cdot \sum_{j=1}^3 \boldsymbol{\delta}_j e^{-i\mathbf{K} \cdot \boldsymbol{\delta}_j} \left[\psi_{+A}^\dagger(\mathbf{r}_i) \psi_{+B}(\mathbf{r}_i) + \psi_{-A}^\dagger(\mathbf{r}_i) \psi_{+B}(\mathbf{r}_i) e^{-i\zeta(\mathbf{r}_i)} \right. \right. \\
&\quad \left. \left. + \psi_{-B}^\dagger(\mathbf{r}_i) \psi_{-A}(\mathbf{r}_i) + \psi_{B-} \psi_{A+}^\dagger e^{i\zeta(\mathbf{r}_i)} \right] - i \boldsymbol{\eta} \cdot \sum_{j=1}^3 \boldsymbol{\delta}_j e^{i\mathbf{K} \cdot \boldsymbol{\delta}_j} \left[\psi_{+B}^\dagger(\mathbf{r}_i) \psi_{+A}(\mathbf{r}_i) \right. \right. \\
&\quad \left. \left. + \psi_{+B}^\dagger(\mathbf{r}_i) \psi_{-A}(\mathbf{r}_i) e^{i\zeta(\mathbf{r}_i)} + \psi_{-A}^\dagger(\mathbf{r}_i) \psi_{-B}(\mathbf{r}_i) + \psi_{+A}^\dagger(\mathbf{r}_i) \psi_{-B}(\mathbf{r}_i) e^{-i\zeta(\mathbf{r}_i)} \right] \right), \\
&= \int d^2\mathbf{r} \Psi_{\tau, \sigma, s}^\dagger \left(H_{\text{B-R}} + \sum_{\mathbf{r}_a} H_{\text{spin-valley}} \right) \Psi_{\tau, \sigma, s},
\end{aligned} \tag{2.15}$$

where the spin-valley isotropic basis are

$$\Psi_{\tau, \sigma, s}^\dagger(\mathbf{r}) = \begin{pmatrix} \psi_{+A, s}^\dagger & \psi_{+B, s}^\dagger & -\psi_{-B, s}^\dagger & \psi_{-A, s}^\dagger \end{pmatrix}. \tag{2.16}$$

such that,

$$H_{\text{B-R}} = \lambda_R (\tau_0 \sigma_x s_y - \tau_z \sigma_y s_x), \tag{2.17}$$

$$H_{\text{spin-valley}} = \frac{i \lambda_R}{4} (\gamma_- \tau_- s_- - \gamma_+ \tau_+ s_+) \delta(\mathbf{r}_i - \mathbf{r}_a), \tag{2.18}$$

where $\lambda_R = at_{\text{so}}\sqrt{3}$ and $\gamma_{\pm} = e^{\pm i\zeta(\mathbf{r}_a)}$. The first Hamiltonian has the standard form of the Bychkov-Rashba type SOC [54] for graphene $\mathbf{v} = v_F \boldsymbol{\sigma} + \dots$, as one anticipates. The second term, however, is the spin valley interaction term that is originated by the adatoms

and merits further discussion. During the quasiparticle scattering from the adatoms, this term results in an intervalley scattering of the carrier along with the flip of their spin degrees of freedom. The spin-valley locking that we derived by only considering the effect of adatoms, is suggested to emerge in graphene/TMD heterojunctions [62]. The

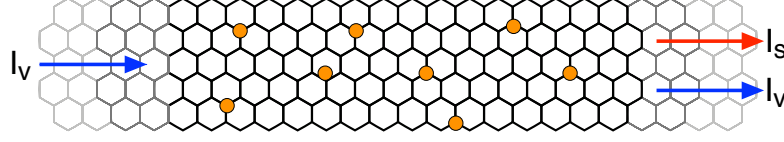


Figure 2.2: (Color online) The schematics of a finite width graphene nanoribbon with randomly deposited adatoms on atomic sites. The spin-orbit interaction (2.11) in this system induces the spin-valley locking (2.18) that can be utilized to generate spin current I_s from an injected valley current I_v .

spin valley mixing term (2.18), which is present in TMDs (see Ref. [63] and references therein), permits the realization of spin valley device, Fig.2.2, where the spin current can be created via valley current and vice versa [64]. The spin-valley locking also induces spin diffusion anisotropy, and coincidentally, materials possessing anisotropic spin lifetime are good candidates for spintronics applications[62]. This indicates that the intrinsic graphene could be engineered by the external mechanism and adatom deposition in order to modulate its features to function as a spin valley filter [16, 17, 65–67]. This additional term can result in the simultaneous valley and spin Hall effects, protection of the spin or valley index (as there is no spin or valley alone flipping) and spin-valley filtering [6, 67, 68].

We, thus, showed, in Eqs.2.17 and 2.18, that randomly adding adatoms on top of carbon atoms in graphene produces a strong Rashba effect as well as a spin dependent intervalley scattering which is not addressed in previous studies. Next, to compare the intervalley and intravalley transition rates, we consider the spin independent valley mixing which occurs in the presence of point-like short-range impurities.

2.2.2. Intervalley scattering

Some of the intriguing electronic properties of graphene are the so called minimal conductivity [69–71] and absence of localization [72] at low temperature near the Dirac point where the density of states tends to zero that is lacking in other materials[73, 74]. The studies show that most of these electronic properties in graphene are controlled by the impurities [71, 74–77]. There are typically two important types of disorder, 1) long range: Coulomb interaction due to the charged impurities and lattice corrugations, and 2) the

short range uncorrelated disorder [78–80],

$$V(\mathbf{r}) = \sum_{\mathbf{r}_i} \lambda_B(\mathbf{r}-\mathbf{r}_i) \psi_A^\dagger(\mathbf{r}_i) \psi_A(\mathbf{r}_i) + \sum_{\mathbf{r}_i, j} \lambda_B(\mathbf{r}-\mathbf{r}_i-\boldsymbol{\delta}_j) \psi_B^\dagger(\mathbf{r}_i+\boldsymbol{\delta}_j) \psi_B(\mathbf{r}_i+\boldsymbol{\delta}_j). \quad (2.19)$$

More importantly, the short-range impurities are the source of the intervalley scattering which dominates the momentum relaxation in graphene [81].

In the presence of spin-valley coupling, intervalley scattering also mediates the transport of spin. These features indicate that an accurate theory of transport in graphene needs to consider the interplay of all such degrees of freedom. Furthermore, the valley degrees of freedom have a defining role in describing weak localization or weak antilocalization transport regimes [73, 82]. Therefore the study of intervalley scattering is essential for the realization of the spin-valley coupled transport.

We next write down the hopping Hamiltonian for the short-range impurity model. In second quantization language for the potential (2.19) we write

$$\begin{aligned} V(\mathbf{r}) &= \sum_{\mathbf{r}_i} \lambda_A \left(\psi_{+A}^\dagger(\mathbf{r}_i) e^{-i\mathbf{K}\cdot\mathbf{r}_i} + \psi_{-A}^\dagger(\mathbf{r}_i) e^{i\mathbf{K}\cdot\mathbf{r}_i} \right) \left(\psi_{+A}(\mathbf{r}_i) e^{i\mathbf{K}\cdot\mathbf{r}_i} + \psi_{-A}(\mathbf{r}_i) e^{-i\mathbf{K}\cdot\mathbf{r}_i} \right) \\ &\quad + \sum_{\mathbf{r}_i, j} \lambda_B \left(\psi_{+B}^\dagger(\mathbf{r}_i + \boldsymbol{\delta}_j) e^{-i\mathbf{K}\cdot(\mathbf{r}_i+\boldsymbol{\delta}_j)} + \psi_{-B}^\dagger(\mathbf{r}_i + \boldsymbol{\delta}_j) e^{i\mathbf{K}\cdot(\mathbf{r}_i+\boldsymbol{\delta}_j)} \right) \times \\ &\quad \left(\psi_{+B}(\mathbf{r}_i + \boldsymbol{\delta}_j) e^{i\mathbf{K}\cdot(\mathbf{r}_i+\boldsymbol{\delta}_j)} + \psi_{-B}(\mathbf{r}_i + \boldsymbol{\delta}_j) e^{-i\mathbf{K}\cdot(\mathbf{r}_i+\boldsymbol{\delta}_j)} \right), \\ &= \sum_{\mathbf{r}_i} \lambda_A \left(\psi_{+A}^\dagger(\mathbf{r}_i) \psi_{+A}(\mathbf{r}_i) + \psi_{+A}^\dagger(\mathbf{r}_i) \psi_{-A}(\mathbf{r}_i) e^{-i\zeta(\mathbf{r}_i)} + \psi_{-A}^\dagger(\mathbf{r}_i) \psi_{+A}(\mathbf{r}_i) e^{i\zeta(\mathbf{r}_i)} \right. \\ &\quad \left. + \psi_{-A}^\dagger(\mathbf{r}_i) \psi_{-A}(\mathbf{r}_i) \right) \\ &\quad + \sum_{\mathbf{r}_i, j} \lambda_B \left(\psi_{+B}^\dagger(\mathbf{r}_i + \boldsymbol{\delta}_j) \psi_{+B}(\mathbf{r}_i + \boldsymbol{\delta}_j) + \psi_{+B}^\dagger(\mathbf{r}_i + \boldsymbol{\delta}_j) \psi_{-B}(\mathbf{r}_i + \boldsymbol{\delta}_j) e^{-i\zeta(\mathbf{r}_i)} \right. \\ &\quad \left. + \psi_{-B}^\dagger(\mathbf{r}_i + \boldsymbol{\delta}_j) \psi_{+B}(\mathbf{r}_i + \boldsymbol{\delta}_j) e^{i\zeta(\mathbf{r}_i)} + \psi_{-B}^\dagger(\mathbf{r}_i + \boldsymbol{\delta}_j) \psi_{-B}(\mathbf{r}_i + \boldsymbol{\delta}_j) \right), \\ &= \sum_{\mathbf{r}_i} \left\{ \lambda_A \left(\psi_{+A}^\dagger \psi_{+A} + \psi_{+A}^\dagger \psi_{-A} e^{-i\zeta(\mathbf{r}_i)} + \psi_{-A}^\dagger \psi_{+A} e^{i\zeta(\mathbf{r}_i)} + \psi_{-A}^\dagger \psi_{-A} \right) + \right. \\ &\quad \left. \lambda_B \left(\psi_{+B}^\dagger \psi_{+B} + \frac{4\pi}{\sqrt{3}} \psi_{+B}^\dagger \psi_{-B} e^{-i\zeta(\mathbf{r}_i)} - \frac{4\pi}{\sqrt{3}} \psi_{-B}^\dagger \psi_{+B} e^{i\zeta(\mathbf{r}_i)} + \psi_{-B}^\dagger \psi_{-B} \right) \right\} \\ &= \sum_{\mathbf{r}_i} \Psi^\dagger \mathbb{V}(\mathbf{r}_i) \Psi, \end{aligned} \quad (2.20)$$

where \mathbb{V} is defined below and $\lambda_A \equiv \lambda_A(\mathbf{r} - \mathbf{r}_i)$ and $\lambda_B \equiv \lambda_B(\mathbf{r} - \mathbf{r}_i - \boldsymbol{\delta}_j)$. Note that, to obtain the last line we have used the Taylor expansion for the envelope function around

sublattice B such that

$$\psi_{\tau,B}^{(\dagger)}(\mathbf{r}_i + \boldsymbol{\delta}_j) = \psi_{\tau,B}^{(\dagger)}(\mathbf{r}_i) + \boldsymbol{\delta}_j \cdot \nabla \psi_{\tau,B}^{(\dagger)}(\mathbf{r}_i) + O(|\boldsymbol{\delta}_j|^2), \quad (2.21)$$

which consequently, in the limit $\delta \ll 1$, yields

$$\psi_{\tau,B}^{(\dagger)}(\mathbf{r}_i + \boldsymbol{\delta}_j) \psi_{\tau,B}(\mathbf{r}_i + \boldsymbol{\delta}_j) \approx (1 + \boldsymbol{\delta}_j \cdot \nabla) \psi_{\tau,B}^{(\dagger)}(\mathbf{r}_i) \psi_{\tau,B}(\mathbf{r}_i), \quad (2.22)$$

$$\begin{aligned} \psi_{\tau',B}^{(\dagger)}(\mathbf{r}_i + \boldsymbol{\delta}_j) \psi_{\tau,B}(\mathbf{r}_i + \boldsymbol{\delta}_j) e^{i\tau\zeta(\mathbf{r}_i)} &\approx (1 - 2i\tau \mathbf{K} \cdot \boldsymbol{\delta}_j) \psi_{\tau,B}^{(\dagger)}(\mathbf{r}_i) \psi_{\tau,B}(\mathbf{r}_i) e^{i\tau\zeta(\mathbf{r}_i)} \\ &+ \boldsymbol{\delta}_j \cdot \nabla \left(\psi_{\tau,B}^{(\dagger)}(\mathbf{r}_i) \psi_{\tau,B}(\mathbf{r}_i) e^{i\tau\zeta(\mathbf{r}_i)} \right), \end{aligned} \quad (2.23)$$

where $\tau, \tau' = \pm$ are valley indices and in the continuum limit terms involving total derivatives will vanish. Also note that

$$\sum_j e^{\pm i\mathbf{K} \cdot \boldsymbol{\delta}_j} = \sum_j e^{\pm 2i\mathbf{K} \cdot \boldsymbol{\delta}_j} = 0, \quad \sum_j \mathbf{K} \cdot \boldsymbol{\delta}_j e^{\pm 2i\mathbf{K} \cdot \boldsymbol{\delta}_j} = -\frac{2\pi i}{\sqrt{3}}. \quad (2.24)$$

This allows us to ignore the terms of orders δ such that in the limit $\lambda_B \gg \lambda_B \delta \gg \lambda_B \delta^2$ we obtain the matrix

$$\begin{aligned} \mathbb{V} = & \left[\lambda_+ \tau_0 \otimes \sigma_0 + \lambda_- \tau_3 \otimes \sigma_3 + \frac{\lambda_A}{4} \left(e^{-2i\zeta(\mathbf{r}_i)} \tau_+ \otimes \sigma_+ + e^{2i\zeta(\mathbf{r}_i)} \tau_- \otimes \sigma_- \right) \right. \\ & \left. - \frac{\lambda_B}{4} \left(e^{2i\zeta(\mathbf{r}_i)} \tau_- \otimes \sigma_+ + e^{-2i\zeta(\mathbf{r}_i)} \tau_+ \otimes \sigma_- \right) \right] \otimes s_0, \end{aligned} \quad (2.25)$$

where $\lambda_{\pm} = \frac{\lambda_B \pm \lambda_A}{2}$. As we see from the Hamiltonian, the impurity potential gives rise to various valley orbit coupling terms that each term has its own merit of discussion. The impurity potential term as a matrix gives

$$\mathbb{V} = \begin{matrix} & \psi_{+A} & \psi_{+B} & -\psi_{-B} & \psi_{-A} \\ \begin{matrix} \psi_{+A}^\dagger \\ \psi_{+B}^\dagger \\ -\psi_{-B}^\dagger \\ \psi_{-A}^\dagger \end{matrix} & \begin{pmatrix} \lambda_A & 0 & 0 & \lambda_A e^{-2i\zeta(\mathbf{r}_i)} \\ 0 & \lambda_B & -\tilde{\lambda}_B e^{-2i\zeta(\mathbf{r}_i)} & 0 \\ 0 & -\tilde{\lambda}_B e^{2i\zeta(\mathbf{r}_i)} & \lambda_B & 0 \\ \lambda_A e^{2i\zeta(\mathbf{r}_i)} & 0 & 0 & \lambda_A \end{pmatrix} \end{matrix}, \quad (2.26)$$

where $\tilde{\lambda}_B = \frac{4\pi}{\sqrt{3}} \lambda_B$. Note that the terms along the diagonal are intravalley scattering whereas the off diagonal terms induce the intervalley scatterings. In the next section we will compute the transition rates due to these different transitions.

2.3. Spin scattering rates: Fermi's golden rule

Now we compute the transition rates using Fermi's golden rule in the presence of short-range defects and local spin orbit coupling. By solving the eigenvalue problem in graphene, the electronic states (positive energy) in the valley isotropic basis (2.6) gives

$$|+\rangle = \begin{pmatrix} 1 \\ e^{i\varphi} \\ 0 \\ 0 \end{pmatrix} e^{i\mathbf{k}\cdot\mathbf{r}}, \quad \text{and} \quad |-\rangle = \begin{pmatrix} 0 \\ 0 \\ -e^{-i\varphi} \\ 1 \end{pmatrix} e^{i\mathbf{k}\cdot\mathbf{r}}, \quad (2.27)$$

where the indices \pm refers to two inequivalent valleys in graphene and $\varphi = \tan^{-1}(k_y/k_x)$. The intervalley transition rate from an initial state into a final state using Fermi's Golden Rule for uncorrelated point-like impurities is given by

$$\frac{1}{\tau(k)} = n_{\text{imp}} \int k' dk' \int_0^{2\pi} \frac{d\varphi'}{2\pi} |\langle \text{in} | \mathbb{V} | \text{fin} \rangle|^2 \delta(\varepsilon_{k'} - \varepsilon_k). \quad (2.28)$$

Therefore, the transition matrix elements give

$$\mathbb{V}_{++} = \langle + | \mathbb{V} | + \rangle = (\lambda_A + \lambda_B e^{-i(\varphi - \varphi')}) = \langle - | \mathbb{V} | - \rangle^* = \mathbb{V}_{--}^*$$

$$\mathbb{V}_{+-} = \langle + | \mathbb{V} | - \rangle = e^{-2i\zeta(\mathbf{r}_i)} (\lambda_A + \tilde{\lambda}_B e^{-i(\varphi + \varphi')}) = \langle - | \mathbb{V} | + \rangle^* = \mathbb{V}_{-+}^*.$$

Therefore

$$|\mathbb{V}_{++}|^2 = |\mathbb{V}_{--}|^2 = \lambda_A^2 + \lambda_B^2 + 2\lambda_A\lambda_B \cos(\varphi - \varphi'), \quad (2.29)$$

$$|\mathbb{V}_{+-}|^2 = |\mathbb{V}_{-+}|^2 = \lambda_A^2 + \tilde{\lambda}_B^2 + 2\lambda_A\tilde{\lambda}_B \cos(\varphi + \varphi'). \quad (2.30)$$

Then the rates of intervalley and intravalley scattering are

$$\frac{1}{\tau} \propto \begin{cases} \lambda_A^2 + \lambda_B^2 + 2\lambda_A\lambda_B \cos \varphi' & \text{Intra-Valley,} \\ \lambda_A^2 + \lambda_B^2 - 2\lambda_A\lambda_B \cos \varphi' & \text{Inter-Valley.} \end{cases} \quad (2.31)$$

To compute the matrix element of the SOC we find that

$$\langle \tau, s | H_{\text{SOC}} | \tau, s \rangle = 0 \quad (2.32)$$

$$|\langle \tau, s | H_{\text{SOC}} | \tau, s' \rangle|^2 = |\gamma_-|^2 + |\gamma_+|^2 + 2\gamma_+\gamma_- \cos(\varphi + \varphi') \quad (2.33)$$

$$|\langle \tau, s | H_{\text{SOC}} | \tau', s' \rangle|^2 = 2|\gamma_\tau|^2 \cos^2\left(\frac{\varphi + \varphi'}{2}\right) \quad (2.34)$$

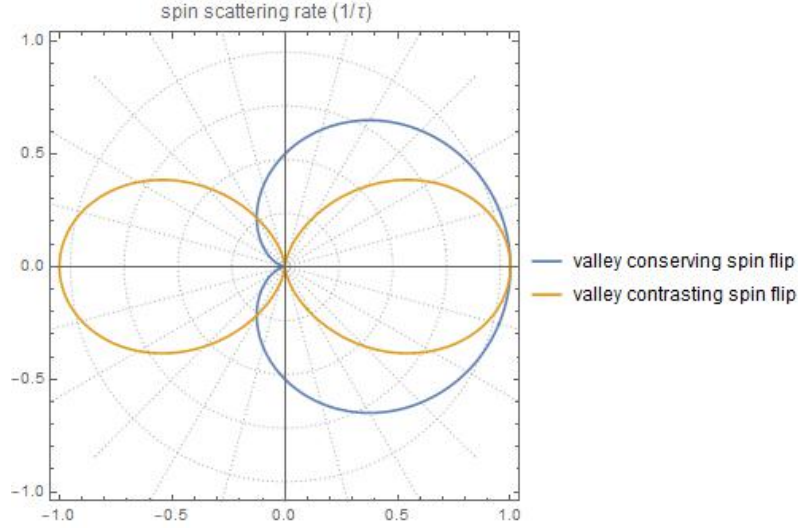


Figure 2.3: (Color online) The spin scattering rates for the adatom engineered graphene that induces SOC given in (2.17) and (2.18). During the intravalley scattering the suppression of back scattering happens while for in the valley mixed spin flips the backscattering is allowed.

where s and s' are the spin degrees of freedom and picking either \uparrow or \downarrow . The transition rates show that there is difference between the valley conserved and valley contrasting spin flip scatterings in terms of the backscattering. We have plotted these rates in Fig. 2.3 for further discussions. It turns out that the well-known suppression of the backscattering, which is a feature of the Dirac particles in graphene, is removed in the case of the SOC induced by the adatoms which allows for a novel valley mixed spin scatterings. Therefore, while the valley contrasting spin flip forbids the backscattering, the valley conserving spin flip permits the Dirac particles to be back scattered.

This new backscattering attributes of the adatom engineered graphene opens new fronts for its applications as a spin-valley qubit where through the intervalley scattering the initial states can be restored [1]. In order to understand the coherent dynamics of the degrees of freedom in graphene, such as the coupling of spin and valley, we next try to establish a quantum kinetic model for the Dirac Hamiltonian in the presence of adatoms. After constructing the kinetic model, for better interpretation, we will reduce it to a diffusion model written in real space [26].

2.4. Quantum transport equation

The dynamics of a statistical system is governed by *Liouville's theorem* which describes the time evolution of the N -body distribution function. This large set of variables, $6N$ (N being the number of the atoms), makes the Liouville's equation complex and impractical for analytical and numerical use [26]. Contrary to Liouville's equation which in essence is a many-body formulation, on the other hand, the *Boltzmann equation*, describing the

statistical dynamics of a system out of equilibrium, is formulated for a single-particle distribution function and hence more functional [26, 27].

In the kinetics model the particles tend to go towards the equilibration by experiencing collisions. The Boltzmann transport equation also takes into account the scatterings through a collision term that balances the kinetics of the carriers. There are two directions in using the Boltzmann transport equation to describe the physical quantities. One way is by solving the equation for the distribution function and use it to find the form of the quantity under study. We alternatively apply approximations to the transport equation which in turn gives the *Drift-Diffusion models* of transport.

In the quantum transport equation, the main object that is described is the quasiparticle distribution function $f(\mathbf{k}, \mathbf{x}, \varepsilon, t)$ and when deriving the drift-diffusion model, from the quantum transport equation, its counterpart will be the density matrix $\rho(\mathbf{x}, t, \varepsilon)$.

We attempt to generate a reliable quantum Boltzmann equation for carriers having coherent spin and valley degrees of freedom driven by external fields. We assume these fields have weak spatial and temporal dependence and we stay within the response limit so a quasi-stationary transport equation is justified.

We start the derivation of quantum transport equation by studying the time evolution of the density matrix governed by quantum Liouville's equation,

$$i\dot{\rho} = [H, \rho]. \quad (2.35)$$

For a system in equilibrium the density matrix is a function of the unperturbed Hamiltonian $\rho(H_0)$ [83, 84]. In the presence of external fields however the density matrix will deviate from its equilibrium form such that

$$\rho(t) = \rho(H_0) + \delta\rho(t), \quad (2.36)$$

where the non-equilibrium part, when the external fields vanish, will relax into the equilibrium. Furthermore, we assume an initial condition on time t such that the fields were absent at very past, namely,

$$\delta\rho(t = -\infty) = 0, \quad (2.37)$$

where we assume that the non-equilibrium part to have the time dependent form as $\delta\rho(t) = f e^{\alpha t}$, $\alpha > 0$. We consider an impure Graphene sample subjected to external in plane electric field such that now the one particle Hamiltonian for the system is

$$H = H_0 + V(\mathbf{x}) + H_{\text{ext}}, \quad (2.38)$$

where H_0 is the Dirac Hamiltonian for Graphene in the vicinity of a single cone

$$H_0 = v_F \boldsymbol{\sigma} \cdot \mathbf{p}, \quad (2.39)$$

and the disorder potential and the external field is given by

$$V(\mathbf{x}) = \sum_i V(\mathbf{x} - \{\mathbf{x}_i\}), \quad H_{\text{ext}} = -e\mathbf{E} \cdot \mathbf{x}. \quad (2.40)$$

such that the electric field is such that $E = E_0 e^{|\alpha|t}$ and is turned off at the far past, namely, $E(t = -\infty) \rightarrow 0$. Therefore the equation for the density matrix now will read

$$i \frac{\partial \delta \rho}{\partial t} = [H_0 + V(\mathbf{x}), \delta \rho]_- + [H_{\text{ext}}, \rho_0]_- + \dots \quad (2.41)$$

we are interested in studying this equation in linear response regime where the solutions are in first order in electric field but has a power series expansion in terms of impurity strength. Therefore we project the Liouville's equation in the momentum space (plane wave basis) where the Hamiltonian is diagonal and noting that $\langle k | \delta \rho | k' \rangle = e^{\alpha t} f_{kk'}$, we then write

$$i\alpha f_{kk'} = H_0(\mathbf{k}) f_{kk'} - f_{kk'} H_0(\mathbf{k}') + \sum_{k''} \left(V_{kk''} f_{k''k'} - f_{kk''} V_{k''k'} \right) - e\mathbf{E} \cdot [\mathbf{x}, \rho_0]_{kk'}. \quad (2.42)$$

By splitting the projected non-equilibrium density matrix into diagonal and off diagonal elements, i.e.,

$$f_{kk'} = f_{kk'} \delta_{kk'} + f_{kk'} (1 - \delta_{kk'}), \quad (2.43)$$

we manage to separate the matrix equation into two coupled equations in term of diagonal and off diagonal elements. The off diagonal part, where $k \neq k'$, reads

$$\begin{aligned} i\alpha f_{kk'} &= H_0(\mathbf{k}) f_{kk'} - f_{kk'} H_0(\mathbf{k}') + V_{kk'} f_{k'} - f_k V_{kk'} + V_k f_{kk'} - f_{kk'} V_{k'} \\ &+ \sum_{k'' \neq k, k'} \left(V_{kk''} f_{k''k'} - f_{kk''} V_{k''k'} \right) - e\mathbf{E} \cdot [\mathbf{x}, \rho_0]_{kk'}, \end{aligned} \quad (2.44)$$

and diagonal part gives

$$i\alpha f_k = H_0(\mathbf{k}) f_k - f_k H_0(\mathbf{k}) + \sum_{k' \neq k} \left(V_{kk'} f_{k'k} - f_{kk'} V_{k'k} \right) - e\mathbf{E} \cdot [\mathbf{x}, \rho_0]_{kk}. \quad (2.45)$$

We now assume that dominant contribution to the non equilibrium part is coming from the band diagonal part of the distribution function and the offdiagonal terms, that are induced by the external fields, are relatively weak, namely, $f_k \gg f_{kk'}$, [83, 84]. Hence the final evolution equation, which will reduce into a Boltzmann type transport equation, must be

written for the diagonal distribution function. Up to the leading order in the impurity potential the off diagonal equation then becomes

$$i\alpha f_{kk'} - \left(H_0(\mathbf{k}) f_{kk'} - f_{kk'} H_0(\mathbf{k}') \right) = \left(V_{kk'} f_{k'} - f_k V_{kk'} \right). \quad (2.46)$$

Subsequently, this equation can be solved by introducing two Green's functions namely, i.e

$$G_k^{R(A)}(z) = \left(z + (-)i\alpha/2 - H_0(\mathbf{k}) \right)^{-1}, \quad (2.47)$$

which gives the solution for the diagonal distribution function as

$$f_{kk'} = \frac{1}{2\pi i} \int_{-\infty}^{+\infty} dz G_k^R(z) \left(V_{kk'} f_{k'} - f_k V_{kk'} \right) G_{k'}^A(z). \quad (2.48)$$

Next, plugging this solution back into the diagonal equation gives

$$\alpha f_k + i[H_0(\mathbf{k}), f_k] - e\mathbf{E} \cdot [\nabla_{\mathbf{k}}, f]_k = \mathbb{I}[f_k], \quad (2.49)$$

where the collision integral due to impurity potential reads

$$\mathbb{I}[f_k] = \frac{1}{2\pi} \int dz \sum_{k'} \left\{ V_{kk'} G_{k'}^R (V_{k'k} f_k - f_{k'} V_{k'k}) G_k^A - G_k^R (V_{kk'} f_{k'} - f_k V_{kk'}) G_{k'}^A V_{k'k} \right\}. \quad (2.50)$$

To describe the semiclassical dynamics of quantum carrier, and to obtain a distribution function which is written both in position and momentum coordinates, we transform this equation into Wigner coordinates. In the new representation normal product is transferred into the $*$ -products [85] such that up to first order it yields

$$A B \longrightarrow A \star B \approx A B + \frac{i}{2} [A, B]_{P.B} + \dots, \quad (2.51)$$

where $\star = \exp \frac{i}{2} (\overleftarrow{\partial}_{\mathbf{x}} \overrightarrow{\partial}_{\mathbf{k}} - \overleftarrow{\partial}_{\mathbf{k}} \overrightarrow{\partial}_{\mathbf{x}})$. Working out the Poisson brackets we obtain the semiclassical Boltzmann equation for Graphene as

$$\partial_t f(\mathbf{k}, \mathbf{x}) + i[H_0, f(\mathbf{k}, \mathbf{x})]_- + \frac{v_F}{2} [\boldsymbol{\sigma}, \nabla_{\mathbf{x}} f(\mathbf{k}, \mathbf{x})]_+ - e\mathbf{E} \cdot \nabla_{\mathbf{k}} f(\mathbf{k}, \mathbf{x}) = \mathbb{I}[f(\mathbf{k}, \mathbf{x})]. \quad (2.52)$$

The semiclassical equation we derived and its solutions are the main tools to describe transport in a system. As it appears the equation is written for a matrix distribution function. Next, using the parametrization of the matrix distribution function as $f = n + \mathbf{s} \cdot \boldsymbol{\sigma}$, and assuming that the Hamiltonian is only spin dependent and applying the relaxation time approximation, then the matrix equation can be written in two coupled scalar equations for charge and pseudo-spin such as

$$\partial_t n - e \mathbf{E} \cdot \nabla_{\mathbf{k}} n + v_F \nabla_{\mathbf{x}} \cdot \mathbf{s} = -\frac{n - n_0}{\tau_p}, \quad (2.53)$$

$$\partial_t \mathbf{s} - e (\mathbf{E} \cdot \nabla_{\mathbf{k}}) \mathbf{s} + v_F \nabla_{\mathbf{x}} n + 2v_F \mathbf{s} \times \mathbf{k} = -\frac{\mathbf{s} - \mathbf{s}_0}{\tau_s}. \quad (2.54)$$

These calculations demonstrate that the kinetic equation for a two band system, essentially, describes the coupled dynamics of charge and spin. The above equations can be understood as two balance equations that include the relaxation, diffusion, precession and the flip mechanisms of the carriers during the scattering. In the following we derive the diffusion equations for graphene and its intuitive semiclassical interpretations by first approximating the transport equation and solving it.

2.4.1. Collision kernel: Disorder scattering

To model the disorder in the system, suppose that the spin-less impurities are distributed randomly throughout the system. The strength of these impurities are described by the potential

$$V(\mathbf{x}) = \sum_i V(\mathbf{x} - \{\mathbf{x}_i\}), \quad (2.55)$$

where \mathbf{x}_i 's are the position of the random impurities. Now, substituting this scalar potential into the collision integral we get

$$\mathbb{I}[f] = n_{\text{imp}} \sum_{\mathbf{k}'} |\tilde{V}(\mathbf{k} - \mathbf{k}')|^2 \int \frac{dz}{2\pi} \left\{ G_{k'}^R(f_k - f_{k'}) G_k^A - G_k^R(f_{k'} - f_k) G_{k'}^A \right\}, \quad (2.56)$$

where we have used the notation

$$V_{kk'} V_{k'k} = \langle k | V(\mathbf{x}, \{\mathbf{x}_i\}) | k' \rangle \langle k' | V(\mathbf{x}, \{\mathbf{x}_i\}) | k \rangle, \quad (2.57)$$

and averaged over many impurity instances to obtain

$$\overline{V_{kk'} V_{k'k}} = n_{\text{imp}} |\tilde{V}(\mathbf{k} - \mathbf{k}')|^2. \quad (2.58)$$

On the other hand, the matrix Green's function for graphene is given by

$$G_{\mathbf{k}}^R(z) = \sum_{\xi} \frac{(1 + \xi \boldsymbol{\sigma} \cdot \hat{\mathbf{k}})/2}{z - \varepsilon_k^{\xi} - i0}, \quad (2.59)$$

where ξ is the chirality index which for a single cone (positive) it coincides with the band index. Thus within the first Born approximation the collision operator becomes

$$I[f] = n_{\text{imp}} \sum_{\mathbf{k}', \xi, \xi'} |\tilde{V}(\mathbf{k} - \mathbf{k}')|^2 \int \frac{dz}{2\pi} \left(\frac{\Lambda_{k'k}^{\xi' \xi}}{(z - \varepsilon_{k'}^{\xi'} + i0)(z - \varepsilon_k^{\xi} - i0)} \right)$$

$$- \frac{\Lambda_{kk'}^{\xi\xi'}}{(z - \varepsilon_{k'}^{\xi'} - i0)(z - \varepsilon_k^\xi + i0)}, \quad (2.60)$$

where the transition matrix is given by

$$\Lambda_{kk'}^{\xi\xi'} = \frac{1 + \xi \boldsymbol{\sigma} \cdot \hat{\mathbf{k}}}{2} (f_{k'} - f_k) \frac{1 + \xi' \boldsymbol{\sigma} \cdot \hat{\mathbf{k}}'}{2}. \quad (2.61)$$

The energy integrand has two set of poles on both upper and lower planes. Closing the contour in the lower plane the energy integral is simply

$$\sum_{\mathbf{k}'} \int_{\text{lower}} \frac{dz}{2\pi} \frac{1}{(z - \varepsilon_{k'}^{\xi'} + i0)(z - \varepsilon_k^\xi - i0)} = -\frac{i}{2} \sum_{\mathbf{k}'} \frac{1}{\varepsilon_{k'}^{\xi'} - \varepsilon_k^\xi - i0}, \quad (2.62)$$

and noting that there is yet a momentum integral under which we use the identity from complex analysis

$$\frac{1}{\varepsilon_{k'}^{\xi'} - \varepsilon_k^\xi - i0} = \text{P.V} \left(\frac{1}{\varepsilon_{k'}^{\xi'} - \varepsilon_k^\xi} \right) + i\pi \delta(\varepsilon_k^\xi - \varepsilon_{k'}^{\xi'}). \quad (2.63)$$

The principal value parts from the collision terms cancel identically and surviving term is the delta function giving the Fermi's golden rule and setting the condition for the elastic scattering i.e

$$I[f] = \frac{\pi n_{\text{imp}}}{2} \sum_{k', \xi, \xi'} |u(k - k')|^2 (\Lambda_{kk'}^{\xi\xi'} - \Lambda_{k'k}^{\xi'\xi}) \delta(\varepsilon_k^\xi - \varepsilon_{k'}^{\xi'}). \quad (2.64)$$

which is essentially the Fermi's golden rule, extended to quantum transport.

By doing the momentum integral explicitly we can obtain a bound for the relaxation time in the presence of short-range disorder. Then the relaxation time is expressed as

$$\begin{aligned} \frac{f_0(k) - f(k)}{\tau} &\equiv I[f] \\ &= \frac{\pi n_{\text{imp}}}{2} \sum_{\mu, \mu'} \int \frac{k' dk'}{2\pi} \int \frac{d\phi'}{2\pi} |V(k - k')|^2 (\Lambda_{kk'}^{\mu\mu'} - \Lambda_{k'k}^{\mu'\mu}) \delta(\varepsilon_k^\mu - \varepsilon_{k'}^{\mu'}). \end{aligned} \quad (2.65)$$

The relaxation time is then given by

$$\frac{1}{\tau} = \frac{\pi n_{\text{imp}} V^2}{2} g(\varepsilon_F), \quad (2.66)$$

where $g(\varepsilon_F) = \frac{|\varepsilon_F|}{2\pi v_F^2}$ is the density of states at Fermi energy [86].

2.4.2. Magnetotransport

To compute the deviation from the equilibrium distribution in linear response regime we expand the non-equilibrium distribution function in terms of equilibrium distribution. Assuming that the distribution function has a power series expansion in term of the weak electric field (linear response) we write

$$f(\mathbf{E}, \mathbf{B}; \mathbf{k}) = f_0 + \mathbf{O}(\mathbf{E}, \mathbf{B}) \cdot \nabla_{\mathbf{k}} f, \quad (2.67)$$

where the function $\mathbf{O}(\mathbf{E}, \mathbf{B})$ is first order in the weak field \mathbf{E} . The expansion can be used to self consistently generate higher order corrections to the distribution function. Substituting this ansatz and keeping terms to first order the transport equation gives

$$-e\tau(\mathbf{E} + \mathbf{v} \times \mathbf{B}) \cdot \nabla_{\mathbf{k}} \left(f_0 + \mathbf{O} \cdot \mathbf{v} \frac{\partial f_0}{\partial \varepsilon} \right) = -\mathbf{O} \cdot \mathbf{v} \frac{\partial f_0}{\partial \varepsilon}, \quad (2.68)$$

then applying the momentum derivative and noting that $\nabla_{\mathbf{k}} f_0 = \mathbf{v} \frac{\partial f_0}{\partial \varepsilon}$, and the band velocity as $\mathbf{v} = v_F \hat{\mathbf{k}}$ gives

$$-e\tau(\mathbf{E} + \mathbf{v} \times \mathbf{B}) \cdot \left(\mathbf{v} \frac{\partial f_0}{\partial \varepsilon} + \nabla_{\mathbf{k}}(\mathbf{O} \cdot \mathbf{v}) \frac{\partial f_0}{\partial \varepsilon} + \mathbf{O}(\mathbf{E}, \mathbf{B}) \cdot \mathbf{v} \frac{\partial^2 f_0}{\partial \varepsilon^2} \right) = -\mathbf{O}(\mathbf{E}, \mathbf{B}) \cdot \mathbf{v} \frac{\partial f_0}{\partial \varepsilon}. \quad (2.69)$$

Next, we consider only the first derivatives of the energy which yields

$$-e\tau(\mathbf{E} + \mathbf{v} \times \mathbf{B}) \cdot \left(\mathbf{v} \frac{\partial f_0}{\partial \varepsilon} + \mathbf{O}(\mathbf{E}, \mathbf{B}) \frac{v_F^2}{\varepsilon_k} \frac{\partial f_0}{\partial \varepsilon} \right) = -\mathbf{O}(\mathbf{E}, \mathbf{B}) \cdot \mathbf{v} \frac{\partial f_0}{\partial \varepsilon}, \quad (2.70)$$

and then taking into account terms of up to the first order in the electric field and noting that $\partial v_i / \partial p_j = v_F^2 / \varepsilon_k$ we simply obtain a vector equation, namely,

$$\mathbf{E} = \frac{1}{e\tau} \mathbf{O}(\mathbf{E}, \mathbf{B}) - \frac{v_F^2}{\varepsilon_k} \mathbf{B} \times \mathbf{O}(\mathbf{E}, \mathbf{B}), \quad (2.71)$$

which is solved to yield the generator of the small deviation from the equilibrium as

$$\mathbf{O}(\mathbf{E}, \mathbf{B}) = \frac{e\tau}{1 + \tau^2 (ev_F^2 \mathbf{B} / \varepsilon_k)^2} (\mathbf{E} + e\tau \frac{v_F^2}{\varepsilon_k} \mathbf{B} \times \mathbf{E}), \quad (2.72)$$

that consequently produces the non-equilibrium part of the distribution [86]

$$f(\mathbf{E}, \mathbf{B}) = f_0 + \frac{e\tau}{1 + \tau^2 \omega^2} (\mathbf{E} + e\tau \frac{v_F^2}{\varepsilon_k} \mathbf{B} \times \mathbf{E}) \cdot \mathbf{v} \frac{\partial f_0}{\partial \varepsilon}, \quad (2.73)$$

where we introduced the cyclotron frequency in Graphene as

$$\omega = \frac{ev_F^2}{\varepsilon_k} B. \quad (2.74)$$

Using this solution the charge current from the transport equation gives

$$\begin{aligned} J_i &= -e \sum_k v_i f, \\ &= -e \sum_k \frac{\partial f_0}{\partial \varepsilon} \frac{e\tau}{1 + \tau^2 \omega^2} v_i v_j E_j - e \sum_k \frac{\partial f_0}{\partial \varepsilon} \frac{e\tau^2 \omega}{1 + \tau^2 \omega^2} \varepsilon_{3\ell j} v_i v_j E_\ell, \end{aligned} \quad (2.75)$$

changing the summation into integrals via

$$\sum_{\mathbf{k}} \rightarrow \int \frac{\varepsilon_k d\varepsilon_k}{2\pi v_F^2} \int \frac{d\phi}{2\pi}, \quad (2.76)$$

and noting that the density of state (DOS) for Graphene can be written as

$$\text{DOS}(\varepsilon_F) = \sum_{\mathbf{k}} \delta(\varepsilon_k - \varepsilon_F) = \int \frac{\varepsilon_k d\varepsilon_k}{2\pi v_F^2} \left(-\frac{\partial f_0}{\partial \varepsilon} \right), \quad (2.77)$$

and noting that for graphene $\langle v_i v_j \rangle_\phi = \delta_{ij} v_F^2/2$, we obtain the current as

$$J_i = \frac{e^2 v_F^2 \nu(\varepsilon_F)}{2} \left(\frac{\tau}{1 + \tau^2 \omega^2} \delta_{ij} E_j - \frac{\omega \tau^2}{1 + \tau^2 \omega^2} \varepsilon_{ij3} E_j \right), \quad (2.78)$$

hence the conductivity tensor consist of diagonal and transverse (Hall) parts is given by

$$\sigma_{ij} = \frac{e^2 v_F^2 \nu(\varepsilon_F)}{2} \left(\frac{\tau}{1 + \tau^2 \omega^2} \delta_{ij} - \frac{\omega \tau^2}{1 + \tau^2 \omega^2} \varepsilon_{ij3} \right). \quad (2.79)$$

2.5. Diffusion model

For a real physical setting, the transport equation can be further simplified. We consider an inhomogeneous system in the presence of an external electric field then we write

$$\partial_t f(k, x) + i[\mathcal{H}_0(k), f(k, x)]_- + \frac{v_F}{2} [\sigma; \nabla_x f(k, x)]_+ - e E \cdot \nabla_p f(k, x) = \mathbb{I}[f(k, x)], \quad (2.80)$$

where the collision integral is

$$\mathbb{I}[f(k, x)] = \frac{1}{2\pi} \int dz \sum_{\mathbf{k}'} |\mathbb{V}_{\mathbf{k}\mathbf{k}'}|^2 \left(G_{\mathbf{k}'z}^R (f_{\mathbf{k}'} - f_{\mathbf{k}}) G_{\mathbf{k}z}^A - G_{\mathbf{k}z}^R (f_{\mathbf{k}} - f_{\mathbf{k}'}) G_{\mathbf{k}'z}^A \right). \quad (2.81)$$

Note that the matrix Green's function for the free Graphene Hamiltonian can be written in terms of projection operators as

$$G(\mathbf{k}, z) = \sum_{\mu} \mathcal{P}_{\mathbf{k}}^{\mu} G_{\mu}(k, z) \quad (2.82)$$

where $\mu = \pm$ being the band index

$$\mathcal{P}_{\mathbf{k}}^{\mu} = \frac{1 + \mu \sigma_{\mathbf{k}}}{2}, \quad G_{\mu}(k, z) = \frac{1}{z - \xi_k^{\mu}}, \quad (2.83)$$

one has similar relation for the retarded, advanced function and $\xi_k^{\mu} = \mu v_F k$, is the kinetic energy counted from the Fermi level. Furthermore, the spectral function becomes

$$\mathbb{G}^R(\mathbf{k}, z) - \mathbb{G}^A(\mathbf{k}, z) = -2i\pi \sum_{\mu} \mathcal{P}_{\mathbf{k}}^{\mu} \delta(z - \varepsilon_k^{\mu}), \quad (2.84)$$

One can use this result by adding retarded and advanced function to the collision integral and rewritten it as

$$\begin{aligned} \mathbb{I}[f(\mathbf{k}, \mathbf{x})] &= \frac{1}{2\pi} \int dz \sum_{\mathbf{k}'} |\mathbb{V}_{\mathbf{k}\mathbf{k}'}|^2 \left[\mathbb{G}_{\mathbf{k}'z}^R (f_{\mathbf{k}'} - f_{\mathbf{k}}) (\mathbb{G}_{\mathbf{k}z}^A - \mathbb{G}_{\mathbf{k}z}^R) - (\mathbb{G}_{\mathbf{k}z}^R - \mathbb{G}_{\mathbf{k}z}^A) (f_{\mathbf{k}} - f_{\mathbf{k}'}) \mathbb{G}_{\mathbf{k}'z}^A \right], \\ &= i \sum_{\mathbf{k}'} |\mathbb{V}_{\mathbf{k}\mathbf{k}'}|^2 (\mathbb{G}_{\mathbf{k}'z}^R f_{\mathbf{k}'} - f_{\mathbf{k}'} \mathbb{G}_{\mathbf{k}'z}^A) - i \sum_{\mathbf{k}'} |\mathbb{V}_{\mathbf{k}\mathbf{k}'}|^2 (\mathbb{G}_{\mathbf{k}'z}^R f_{\mathbf{k}} - f_{\mathbf{k}} \mathbb{G}_{\mathbf{k}'z}^A) \\ &= i \frac{\rho}{\tau} - \frac{f_{\mathbf{k}}}{\tau} \end{aligned} \quad (2.85)$$

where in second line it is straightforward to compute the sums by changing them into integrals. The second term is proportional with the scattering rate of carriers from impurity with distribution function $f(k)$ while the first term is approximated as the scattering rate for carriers given with general momentum resolved, energy dependent distribution function as

$$\mathfrak{g}_{\mathbf{k}''\varepsilon} = \frac{1}{2i\pi} \left(\mathbb{G}_{\mathbf{k}''\varepsilon}^R f_{\mathbf{k}''} - f_{\mathbf{k}''} \mathbb{G}_{\mathbf{k}''\varepsilon}^A \right), \quad \rho_{\varepsilon} = \sum_{\mathbf{k}''} \mathfrak{g}_{\mathbf{k}''\varepsilon}, \quad (2.86)$$

these assumptions help to conveniently simplify the collision integral. Then the resultant transport equation becomes

$$\partial_t f(\mathbf{k}, \mathbf{x}) + i[\mathcal{H}_0(k), f(\mathbf{k}, \mathbf{x})]_- + \frac{v_F}{2} [\sigma; \nabla_x f(\mathbf{k}, \mathbf{x})]_+ = i \frac{\rho_{\varepsilon}}{\tau} - \frac{f(\mathbf{k}, \mathbf{x})}{\tau}. \quad (2.87)$$

We, furthermore, multiply the transport equation with the retarded and advanced functions from the left and right respectively and then subtract two relations to obtain the quantum Boltzmann equation [87],

$$(\partial_t + \tau^{-1}) \mathfrak{g}_{\mathbf{k},\varepsilon} + i[\mathcal{H}_0(k), \mathfrak{g}_{\mathbf{k},\varepsilon}]_- + \frac{v_F}{2} [\sigma; \nabla_x \mathfrak{g}_{\mathbf{k},\varepsilon}]_+ = i\tau_k^{-1} (\mathbb{G}_{\mathbf{k}\varepsilon}^R \rho_{\varepsilon} - \rho_{\varepsilon} \mathbb{G}_{\mathbf{k}\varepsilon}^A). \quad (2.88)$$

We solve this equation using Laplace transform, which is equivalent to setting the time dependence of the distribution function $\mathfrak{g}_{\mathbf{k},\varepsilon}(t) = \mathfrak{g}_{\mathbf{k},\varepsilon} e^{|\alpha|t}$ which is consistent with out

boundary condition that $\mathbf{g}_{\mathbf{k},\varepsilon}(-\infty) = 0$, and finally it yields

$$(\Omega + i\mathbb{L}_k) \mathbf{g} = \mathfrak{L}, \quad \mathbb{L}_k = [\mathcal{H}_0(k), \quad]_- \quad (2.89)$$

and $\Omega = \alpha + \frac{1}{\tau}$. The left side can be understood as the fast relaxation into equilibrium which is mediated with the terms in right hand side as scattering and anisotropic deviation from local density distribution given by $\mathfrak{L}_{\mathbf{k},\varepsilon} = \mathfrak{L}_{\mathbf{k},\varepsilon}^{(0)} + \mathfrak{L}_{\mathbf{k},\varepsilon}^{(1)}$ where

$$\mathfrak{L}_{\mathbf{k},\varepsilon}^{(0)} = i\tau_k^{-1} (\mathbb{G}_{\mathbf{k}\varepsilon}^R \rho_\varepsilon - \rho_\varepsilon \mathbb{G}_{\mathbf{k}\varepsilon}^A), \quad (2.90)$$

$$\mathfrak{L}_{\mathbf{k}\varepsilon}^{(1)} = -\frac{vf}{2} [\sigma; \nabla_x \mathbf{g}_{\mathbf{k},\varepsilon}]_+. \quad (2.91)$$

The solution to the transport equation reads

$$\mathbf{g}_{\mathbf{k},\varepsilon} = \frac{1}{2\pi} \int dz' \mathbf{G}_{\mathbf{k}z'}^+ \mathfrak{L}_{\mathbf{k},\varepsilon} \mathbf{G}_{\mathbf{k}z'}^-, \quad (2.92)$$

with the matrix retarded and advanced Green's function given by [88, 89]

$$\mathbf{G}_{\mathbf{k}z'}^{(\pm)} = \frac{1}{z' - \mathcal{H}_0(k) \pm i\frac{\Omega}{2}} = \frac{1}{2} \left(\frac{1 + \sigma_{\hat{\mathbf{k}}}}{z' - \xi_k \pm i\frac{\Omega}{2}} + \frac{1 - \sigma_{\hat{\mathbf{k}}}}{z' + \xi_k \pm i\frac{\Omega}{2}} \right), \quad (2.93)$$

where $\sigma_{\hat{\mathbf{k}}} = \sigma \cdot \hat{\mathbf{k}}$. Therefore the solutions have two set of simple singularities two of them $z' = \pm \xi_k - i\frac{\Omega}{2}$ for the retarded function residing on the upper plane and the other two $z' = \pm \xi_k + i\frac{\Omega}{2}$ for the advanced function and lying on the lower plane. Computing the z' integral over either the upper or lower half plane consequently gives,

$$\mathbf{g}_{\mathbf{k},\varepsilon} = \zeta_1 \mathfrak{L}_{\mathbf{k},\varepsilon} + \zeta_2 [\sigma_{\hat{\mathbf{k}}}, \mathfrak{L}_{\mathbf{k},\varepsilon}]_- + \zeta_3 \sigma_{\hat{\mathbf{k}}} \mathfrak{L}_{\mathbf{k},\varepsilon} \sigma_{\hat{\mathbf{k}}} = \mathbb{D}[\mathfrak{L}_{\mathbf{k},\varepsilon}] \quad (2.94)$$

where

$$\zeta_1 = \frac{2\xi_k^2 + \Omega^2}{\Omega(4\xi_k^2 + \Omega^2)}, \quad \zeta_2 = \frac{-i\xi_k}{(4\xi_k^2 + \Omega^2)}, \quad \zeta_3 = \frac{2\xi_k^2}{\Omega(4\xi_k^2 + \Omega^2)}. \quad (2.95)$$

We can establish the different corrections by iteration and get

$$\mathbf{g}_{\mathbf{k}\varepsilon}^{(0)} = \mathbb{D}[\mathfrak{L}_{\mathbf{k},\varepsilon}^{(0)}(\rho)], \quad (2.96)$$

$$\mathbf{g}_{\mathbf{k}\varepsilon}^{(i)} = \mathbb{D}[\mathfrak{L}_{\mathbf{k},\varepsilon}^{(1)}(\mathbf{g}_{\mathbf{k}\varepsilon}^{(i-1)})], \quad i \geq 1, \quad (2.97)$$

hence up to the second order the perturbative solutions give (see the Appendix. C)

$$\mathbf{g}_{\mathbf{k}\varepsilon} = \mathbf{g}_{\mathbf{k}\varepsilon}^{(0)} + \mathbf{g}_{\mathbf{k}\varepsilon}^{(1)} + \mathbf{g}_{\mathbf{k}\varepsilon}^{(2)}. \quad (2.98)$$

Note that here we are interested in quasi stationary system where $\alpha\tau \ll 1$ hence $\Omega \approx \tau^{-1}$. This limit reflects that the relaxation due to the impurity scattering is such short that takes long time for the system to reach equilibrium which can happen in highly diffusive

systems. As it is clear this limit is favorable in studying the coupled dynamics of charge and spin. In the following we try to obtain a quantitative interpretation of charge and pseudo-spin transport in graphene.

Next we attempt to obtain explicit form of the solutions by parameterizing the density matrix as $\rho = n/2 + \sigma \cdot \mathbf{s} + \sigma_3 \mathbf{s}_3$. Substituting these results back into the kinetic equation in clean system limit where $\gamma = \varepsilon_F \tau \ll 1$ one obtains the set of diffusion equations describing the coupling charge and pseudo-spin dynamics (Appendix A), [87, 89–91],

$$D \tilde{\nabla}^2 n + v_F \tilde{\nabla} \cdot \mathbf{s} = 0, \quad (2.99)$$

$$D \tilde{\nabla}^2 \mathbf{s} + D_s \tilde{\nabla}(\tilde{\nabla} \cdot \mathbf{s}) + \frac{v_F}{2} \tilde{\nabla} n = \frac{\mathbf{s}}{\tau_s}, \quad (2.100)$$

$$D \tilde{\nabla}^2 s_z - \frac{\gamma}{1 + 4\gamma^2} \frac{v_F}{2} (\hat{\mathbf{z}} \times \tilde{\nabla}) \cdot \mathbf{s} = \frac{s_z}{\tau_s}, \quad (2.101)$$

where noting that τ and τ_s are charge and pseudo-spin relaxation times, respectively, and we defined

$$\tau_s = \frac{(1 + 4\gamma^2)^2}{\gamma^2} \tau, \quad D = \frac{v_F^2}{2} \tau, \quad D_s = \frac{v_F^2}{2} \tau_s. \quad (2.102)$$

The first equation gives the coupled diffusion of the charge and its compensation by the pseudospin polarization vector, whereas the second and third equations describe the diffusion, precession and relaxation of the in-plane and out of plane pseudospin components.

2.6. Pseudospin Edelstein effect

First, one notes that the charge and pseudo-spin relax differently to the equilibrium. According to the continuity equation, we have

$$\partial_t n + \nabla_{\mathbf{x}} \cdot \mathbf{J} = 0, \quad (2.103)$$

therefore we immediately read off from the third equation that

$$\mathbf{J} = v_F \mathbf{s} - D \nabla_{\mathbf{x}} n \quad (2.104)$$

For diffusion under field, the electric field can be coupled to equations via the condition [91]

$$\nabla_{\mathbf{x}} \rightarrow \nabla_{\mathbf{x}} - e \mathbf{E} \partial_{\varepsilon}, \quad (2.105)$$

and noting that the mean free path is $\ell = v_F \tau$, one obtains the Einstein relation that indicating that the charge in graphene is separated into a dynamical part due to the diffusion

and bias plus pseudospin charge, i.e.,

$$\mathbf{J}_{\text{charge}} = (-D \nabla_{\mathbf{x}} + e \mathbf{E} \frac{\ell}{2} \partial_{\epsilon}) n + v_F \mathbf{s}. \quad (2.106)$$

Note that the first term is dynamical since it is driven due to the external perturbation and charge imbalance. To understand this better, we use the unitary map that diagonalize the graphene Hamiltonian and write down the carrier distribution accordingly as

$$f(\mathbf{k}, \mathbf{x}) = n(\mathbf{k}, \mathbf{x}) \mathbf{1} + \tilde{\mathbf{v}}(\phi) \cdot \mathbf{s}(\mathbf{k}, \mathbf{x}), \quad (2.107)$$

where n is the scalar charge density, \mathbf{s} is the pseudospin part of the charge, $\tilde{\mathbf{v}}(\phi) = \tilde{\sigma} = U \sigma U^\dagger$, and note that

$$\tilde{\sigma}_x = \begin{pmatrix} \cos \phi & i \sin \phi e^{-i\phi} \\ -i \sin \phi e^{i\phi} & -\cos \phi \end{pmatrix}, \quad \tilde{\sigma}_y = \begin{pmatrix} \sin \phi & -i \cos \phi e^{-i\phi} \\ i \cos \phi e^{i\phi} & -\sin \phi \end{pmatrix}. \quad (2.108)$$

Now defining the general momentum resolved carrier distribution as

$$\rho(\mathbf{x}) = \int d\mathbf{k} (G^R f - f G^A), \quad (2.109)$$

and averaging over the random angle by noting that $\langle \tilde{\sigma}_x \rangle_\phi = \sigma_x$ and $\langle \tilde{\sigma}_y \rangle_\phi = \sigma_y$ one obtains

$$\rho(\mathbf{x}) = n(\mathbf{x}) \mathbf{1} + \sigma \cdot \mathbf{s}(\mathbf{x}). \quad (2.110)$$

This indicates that a part of the charge distribution that corresponds to the pseudospin is in fact the residue charge density which is driven by the band coherence near the Dirac points. One notes that if the band coherence is neglected or the Fermi energy is far from the Dirac point then this residue (pseudospin) charge will vanish.

We next solve the diffusion equations in a 1D graphene nanoribbon and find that depending on the degree of the polarization there will be pseudospin accumulation on the boundaries of the sample. The diffusion equations decouple for the y and z components of the pseudospin and give

$$D \partial_x^2 n + v_F \partial_x s^x = 0, \quad (2.111)$$

$$(D + D_s) \partial_x^2 s^x - \frac{s^x}{\tau_s} = -\frac{v_F}{2} \partial_x n, \quad (2.112)$$

$$(D + D_s) \partial_x^2 s^y - \frac{s^y}{\tau_s} = 0, \quad (2.113)$$

$$D \partial_x^2 s^z - \frac{s^z}{\tau_s} = -\frac{\gamma}{1 + 4\gamma^2} \frac{v_F}{2} \partial_x s^y. \quad (2.114)$$

The first equation is simply the continuity equation giving a formula for the current as

$$D\partial_x n + v_F s^x = I = \text{constant}. \quad (2.115)$$

The first term in this equation is the usual local charge accumulation whereas the second term is directly proportional to the distribution of the helicity states pseudospin in the x -direction and indicates the pseudospin magnetization. One notes that the relation is also time reversal invariant. Entering of the pseudospin magnetization into the current formula is rather an unusual contribution since one would assume that the pseudospin current (if considered to be nonmagnetic) to be present here as of the form $\partial_x s^x$ [89]. This suggests that injecting an electric current, as a result, can induce pseudospin density which alike the charge density will decay away from the contacts, but, besides, it also will generate pseudospin polarization: the pseudospin magnetoelectric effect. To see this, we first solve for $\partial_x n$ and plugging in the second equation to obtain

$$(D + D_s) \partial_x^2 s^x - \left(\frac{1}{\tau} + \frac{1}{\tau_s} \right) s^x = -\frac{I}{\ell} \quad (2.116)$$

and solving this gives

$$s^x(x) = \frac{I}{v_F} \left(\frac{\tau_s}{\tau + \tau_s} \right) + c_1 e^{\sqrt{\frac{2}{\tau\tau_s}} \frac{x}{v_F}} + c_2 e^{-\sqrt{\frac{2}{\tau\tau_s}} \frac{x}{v_F}}. \quad (2.117)$$

Next we assume a sample extended in x -direction with length L where the boundaries are at $x = \pm \frac{L}{2}$. We further suppose that there is a constant charge injection to the system from the left boundary such that

$$J \Big|_{x=\pm \frac{L}{2}} = I, \quad (2.118)$$

$$J_s^x \Big|_{x=-\frac{L}{2}} = \eta I, \quad (2.119)$$

$$J_s^x \Big|_{x=\frac{L}{2}} = 0 \quad (2.120)$$

where J_{s_x} is the pseudospin current and naturally we assume that on the first interface there is a polarization degree given by η whereas at the right interface the pseudospin finally decays and relaxes to zero [89, 92]. The solution finally gives

$$s^x(x) = \frac{I}{v_F} \left(\frac{\tau}{\tau + \tau_s} - \eta \frac{\sqrt{2\tau\tau_s}}{\tau} \frac{\cosh \sqrt{\frac{2}{\ell\ell_s}}(x - L/2)}{\sinh \sqrt{\frac{2}{\ell\ell_s}} L} \right). \quad (2.121)$$

Assuming that the relaxation time for charge and pseudospin happen at the same rate

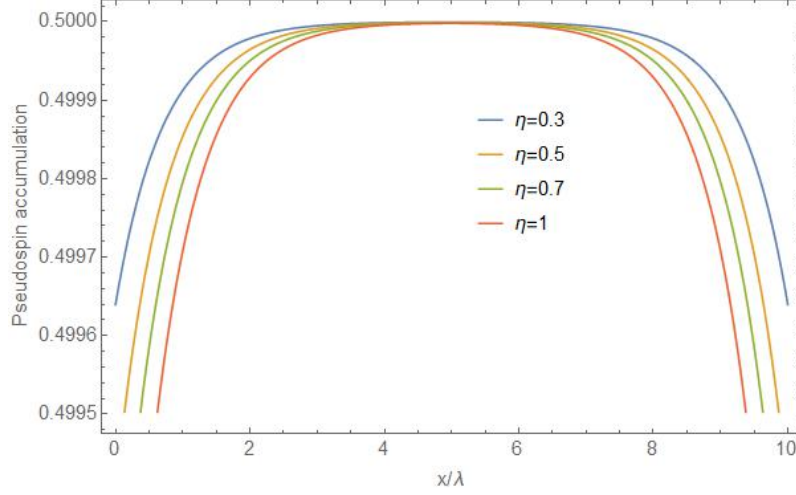


Figure 2.4: (Color online) Diffusion of the pseudospin accumulation (2.122) inside a graphene conductor along the x -direction plotted with the different degrees of polarization η . The decay rate follows a Gaussian pattern with spread peak as one expects from diffusion equation.

such that $\tau = \tau_s$ then we obtain

$$s^x(x) = \frac{I}{v_F} \left(\frac{1}{2} - \eta \sqrt{2} \frac{\cosh \frac{\sqrt{2}(x-L/2)}{\ell}}{\sinh \frac{\sqrt{2}L}{\ell}} \right). \quad (2.122)$$

Consequently we realize that the pseudospin accumulates at the boundaries and are given by

$$s^x(x = -L/2) = \frac{I}{v_F} \left(\frac{1}{2} - \eta \sqrt{2} \tanh \frac{\sqrt{2}L}{\ell} \right), \quad (2.123)$$

$$s^x(x = L/2) = \frac{I}{v_F} \left(\frac{1}{2} - \eta \frac{\sqrt{2}}{\sinh \frac{\sqrt{2}L}{\ell}} \right). \quad (2.124)$$

One furthermore observes that the equal interface accumulation of pseudospin happens at the ballistic regime where the size of the sample is comparable with the mean free path (Fig.2.5)

$$L = \frac{\ell}{\sqrt{2}} \cosh^{-1} \left(\frac{1 + \sqrt{5}}{2} \right) \approx 0.74 \ell. \quad (2.125)$$

To realize the symmetries of pure graphene hinders its technological and engineering applications. To overcome this obstacle, few approaches are presented to break the symmetries of graphene such as breaking the sublattice symmetry. The pseudospin symmetry breaking is thus favorable to realize the pseudospin magnetism in graphene.

Noting the current formula then the charge density gives

$$n(x) = \frac{I}{v_F} \left(\frac{2\tau}{\tau + \tau_f} \right) \frac{x}{\ell} - \frac{2}{\ell} \int dx s^x(x). \quad (2.126)$$

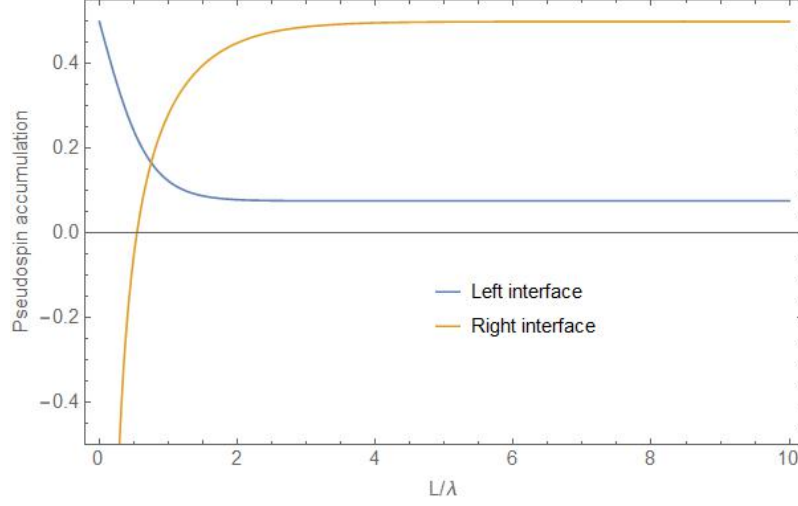


Figure 2.5: (Color online) Pseudospin accumulation in the right (2.124) and left (2.123) interface of a graphene nanoribbon with polarization degree $\eta = 0.3$. There is a critical length where the accumulation in both the interfaces are identical. Eventually the accumulation at the interfaces leak to the bulk and reach a constant value.

2.7. Conclusion

In summary, we illustrated that using a suitable local envelope function to describe the electronic structure in graphene gives rise to the novel effective interplay between the relevant degrees of freedom. These interactions are vital for the realization of spintronics and valleytronics devices that puts the many useful degrees of freedom of graphene into use as an alternative way of transporting information. These effective interactions are induced by external impurities. Hence impurities can be useful in improving the graphene device functionality. We demonstrated that the adsorption mechanism, by randomly depositing adatoms on top of the sublattice vertices, along with a short-range impurity model, that initiates the intervalley coupling, effectively bring about the interplay of the spin and valley degrees of freedom. Furthermore, we calculated the valley and spin relaxation rates and gave an analytical expression for them.

We provided a ground-up construction of the quantum transport equation using quantum Liouville's equation. We then applied the gradient approximation and then by integrating out the extra degrees of freedom obtained a real space quantum diffusion equation describing the coupled dynamics of charge and other degrees of freedom in graphene. In graphene, we illustrated that to explore the charge transport one has to consider the charge pseudospin degrees of freedom as well. The pseudospin polarization effectively dictates that upon applying electric current graphene can be pseudospin magnetized.

Chapter 3

ANOMALOUS TRANSPORT IN WEYL SEMIMETALS

3.1. Introduction

Dirac and Weyl semimetals (WSM) are members of materials with topological properties. They are intermediate phases between a trivial insulator and a topological insulator. Both of these materials can be taught as the three dimensional version of graphene in the sense that they obey the three dimensional Dirac/Weyl equation. Dirac semimetals (DSM) have been predicted to occur in band inversion crystals with strong spin orbit coupling in the presence of space inversion and time reversal symmetries. As a result, the valance and conduction bands cross at discrete points in the Brillouin zone forming the gapless modes at the bulk Fermi surface, giving rise to a semimetallic feature [93–96].

The presence of both the time reversal and inversion symmetries in DSMs naturally result in degenerate Dirac nodes [94]. Another topological phase may appear if one or two of these symmetries are broken, giving rise to non degenerate Weyl semimetallic phase [97–100], where the cones which were degenerate in the Dirac phase get separated in the Weyl phase. Each cone has definite handedness, which protects against gapping out as the only way to get chiral fermions out is to pair them with the opposite chirality. Crystals featuring WSM phases, contrary to other types of Dirac matter, [98, 101, 102] have unique topological features in addition to the Weyl nodes [98, 103, 104]. These nodes are connected only at the boundary of the crystal via a peculiar half loop surface states known as the Fermi arcs [102, 105–108]. The notion of chirality is a feature of the Weyl equation (the massless version of Dirac equation) which, according to the fermion doubling theorem, predicts that the massless solutions (Weyl fermions) always come in pairs each with definite helicity [103, 109]. For isotropic Weyl cones, the helicity is specified by the operator

$$\chi = \boldsymbol{\sigma} \cdot \hat{\mathbf{p}},$$

where $\boldsymbol{\sigma}$ and $\hat{\mathbf{p}}$ are the spin and momentum direction vectors of the particle, respectively.

In this study, we consider WSM with broken time reversal and inversion symmetry, where the bands touch at two points in the Brillouin zone. Here each Weyl node carries opposite chirality as the *source* and *sink* of the Berry flux [110].

WSM phase has been the object of recent attention because of the unique band structure featuring chiral fermions. The most important characteristic associated with the chiral fermions is the existence of quantum anomalies [111]. Therefore the discovery of WSM allows the realization of quantum anomalies associated with the Weyl fermions such as chiral anomaly and chiral magnetic effect in the crystal lattice[112–116].

When both the time reversal (by applying a magnetic field \mathbf{B}) and inversion symmetries are broken, as we will show in this chapter, the separate Weyl nodes cross at different energies. Application of an electric field \mathbf{E} causes the constant pump of charge between the nodes indicating the nonequilibrium feature of chiral transport [117–119]. This axial current is larger when the electric field is locked parallel to the magnetic field and vanishes when the fields are perpendicular [120].

To better understand the chiral kinetics, we first develop a quantum transport equation for Weyl Hamiltonian in the presence of electromagnetic fields. In the next section, we present our main finding which is the systematic derivation of the effective equations of motion through the band projection. Then using the transport equation model and obtaining the distributions function we compute the chiral current and clarify its microscopic origin. We finally illustrate that the chiral magnetic effect is directly linked to the flux of the Berry monopoles indicating a topological origin.

3.2. Nonabelian Boltzmann equation and $U(1)$ gauge fields

In this section we construct a general nonabelian (matrix) quantum transport model in the presence of electromagnetic fields to examine the chiral transport in Weyl systems we focus on a single Weyl cone, given by the Hamiltonian

$$H = v_F \mathbf{p} \cdot \boldsymbol{\sigma}, \quad (3.1)$$

where \mathbf{p} is the momentum vector in 3D and the Pauli matrices $\boldsymbol{\sigma} = (\sigma_x, \sigma_y, \sigma_z)$ operating in spin/orbital space. Including the electromagnetic field through minimal coupling into the Hamiltonian now the Liouville's equation in position basis gives

$$\begin{aligned} i\dot{\rho}(\mathbf{x}_1, \mathbf{x}_2) &= \int d\mathbf{x}' \left(\langle \mathbf{x}_1 | H | \mathbf{x}' \rangle \rho(\mathbf{x}', \mathbf{x}_2) - \rho(\mathbf{x}_1, \mathbf{x}') \langle \mathbf{x}' | H | \mathbf{x}_2 \rangle \right) \\ &= v_F \int d\mathbf{x}' \left(\langle \mathbf{x}_1 | \boldsymbol{\sigma} \cdot (\mathbf{p} - e\mathbf{A}) | \mathbf{x}' \rangle \rho(\mathbf{x}', \mathbf{x}_2) - \rho(\mathbf{x}_1, \mathbf{x}') \langle \mathbf{x}' | (\mathbf{p} - e\mathbf{A}) \cdot \boldsymbol{\sigma} | \mathbf{x}_2 \rangle \right) \end{aligned}$$

$$= v_F \left\{ \boldsymbol{\sigma} \cdot \left(-i \vec{\nabla}_{\mathbf{x}_1} - e \mathbf{A}(\mathbf{x}_1) \right) \rho(\mathbf{x}_1, \mathbf{x}_2) - \rho(\mathbf{x}_1, \mathbf{x}_2) \left(i \overleftarrow{\nabla}_{\mathbf{x}_2} - e \mathbf{A}(\mathbf{x}_2) \right) \cdot \boldsymbol{\sigma} \right\}. \quad (3.2)$$

Next we transform to the center of mass and relative coordinates system (x, r) :

$$\mathbf{x} = \frac{\mathbf{x}_1 + \mathbf{x}_2}{2}, \quad \mathbf{r} = \mathbf{x}_1 - \mathbf{x}_2. \quad (3.3)$$

Therefore, in terms of the new coordinate, we have

$$\mathbf{x}_{1(2)} = \mathbf{x} + (-)\frac{\mathbf{r}}{2}, \quad \nabla_{\mathbf{x}_{1(2)}} = \frac{1}{2}\nabla_{\mathbf{x}} + (-)\nabla_{\mathbf{r}}. \quad (3.4)$$

Now, assuming slowly varying fields and Taylor expansion in terms of the relative distance \mathbf{r} , we obtain the following formula for the vector potential:

$$\mathbf{A}(\mathbf{x}_1) \approx \mathbf{A}(\mathbf{x}) + \frac{1}{2}(\mathbf{r} \cdot \nabla_{\mathbf{x}})\mathbf{A}, \quad \mathbf{A}(\mathbf{x}_2) \approx \mathbf{A}(\mathbf{x}) - \frac{1}{2}(\mathbf{r} \cdot \nabla_{\mathbf{x}})\mathbf{A}. \quad (3.5)$$

For the kinetic momentum we obtain

$$-i\nabla_{\mathbf{x}_1} - e\mathbf{A}(\mathbf{x}_1) = -\frac{i}{2}\nabla_{\mathbf{x}} - i\nabla_{\mathbf{r}} - e\mathbf{A} - \frac{e}{2}(\mathbf{r} \cdot \nabla_{\mathbf{x}})\mathbf{A}, \quad (3.6)$$

$$i\nabla_{\mathbf{x}_2} - e\mathbf{A}(\mathbf{x}_2) = \frac{i}{2}\nabla_{\mathbf{x}} - i\nabla_{\mathbf{r}} - e\mathbf{A} + \frac{e}{2}(\mathbf{r} \cdot \nabla_{\mathbf{x}})\mathbf{A}, \quad (3.7)$$

and the Liouville's equation becomes

$$i\dot{\rho}(\mathbf{r}, \mathbf{x}) = v_F \left\{ \boldsymbol{\sigma} \cdot \left[-\frac{i}{2}\nabla_{\mathbf{x}} - i\nabla_{\mathbf{r}} - e\mathbf{A} - \frac{e}{2}(\mathbf{r} \cdot \nabla_{\mathbf{x}})\mathbf{A} \right] \rho(\mathbf{r}, \mathbf{x}) - \left[\frac{i}{2}\nabla_{\mathbf{x}} - i\nabla_{\mathbf{r}} - e\mathbf{A} + \frac{e}{2}(\mathbf{r} \cdot \nabla_{\mathbf{x}})\mathbf{A} \right] \rho(\mathbf{r}, \mathbf{x}) \cdot \boldsymbol{\sigma} \right\}. \quad (3.8)$$

Next, we perform the Wigner transform of the kinetic equation. The Wigner transformation in the presence of gauge field is given by

$$f(\mathbf{x}, \mathbf{p}) = \int d\mathbf{r} e^{-i(\mathbf{p}+e\mathbf{A})\cdot\mathbf{r}} \rho(\mathbf{r}, \mathbf{x}). \quad (3.9)$$

Applying this transformation to the left hand side and performing the integrals gives

$$\begin{aligned} LHS &= \int d\mathbf{r} e^{-i(\mathbf{p}+e\mathbf{A})\cdot\mathbf{r}} \dot{\rho} = \int d\mathbf{r} \left(\partial_t (e^{-i(\mathbf{p}+e\mathbf{A})\cdot\mathbf{r}} \rho) - ie \mathbf{r} \cdot \dot{\mathbf{A}} e^{-i(\mathbf{p}+e\mathbf{A})\cdot\mathbf{r}} \rho \right) \\ &= (\partial_t - e \mathbf{E} \cdot \nabla_{\mathbf{p}}) f(\mathbf{x}, \mathbf{p}), \end{aligned} \quad (3.10)$$

where $\mathbf{E} = -\dot{\mathbf{A}}$. The right hand side likewise can be cast into the form

$$\begin{aligned} RHS &= \int d\mathbf{r} e^{-i(\mathbf{p}+e\mathbf{A})\cdot\mathbf{r}} \left(\mp \frac{i}{2}\nabla_{\mathbf{x}} - i\nabla_{\mathbf{r}} - e\mathbf{A} \mp \frac{e}{2}(\mathbf{r} \cdot \nabla_{\mathbf{x}})\mathbf{A} \right) \rho(\mathbf{r}, \mathbf{x}), \\ &= \mp \frac{i}{2}\nabla_{\mathbf{x}} f(\mathbf{x}, \mathbf{p}) + \mathbf{p} f(\mathbf{x}, \mathbf{p}) \pm i \frac{e}{2} \mathbf{B} \times \nabla_{\mathbf{p}} f(\mathbf{x}, \mathbf{p}), \end{aligned} \quad (3.11)$$

where we have used

$$e^{-i(\mathbf{p}+e\mathbf{A})\cdot\mathbf{r}} \nabla_{\mathbf{r}}\rho = \nabla_{\mathbf{r}}\left(e^{-i(\mathbf{p}-e\mathbf{A})\cdot\mathbf{r}}\rho\right) + i(\mathbf{p} + e\mathbf{A})e^{-i(\mathbf{p}+e\mathbf{A})\cdot\mathbf{r}} \rho, \quad (3.12)$$

$$e^{-i(\mathbf{p}+e\mathbf{A})\cdot\mathbf{r}} \nabla_{\mathbf{x}}\rho = \nabla_{\mathbf{x}}\left(e^{-i(\mathbf{p}-e\mathbf{A})\cdot\mathbf{r}}\rho\right) + ie \nabla_{\mathbf{x}}(\mathbf{r} \cdot \mathbf{A})e^{-i(\mathbf{p}+e\mathbf{A})\cdot\mathbf{r}} \rho, \quad (3.13)$$

and

$$\int d\mathbf{r} e^{-i(\mathbf{p}+e\mathbf{A})\cdot\mathbf{r}} \nabla_{\mathbf{x}}\rho = i(\mathbf{p} + e\mathbf{A})f(\mathbf{x}, \mathbf{p}), \quad (3.14)$$

$$\int d\mathbf{r} e^{-i(\mathbf{p}+e\mathbf{A})\cdot\mathbf{r}} \nabla_{\mathbf{x}}\rho = \nabla_{\mathbf{x}}f(\mathbf{x}, \mathbf{p}) + ie \int d\mathbf{r} \nabla_{\mathbf{x}}(\mathbf{r} \cdot \mathbf{A})e^{-i(\mathbf{p}+e\mathbf{A})\cdot\mathbf{r}} \rho, \quad (3.15)$$

and finally we reach to the collisionless gauge invariant transport equation

$$\partial_t f - \frac{e}{2}[(\mathbf{E} + v_F \boldsymbol{\sigma} \times \mathbf{B}), \nabla_{\mathbf{p}}f]_+ + \frac{v_F}{2}[\sigma, \nabla_{\mathbf{x}}f]_+ + i[H, f]_- = 0. \quad (3.16)$$

One observes that excluding the last term, which indicates the quantum corrections, and ignoring the nonabelian feature of this equation, by considering the distributions as functions not matrices, one arrives at the standard semiclassical Boltzmann equation for the one band model. The quantum coherence term $i[H, f]_-$, which can be interpreted as the precession of the spin (or other degrees of freedom associated with the two band) due to the momentum space pseudo-magnetic field, is the imprint of the quantum Liouville's equation which is our starting point [121, 122]. To describe the electronic structure of a multi-band system, the system is usually reduced into an effective model with less bands by band projection [123–125]. Adopting this point of view in the Matrix kinetic equation leads to an equivalent transport description written effectively in terms of the band diagonal Hamiltonian. In the following we explicitly carry out the reduction of the matrix kinetic equation (3.16) and demonstrate the connection between the effective equation of motion and the Berry curvature.

3.3. Non-abelian $SU(2)$ gauge, band projection and Berry curvature

The main object of interest in the quantum Boltzmann equation is the single particle distribution (matrix) function. The matrix distribution has diagonal and off-diagonal parts denoting the contributions of the quantum intraband and interband interference effects respectively. To elucidate the physical picture of transport in a multiband system it is customary to derive an effective equation by projecting the original equation into the energy eigenbasis and applying the gradient approximation [123, 124].

The transport equation can be simplified using a unitary transformation that diagonal-

ize the Hamiltonian (3.1) such that

$$U H U^\dagger = H_d = v_F |p| \sigma_z, \quad (3.17)$$

where by solving the eigenvalue problem, one directly finds that the transformation reads

$$U = e^{i\frac{\pi}{2} \boldsymbol{\sigma} \cdot \hat{\mathbf{p}}_\perp} = \frac{1}{\sqrt{2}} \begin{pmatrix} 1 & e^{-i\phi} \\ 1 & -e^{-i\phi} \end{pmatrix}, \quad \mathbf{p}_\perp = \mathbf{p} \times \hat{\mathbf{z}}. \quad (3.18)$$

with $\phi = \tan^{-1}(k_y/k_x)$. Moreover this unitary transformation is momentum dependent (local gauge), therefore it will naturally induce a covariant derivative

$$\nabla_{\mathbf{p}} \longrightarrow \mathbb{D}_{\mathbf{p}} = \nabla_{\mathbf{p}} - i[\mathbb{A}, \quad]_-, \quad \mathbb{A} = iU \nabla_{\mathbf{p}} U^\dagger = \nabla_{\mathbf{p}} \phi (I - \sigma_x). \quad (3.19)$$

Note that vector $\mathbb{A} = (\mathbb{A}_x, \mathbb{A}_y, \mathbb{A}_z)$ is a pure nonabelian $SU(2)$ gauge potential in momentum space with null field strength,

$$\begin{aligned} F_{\mu\nu} &= \partial_\mu \mathbb{A}_\nu - \partial_\nu \mathbb{A}_\mu - i[\mathbb{A}_\mu, \mathbb{A}_\nu]_-, \\ &= i\partial_\mu (U \partial_\nu U^\dagger) - i\partial_\nu (U \partial_\mu U^\dagger) + iU \partial_\mu U^\dagger U \partial_\nu U^\dagger - iU \partial_\nu U^\dagger U \partial_\mu U^\dagger \\ &= i(\partial_\mu U)(\partial_\nu U^\dagger) + iU \partial_{\mu\nu} U^\dagger - i(\partial_\nu U)(\partial_\mu U^\dagger) - iU \partial_{\nu\mu} U^\dagger + iU \partial_\mu U^\dagger U \partial_\nu U^\dagger \\ &\quad - iU \partial_\nu U^\dagger U \partial_\mu U^\dagger, \\ &= 0, \end{aligned} \quad (3.20)$$

indicating that this pure gauge potential has no physical force effect on our system and we have

$$i[\mathbb{A}_\mu, \mathbb{A}_\nu]_- = \partial_\mu \mathbb{A}_\nu - \partial_\nu \mathbb{A}_\mu. \quad (3.21)$$

The transformation also affects the velocity $\mathbf{v} = \nabla_{\mathbf{p}} H$, and results

$$\begin{aligned} \mathbf{v} &= U \nabla_{\mathbf{p}} H U^\dagger, \\ &= \nabla_{\mathbf{p}} H_d + i[\mathbb{A}, H_d]_- = \mathbb{D}_{\mathbf{p}} H_d. \end{aligned} \quad (3.22)$$

The covariant matrix velocity on the other hand can be rewritten as

$$\mathbf{v} = v_F \mathbf{p} + 2v_F \nabla_{\mathbf{p}} \phi \sigma_y, \quad (3.23)$$

where the first part is the orbital velocity of the particle in the band, while second term is the contribution due to the gauge (Berry) connection.

After applying the local gauge transformation (3.18) into the transport equation (3.16),

and considering a stationary and homogeneous system, the transport equation becomes

$$\partial_t f + \frac{1}{2}[\dot{\mathbf{p}}, \mathbb{D}_{\mathbf{p}} f]_+ + \frac{1}{2}[\mathbf{v}, \nabla_{\mathbf{x}} f]_+ + i[H_d, f]_- = 0, \quad (3.24)$$

where the velocity and force matrices are given by

$$\mathbf{v} = v_F U \boldsymbol{\sigma} U^\dagger = v_F(\sigma_z \mathbf{p} + ip[\mathbb{A}, \sigma_z]_-), \quad (3.25)$$

$$\dot{\mathbf{p}} = -e \mathbf{E} - e \mathbf{v} \times \mathbf{B}. \quad (3.26)$$

In order to obtain an effective single band transport equation, we first express the quantum coherence term (the commutator) as

$$[H_d, f]_- = \mathbb{F} = i\partial_t f + \frac{i}{2}[\dot{\mathbf{p}}, \mathbb{D}_{\mathbf{p}} f]_+ + \frac{i}{2}[\mathbf{v}, \nabla_{\mathbf{x}} f]_+, \quad (3.27)$$

where, we assume the gradient terms only add corrections to the solution of the kinetic equation. Next we apply the band projection scheme by first separating the coherence term into band diagonal and off-diagonal equations. The diagonal equation clearly will depend on the band diagonal (intraband) and off-diagonal (interband) distribution functions, f^α and $f^{\alpha\alpha'}$, respectively. Using the gradient expansion, and by note that $f^\alpha \gg f^{\alpha\alpha'}$, we then express the diagonal equation in terms of functional of the intraband distributions and write

$$\begin{aligned} [H_d^\alpha, f^\alpha]_- &= \mathbb{F}_\alpha(f^\alpha, f^{\bar{\alpha}}, f^{\alpha\bar{\alpha}}) \\ &= \mathbb{F}_\alpha^{(1)}(f^\alpha) + \mathbb{F}_\alpha^{(2)}(f^{\alpha\bar{\alpha}}[f^\alpha]) + \mathbb{F}_\alpha^{(3)}(f^{\bar{\alpha}}[f^\alpha]) + \dots \end{aligned} \quad (3.28)$$

The first and dominant correction to the coherence term, we indicate it by $\mathbb{F}_\alpha^{(1)}$, is a functional of the intraband distributions. In the second and the third iterations we select the terms $\mathbb{F}_\alpha^{(2)}$ and $\mathbb{F}_\alpha^{(3)}$ that depend on the interband and the opposite-band distributions. We find that

$$\mathbb{F}_\alpha[f^\alpha] = i\partial_t f^\alpha + i\dot{\mathbf{p}}_i^\alpha \partial_{p_i} f^\alpha + i\mathbf{v}_i^\alpha \partial_{x_i} f^\alpha + \frac{1}{2}(\dot{\mathbf{p}}_i^{\alpha\bar{\alpha}} \mathbb{A}_i^{\bar{\alpha}\alpha} - \dot{\mathbf{p}}_i^{\bar{\alpha}\alpha} \mathbb{A}_i^{\alpha\bar{\alpha}})f^\alpha, \quad (3.29)$$

$$\begin{aligned} \mathbb{F}_\alpha[f^{\alpha\bar{\alpha}}, f^{\bar{\alpha}\alpha}] &= \frac{i}{2}(\dot{\mathbf{p}}_i^{\alpha\bar{\alpha}} \partial_{p_i} f^{\bar{\alpha}\alpha} + \dot{\mathbf{p}}_i^{\bar{\alpha}\alpha} \partial_{p_i} f^{\alpha\bar{\alpha}}) + \frac{i}{2}(\mathbf{v}_i^{\alpha\bar{\alpha}} \partial_{x_i} f^{\bar{\alpha}\alpha} + \mathbf{v}_i^{\bar{\alpha}\alpha} \partial_{x_i} f^{\alpha\bar{\alpha}}) \\ &\quad + \dot{\mathbf{p}}_i^\alpha (\mathbb{A}_i^{\alpha\bar{\alpha}} f^{\bar{\alpha}\alpha} - \mathbb{A}_i^{\bar{\alpha}\alpha} f^{\alpha\bar{\alpha}}) + \frac{1}{2}(\mathbb{A}_i^{\bar{\alpha}} - \mathbb{A}_i^\alpha)(\dot{\mathbf{p}}_i^{\alpha\bar{\alpha}} f^{\bar{\alpha}\alpha} + \dot{\mathbf{p}}_i^{\bar{\alpha}\alpha} f^{\alpha\bar{\alpha}}), \end{aligned} \quad (3.30)$$

$$\mathbb{F}_\alpha[f^{\bar{\alpha}}] = \frac{1}{2}(\mathbb{A}_i^{\alpha\bar{\alpha}} \dot{\mathbf{p}}_i^{\bar{\alpha}\alpha} - \dot{\mathbf{p}}_i^{\alpha\bar{\alpha}} \mathbb{A}_i^{\bar{\alpha}\alpha})f^{\bar{\alpha}}. \quad (3.31)$$

We also express the second and the third iterations as a functional of the intraband distribution by using the band off-diagonal matrix equation (3.27) which contains both the

interband and intraband distributions as well and gives

$$[H_d, f]_-^{\alpha\bar{\alpha}} = \mathbb{F}_{\alpha\bar{\alpha}}(f^\alpha, f^{\bar{\alpha}}, f^{\alpha\bar{\alpha}}). \quad (3.32)$$

The right hand side reads

$$\begin{aligned} \mathbb{F}_{\alpha\bar{\alpha}}(f^\alpha, f^{\bar{\alpha}}, f^{\alpha\bar{\alpha}}) &= \frac{i}{2}(\dot{\mathbf{p}}_i^{\alpha\bar{\alpha}} \partial_{p_i} f^\alpha + \mathbf{v}_i^{\alpha\bar{\alpha}} \partial_{x_i} f^\alpha) - \frac{1}{2}(\dot{\mathbf{p}}_i^\alpha + \dot{\mathbf{p}}_i^{\bar{\alpha}}) \mathcal{A}_i^{\alpha\bar{\alpha}} f^\alpha + i \partial_t f^{\alpha\bar{\alpha}} \\ &\quad + \frac{i}{2}(\dot{\mathbf{p}}_i^\alpha + \dot{\mathbf{p}}_i^{\bar{\alpha}}) [\partial_{p_i} f^{\alpha\bar{\alpha}} - i(\mathbb{A}_i^\alpha - \mathbb{A}_i^{\bar{\alpha}}) f^{\alpha\bar{\alpha}}] + \frac{i}{2}(\mathbf{v}_i^\alpha + \mathbf{v}_i^{\bar{\alpha}}) \partial_{x_i} f^{\alpha\bar{\alpha}} \\ &\quad + \frac{1}{2}(\dot{\mathbf{p}}_i^\alpha + \dot{\mathbf{p}}_i^{\bar{\alpha}}) \mathbb{A}_i^{\alpha\bar{\alpha}} f^{\bar{\alpha}} + \frac{i}{2}(\dot{\mathbf{p}}_i^{\alpha\bar{\alpha}} \partial_{p_i} f^{\bar{\alpha}} + \mathbf{v}_i^{\alpha\bar{\alpha}} \partial_{x_i} f^{\bar{\alpha}}), \end{aligned} \quad (3.33)$$

there we used the fact that the diagonal and off-diagonal elements of the covariant derivative are

$$(\mathbb{D}_{\mathbf{p}} f)^\alpha = \nabla_{\mathbf{p}} f^\alpha - i(\mathbb{A}^{\alpha\bar{\alpha}} f^{\bar{\alpha}\alpha} - f^{\alpha\bar{\alpha}} \mathbb{A}^{\bar{\alpha}\alpha}), \quad (3.34)$$

$$(\mathbb{D}_{\mathbf{p}} f)^{\alpha\bar{\alpha}} = \nabla_{\mathbf{p}} f^{\alpha\bar{\alpha}} - i(\mathbb{A}^{\alpha\bar{\alpha}} f^{\bar{\alpha}} - f^\alpha \mathbb{A}^{\alpha\bar{\alpha}}) - i(\mathbb{A}^\alpha f^{\alpha\bar{\alpha}} - f^{\alpha\bar{\alpha}} \mathbb{A}^{\bar{\alpha}}). \quad (3.35)$$

In order to express the second and third iterations as functional of the only intraband distribution, we first need to solve the (3.32). Considering the contributions from intraband distribution functions yields

$$H_d^\alpha f^{\alpha\bar{\alpha}} - f^{\alpha\bar{\alpha}} H_d^{\bar{\alpha}} = \mathbb{F}_{\alpha\bar{\alpha}}(f^\alpha, f^{\bar{\alpha}} = 0, f^{\alpha\bar{\alpha}} = 0), \quad (3.36)$$

which gives

$$f^{\alpha\bar{\alpha}} = \mathbb{F}_{\alpha\bar{\alpha}}(f^\alpha) (H_d^\alpha - H_d^{\bar{\alpha}})^{-1}, \quad f^{\bar{\alpha}\alpha} = (f^{\alpha\bar{\alpha}})^\dagger = (H_d^{\bar{\alpha}} - H_d^\alpha)^{-1} \mathbb{F}_{\bar{\alpha}\alpha}(f^\alpha). \quad (3.37)$$

Now defining the energy distance between opposite bands as $\Delta_p = \mathcal{H}_d^\alpha - \mathcal{H}_d^{\bar{\alpha}}$ we find that

$$\begin{aligned} f^{\alpha\bar{\alpha}}[f^\alpha] &= \frac{i}{2} \Delta_p^{-1} \left(\dot{\mathbf{p}}_i^{\alpha\bar{\alpha}} \partial_{p_i} + \mathbf{v}_i^{\alpha\bar{\alpha}} \partial_{x_i} + i(\dot{\mathbf{p}}_i^\alpha + \dot{\mathbf{p}}_i^{\bar{\alpha}}) \mathcal{A}_i^{\alpha\bar{\alpha}} \right) f^\alpha, \\ &= -\frac{e}{2} \mathbb{A}^{\alpha\bar{\alpha}} \times \mathbf{B} \cdot \nabla_{\mathbf{p}} f^\alpha - \frac{1}{2} \mathbb{A}^{\alpha\bar{\alpha}} \cdot \nabla_{\mathbf{x}} f^\alpha - \frac{e}{\Delta_p} \mathbf{E} \cdot \mathbb{A}^{\alpha\bar{\alpha}} f^\alpha. \end{aligned} \quad (3.38)$$

Furthermore, noting (3.25), we use the following relations,

$$\dot{\mathbf{p}}^{\alpha\bar{\alpha}} = -ie\Delta_p \mathbb{A}^{\alpha\bar{\alpha}} \times \mathbf{B}, \quad (3.39)$$

$$\mathbf{v}^{\alpha\bar{\alpha}} = -i\Delta_p \mathbb{A}^{\alpha\bar{\alpha}}, \quad (3.40)$$

$$\dot{\mathbf{p}}^\alpha = -e \mathbf{E} - ev_F \mathbf{p} \times \mathbf{B}, \quad (3.41)$$

$$\dot{\mathbf{p}}^{\bar{\alpha}} = -e \mathbf{E} + ev_F \mathbf{p} \times \mathbf{B}, \quad (3.42)$$

$$\mathbf{v}^\alpha = v_F \mathbf{p}, \quad (3.43)$$

$$\mathbf{v}^{\bar{\alpha}} = -v_F \mathbf{p}, \quad (3.44)$$

and express the second iteration as

$$\begin{aligned}
\mathbb{F}_\alpha^{(2)}[f^\alpha] &= \frac{i}{2}(\dot{\mathbf{p}}_i^{\alpha\bar{\alpha}}\partial_{p_i}f^{\bar{\alpha}\alpha} + \mathbf{v}_i^{\alpha\bar{\alpha}}\partial_{x_i}f^{\bar{\alpha}\alpha}) + \dot{\mathbf{p}}_i^\alpha\mathbb{A}_i^{\alpha\bar{\alpha}}f^{\bar{\alpha}\alpha} - h.c., \\
&= \frac{\Delta}{2}\left\{-\frac{e^2}{2}\varepsilon_{ij\ell}\varepsilon_{mnr}(\mathbb{A}_j^{\alpha\bar{\alpha}}\partial_{p_i}\mathbb{A}_m^{\bar{\alpha}\alpha} - h.c.)B_\ell B_n\partial_{p_q}f^\alpha\right. \\
&\quad -\frac{e}{2}\varepsilon_{ij\ell}(\mathbb{A}_j^{\alpha\bar{\alpha}}\partial_{p_i}\mathbb{A}_m^{\bar{\alpha}\alpha} - h.c.)B_\ell\partial_{x_m}f^\alpha - \frac{e^2}{\Delta}\varepsilon_{ij\ell}(\mathbb{A}_j^{\alpha\bar{\alpha}}\mathbb{A}_m^{\bar{\alpha}\alpha} - h.c.)B_\ell E_m\partial_{p_i}f^\alpha \\
&\quad \left.-\frac{e}{\Delta}(\mathbb{A}_i^{\alpha\bar{\alpha}}\mathbb{A}_m^{\bar{\alpha}\alpha} - h.c.)E_m\partial_{x_i}f^\alpha\right\} - (eE_i + e\varepsilon_{ij\ell}v_jB_\ell) \\
&\quad \times \left\{\frac{e}{2}\varepsilon_{mnq}(\mathbb{A}_i^{\alpha\bar{\alpha}}\mathbb{A}_m^{\bar{\alpha}\alpha} - h.c.)B_n\partial_{p_q}f^\alpha - \frac{1}{2}(\mathbb{A}_i^{\alpha\bar{\alpha}}\mathbb{A}_m^{\bar{\alpha}\alpha} - h.c.)\partial_{x_m}f^\alpha\right\}, \\
&= \frac{i\Delta}{2}\left\{-\frac{e^2}{2}\varepsilon_{ij\ell}\varepsilon_{mnq}\varepsilon_{jmr}B_\ell B_n\partial_{p_i}b_r\partial_{p_q}f^\alpha - \frac{e}{2}\varepsilon_{ij\ell}\varepsilon_{jmr}B_\ell\partial_{p_i}b_r\partial_{x_m}f^\alpha\right. \\
&\quad \left.-\frac{e^2}{\Delta}\varepsilon_{ij\ell}\varepsilon_{jmr}B_\ell E_m b_r\partial_{p_i}f^\alpha - \frac{e}{\Delta}\varepsilon_{imr}E_m b_r\partial_{x_i}f^\alpha\right\} + i(-eE_i - e\varepsilon_{ij\ell}v_jB_\ell) \\
&\quad \times \left(-\frac{e}{2}\varepsilon_{mnq}\varepsilon_{imr}B_n b_r\partial_{p_q}f^\alpha - \frac{1}{2}\varepsilon_{imr}\partial_{x_m}f^\alpha\right), \\
&= \frac{i\Delta}{2}\left(-\frac{e^2}{2}\mathbf{B} \times \nabla_p(\mathbf{B} \cdot \mathbf{b}) \cdot \nabla_p f^\alpha - \frac{e}{2}[(\nabla_p \cdot \mathbf{b})\nabla B - \nabla_p(\nabla B \cdot \mathbf{b})] \cdot \nabla_x f^\alpha\right. \\
&\quad \left.-\frac{e^2}{\Delta}\mathbf{B} \times (\mathbf{b} \times \mathbf{E}) \cdot \partial_p f^\alpha - \frac{e}{\Delta}\mathbf{E} \times \mathbf{b} \cdot \nabla_x f^\alpha\right) - \frac{ie^2}{2}\mathbf{B} \times (\mathbf{b} \times \mathbf{E}) \cdot \partial_p f^\alpha \\
&\quad - \frac{ie}{2}\mathbf{E} \cdot \mathbf{b} \cdot \nabla_x f^\alpha + \frac{ie^2}{2}(\mathbf{v} \times \mathbf{B})(\mathbf{b} \cdot \mathbf{B}) \cdot \nabla_p f^\alpha + \frac{ie}{2}\mathbf{b} \times (\mathbf{v} \times \mathbf{B}) \cdot \nabla_x f^\alpha,
\end{aligned}$$

where we have defined the nonabelian Berry curvature as

$$\partial_{p_i}\mathbb{A}_j^{\bar{\alpha}\alpha} - \partial_{p_j}\mathbb{A}_i^{\bar{\alpha}\alpha} = \mathbb{A}_i^{\alpha\bar{\alpha}}\mathbb{A}_j^{\bar{\alpha}\alpha} - \mathbb{A}_j^{\alpha\bar{\alpha}}\mathbb{A}_i^{\bar{\alpha}\alpha} = i\varepsilon_{ij\ell}b_\ell, \quad (3.45)$$

and its derivative

$$\partial_{p_r}(\mathbb{A}_i^{\alpha\bar{\alpha}}\mathbb{A}_j^{\bar{\alpha}\alpha} - \mathbb{A}_j^{\alpha\bar{\alpha}}\mathbb{A}_i^{\bar{\alpha}\alpha}) = i\varepsilon_{ij\ell}\partial_{p_r}b_\ell. \quad (3.46)$$

Now substituting this term back into the equation (3.28) finally we obtain an effective single band transport equation

$$\partial_t f + \dot{\mathbf{p}} \cdot \nabla_{\mathbf{p}} f + \dot{\mathbf{r}} \cdot \nabla_{\mathbf{r}} f = 0, \quad (3.47)$$

with the terms

$$\dot{\mathbf{p}} = \left(-e\mathbf{E} - e\mathbf{v} \times \mathbf{B} - \frac{e^2\Delta}{4}\nabla_{\mathbf{p}}(\mathbf{B} \cdot \mathbf{b}) \times \mathbf{B}\right) + e\left[(-e\mathbf{E} - \frac{e}{2}\mathbf{v} \times \mathbf{B}) \times \mathbf{b}\right] \times \mathbf{B},$$

$$\dot{\mathbf{r}} = \left(\mathbf{v} - \frac{e\Delta}{4}[(\nabla_{\mathbf{p}} \cdot \mathbf{b})\mathbf{B} - \nabla_{\mathbf{p}}(\mathbf{B} \cdot \mathbf{b})]\right) + (-e\mathbf{E} - \frac{e}{2}\mathbf{v} \times \mathbf{B}) \times \mathbf{b},$$

which can be arranged and cast into a familiar form as [115, 118],

$$\dot{\mathbf{r}} = \nabla_{\mathbf{p}} \bar{\varepsilon} + \dot{\mathbf{p}} \times \mathbf{b} = (1 + e \mathbf{b} \cdot \mathbf{B})^{-1} \left(\nabla_{\mathbf{p}} \bar{\varepsilon} + \mathbf{E} \times \mathbf{b} + e (\mathbf{b} \cdot \nabla_{\mathbf{p}} \bar{\varepsilon}) \mathbf{B} \right), \quad (3.48)$$

$$\dot{\mathbf{p}} = e \mathbf{E} + e \dot{\mathbf{r}} \times \mathbf{B} = (1 + e \mathbf{b} \cdot \mathbf{B})^{-1} \left(e \mathbf{E} + e \nabla_{\mathbf{p}} \bar{\varepsilon} \times \mathbf{B} + e^2 (\mathbf{B} \cdot \mathbf{E}) \mathbf{b} \right). \quad (3.49)$$

As it is clear from these equations of motion, there is a correction to the spectrum of Weyl fermions (Fig.3.1) due to the Berry curvature, namely, $\bar{\varepsilon} = \varepsilon + \delta\varepsilon = \varepsilon + m(\mathbf{b} \cdot \mathbf{B})$. Here, $m = \frac{e\Delta}{4}$ is the modified energy of the quasiparticles due to the internal Berry monopole associated with a Weyl nodes and \mathbf{b} is the field of a monopole [125–127]. Also note that the Berry curvature is the reflection of our local gauge analysis of the transport equation, as a result chiral imbalance (chiral anomaly) that is related to is a natural consequence of a chiral system [128, 129]. In the remaining of this chapter, we investigate the chiral

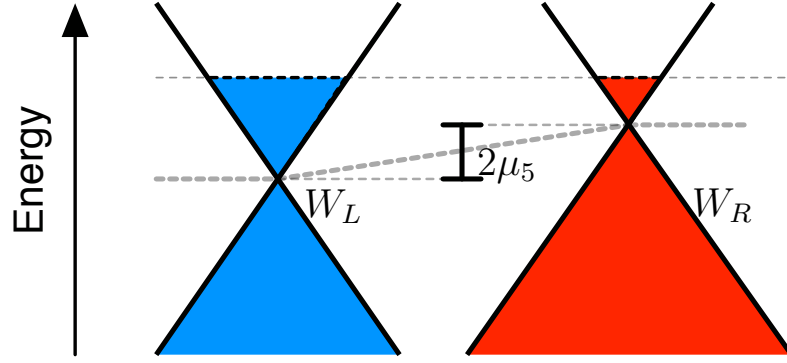


Figure 3.1: (Color online) The energy separation between the left and right Weyl nodes is due to the monopole fields \mathbf{b} (Berry curvature) where $\mu_5 = \frac{e\Delta}{4}(\mathbf{b} \cdot \mathbf{B})$ as given in the anomalous equations of motion. This generates the chemical imbalance between the two chiral fermions giving rise to the chiral anomaly.

anomaly and the chiral magnetic effect using the established kinetic model and anomalous equation of motion for the Weyl system.

3.4. Anomalous equations of motion

In a chiral fermionic system, the magnetic field induces the flow of charge current in the direction of the external electric field generating the chiral magnetic effect, when there is axial chemical potential due to the presence of Berry curvature [120, 130]. In a system with the time reversal and inversion symmetries the effect of the Berry curvature is zero, whereas in Weyl semimetal both the symmetries are broken and Berry curvature is nonzero in the vicinity of the Weyl points. In the previous section we demonstrated, from the kinetic equation point of view, that the Berry monopoles greatly affect the band

velocity of the fermions, and, not surprisingly, this picture also holds true in the wave packet dynamics as well [125]. In general for Weyl Hamiltonian the transport equation reduces to, [115, 118, 124],

$$\partial_t f^\alpha + \dot{\mathbf{r}}^\alpha \cdot \nabla_{\mathbf{x}} f^\alpha + \dot{\mathbf{p}}^\alpha \cdot \nabla_{\mathbf{p}} f^\alpha = - \frac{f^\alpha - f_0^\alpha}{\tau}, \quad (3.50)$$

where the anomalous equation of motion now are prescribed by the contributions from the Berry curvature field and giving

$$\dot{\mathbf{r}}^\alpha = \nabla_{\mathbf{p}} \varepsilon^\alpha + \dot{\mathbf{p}}^\alpha \times \mathbf{b}^\alpha, \quad (3.51)$$

$$\dot{\mathbf{p}}^\alpha = e \mathbf{E} + e \dot{\mathbf{r}}^\alpha \times \mathbf{B}. \quad (3.52)$$

In general the Wigner distribution function $f(\mathbf{x}, \mathbf{p})$ is written in the phase space coordinate, however, our motivation on using the kinetic equation perspective is the coarse grained modeling of chiral kinetics, and therefore we assume that the system under study (Weyl semimetal) is stationary and homogeneous [115, 118]. With these assumptions then the kinetic equation reads

$$\frac{e \mathbf{E} + e v_F \hat{\mathbf{p}} \times \mathbf{B} + e^2 (\mathbf{B} \cdot \mathbf{E}) \mathbf{b}}{1 + e \mathbf{b} \cdot \mathbf{B}} \cdot \nabla_{\mathbf{p}} f = - \frac{f - f_0}{\tau}. \quad (3.53)$$

In order to compute quantities one first need to obtain the distribution function by solving the above transport equation using Chapman-Enskog linearization scheme which ultimately yields

$$f = f^0 - \frac{e\tau}{1 + e \mathbf{b} \cdot \mathbf{B}} (\mathbf{E} + e (\mathbf{B} \cdot \mathbf{E}) \mathbf{b}) \cdot \mathbf{v} \frac{\partial f^0}{\partial \varepsilon}, \quad (3.54)$$

where the electron's band velocity is $\mathbf{v} = v_F \hat{\mathbf{p}}$.

As we discussed at length in Sec.2.4.2, on studying the magnetotransport in the framework of the Kinetic equation, the transport coefficients such as magnetoresistivity and magnetoconductivity are computed via applying the equation (2.73) for the distribution function. Including this result here we obtain the distribution function as

$$\delta f = - \frac{e\tau}{1 + e \mathbf{b} \cdot \mathbf{B} + \tau^2 \left(\frac{v_F^2}{\varepsilon}\right)^2 B^2} \left(\mathbf{E} + \tau \frac{v_F^2}{\varepsilon} \mathbf{B} \times \mathbf{E} + e (\mathbf{B} \cdot \mathbf{E}) \mathbf{b} \right) \cdot \mathbf{v} \frac{\partial f^0}{\partial \varepsilon} \quad (3.55)$$

where for Dirac dispersion we have $\frac{1}{m} = \frac{v_F^2}{\varepsilon}$ and $\mathbf{v} = v_F \hat{\mathbf{p}}$. The first term inside the parenthesis contributes to the dc current whereas the second term generates the Hall current. The third term is the chiral magnetic effect that induces the chiral anomaly.

Next, as an trivial exercise, neglecting the Hall effect one can compute the rate of the

chiral anomaly as

$$\begin{aligned} n_\chi &= \sum_{\mathbf{p}} \delta f(\mathbf{p}), \\ &= e\tau \int \frac{k^2 dk}{2\pi^2} \langle \mathbf{E} \cdot \mathbf{v} \rangle_\Omega \frac{\partial f^0}{\partial \varepsilon} + e^2 \tau (\mathbf{B} \cdot \mathbf{E}) \int \frac{dk}{2\pi^2} \langle \mathbf{b} \cdot \mathbf{v} \rangle_{\mathbf{S}} \frac{\partial f^0}{\partial \varepsilon}, \end{aligned} \quad (3.56)$$

and as a result we obtain

$$n_5 = \frac{e^2 \tau}{4\pi^2 v_F} (\mathbf{B} \cdot \mathbf{E}) \int d\varepsilon \frac{\partial f^0}{\partial \varepsilon}, \quad (3.57)$$

where $n_5 = n_{\chi=+1} - n_{\chi=-1}$ is the chiral imbalance between the two (left and right) Weyl nodes. The first integral in second line vanishes. Hence the non vanishing nonequilibrium charge accumulation (chiral anomaly) is proportional to $\mathbf{B} \cdot \mathbf{E}$ stems from the Berry curvature [115]. Note that

$$\langle \mathbf{b} \cdot \mathbf{v} \rangle_{\mathbf{S}} = \int \frac{k^2 d\Omega}{4\pi} (\mathbf{b} \cdot v_F \hat{\mathbf{p}}) = \frac{1}{4\pi} \oint \mathbf{b} \cdot d\mathbf{S} = \frac{v_F \chi}{2} \quad (3.58)$$

where χ is the quantized Berry flux (Chern number), $d\Omega = d(\cos \theta) d\phi$ is the infinitesimal solid angle and $d\mathbf{S} = k^2 d\Omega \hat{\mathbf{p}}$ is a spherical shell encompassing the monopole charge.

Noticing the energy separation of the Weyl nodes such that $\varepsilon_\tau = \varepsilon_0 + \tau m(\mathbf{b} \cdot \mathbf{B})$, where $m = \frac{e\Delta}{4}$, then the group velocity of the Weyl fermions are

$$\nabla_{\mathbf{p}} \varepsilon_\tau = \mathbf{v} + m \nabla_{\mathbf{p}} (\mathbf{B} \cdot \mathbf{B}). \quad (3.59)$$

Now to compute the current around a single node we write

$$\mathbf{J} = e \sum_{\mathbf{p}} (\mathbf{v} + em \nabla_{\mathbf{p}} (\mathbf{B} \cdot \mathbf{B})) \frac{-e\tau}{1 + e \mathbf{b} \cdot \mathbf{B}} (\mathbf{E} + e (\mathbf{B} \cdot \mathbf{E}) \mathbf{b}) \cdot \mathbf{v} \frac{\partial f^0}{\partial \varepsilon}. \quad (3.60)$$

The chiral magnetic effect is the current due to the magnetic field which will give

$$\begin{aligned} \mathbf{J}_{\text{CME}} &= e^4 \tau m (\mathbf{E} \cdot \mathbf{B}) \mathbf{B} \int \frac{k^2 dk d\Omega}{8\pi^3} (\mathbf{b} \cdot \mathbf{v}) \frac{\partial f^0}{\partial \varepsilon}, \\ &= \frac{e^2 m \chi}{2\pi^2} \left(\frac{e^2 \tau}{4\pi^2} (\mathbf{E} \cdot \mathbf{B}) \int d\varepsilon \frac{\partial f^0}{\partial \varepsilon} \right) \mathbf{B} \\ &= \frac{e^2 m n_5 \chi}{2\pi^2} \mathbf{B}, \end{aligned} \quad (3.61)$$

and the conductivity gives, [115, 116, 130],

$$\sigma_{\text{CME}} = \frac{e^4 \tau m}{8\pi^4} B^2. \quad (3.62)$$

These results that we are obtained from the microscopic standpoint, completely agree with other findings that are based on the different approaches [115, 116, 118].

3.5. Conclusion

We analyzed the kinetic theory of chiral systems, i.e, Weyl semimetal, in the presence of electromagnetic fields by constructing the Quantum Boltzmann equation. Applying a gauge transformation and the using band projection, we then arrived at an effective anomalous kinetic equation where the nonabelian gauge field (curvature) induces corrections in the equations of motion. We then computed the quantum anomalies such as chiral anomaly and chiral magnetic effect in the Weyl system. The transport equation approach to study anomalies in the Weyl system is a standard technique that yields as accurate results as with the conventional field theoretical methods. However, in this approach, as evidenced in the literature, the solution of the kinetic equation was not addressed [115, 118]. However, in our approach, we first solved the effective kinetic equation and obtained the distribution function for the chiral fermions. Using this solution we next computed the charge and the current and obtained the chiral anomaly and the charge current due to the magnetic field. The results for the anomaly related quantities that we obtained from this kinetic outlook, however, are in agreement with other approaches that are based on the field theoretical method.

Chapter 4

COVARIANT TRANSPORT IN TILTED CONES: PSEUDO-RELATIVITY AND LINEAR RESPONSE

4.1. Introduction

Condensed matter systems having Dirac-like linear energy dispersions proved to be a fertile ground to rediscover fundamental particles of nature. The Weyl semimetal (WSM) is a newly discovered phase of matter which hosts yet another emergent excitation of quantum field theory: a long-sought fundamental particle of nature first proposed in 1929 by Herman Weyl as a massless solution to the Dirac equation.[109] Crystals featuring WSM phases, contrary to other types of Dirac matter,[98, 101, 102] have unique topological features such as: the zero-energy excitations in the semimetallic bulk are associated with the chiral Weyl Fermions, having definite handedness near two distinct nodes,[98, 103, 104] whereas these nodes are connected only at the boundary of the crystal via a peculiar half loop surface states known as the Fermi arcs.[102, 105–108] These materials exhibit intriguing and distinct phenomena when exposed to electromagnetic fields, such as chiral anomaly, negative magnetoresistance, and the chiral magnetic effect.[131–133]

Dirac materials, possessing anisotropic and tilted energy cones, where the Fermi surface gains eccentricity and deviates from a standard circular shape, have been reported to exist in the two dimensional organic conductors α -(BEDT-TTF)₂I₃ subjected to pressure and uniaxial strain.[134–136] In these materials, the Dirac crossing occurs away from the high symmetry points of the Brillouin zone and their associated spectrum is modeled with a modified Dirac Hamiltonian. The presence of the tilt largely impacts the magneto-electronic and optical properties in these two-dimensional systems with tilted cones.[134, 136–138] Recently, another type of Weyl cone with no relativistic analog, due to the violation of Lorentz invariance, in transition-metal dichalcogenides hosting Weyl fermions has been reported.[106–108, 139–143] As compared to the abovementioned (moderately) tilted cones in so-called type-I WSMs, the cones are now “overtilted” such that the isoenergy lines are no longer closed ellipses but open hyperbolas. The search

for this new type of WSM, coined type II, is ongoing and some candidate materials have been predicted theoretically.[144–147]

Similar to two-dimensional systems, the tilt of the conical spectrum improves the transport qualities of three-dimensional WSMs by increasing the mobility and conductivity of the carriers. This strongly points out the better electronic and spintronic functionality of the tilted materials compared to other types of Dirac matter. For instance, the reported extremely large and non-saturating magnetoresistance, up to 450,000% in low field and $13 \times 10^6\%$ in high fields,[148–150] suggests a suitable magnetic memory and spintronics applications. Other peculiar properties of WSMs with tilted cone are the large conductivity of about $10^8 \Omega^{-1}\text{cm}^{-1}$ as well as an enlarged chiral anomaly [149, 151] whose origins remain yet unclear and need further theoretical investigation. As evidence to the significance of the Dirac cone tilting, the transport calculations[152–155] show that the anomalous Hall and thermal Hall conductivity, Berry curvature and density of states increase with tilt and peak around the critical tilt value, while optical absorption [156] shows no upper bound. Furthermore, the critical angle between the tilt and the magnetic field sets a threshold for the collapse of the Landau level formation and magnetic breakdown.[157–159]

A very distinct interpretation of tilted Dirac and Weyl systems come from a relativistic perspective where the tilt is identified as the rapidity of a specific Lorentz transformation.[136, 137] In the presence of external fields exploiting the Lorentz covariance, the tilt parameter becomes an essential variable in identifying a boosted frame where the fields transform trivially and this, in turn, facilitates the study of the problem at hand. [136, 160, 161] Besides this rich attribute, there is another motivation that appeals to the use of relativistic argumentation in describing the physics of the titled Weyl cone. The direct diagonalization of the Dirac equation in the presence of external fields is a cumbersome task, [162, 163] while by utilizing a relativistic picture and redefining the fields, this problem can be tackled easily.[136–138, 158, 164] This suggests the use of the covariant formalism that allows for a better understanding of the physics of the tilted Weyl cone phase.

In the present chapter, we address the electric transport properties of two- and three-dimensional Dirac systems and WSMs as a function of the tilt parameter. We show that a relativistic viewpoint in the form of a covariant Boltzmann equation allows for a quantitatively accurate description of the magnetoconductivity in the diffusive transport regime. The tilt in the electronic energy dispersion in the general Weyl Hamiltonian, characterized by the tilt velocity v_0 , is equivalent to drift velocity $v_{\text{drift}} = E/B$ under a suitable Lorentz transformation.[136–138] After obtaining expressions in the relativistically simplified picture where only the magnetic field is present, an inverse Lorentz boost recovers

the results in the original frame. Additionally, we demonstrate and elucidate how the DC conductivity increases in moderately tilted type-I WSM in terms of the tilting degree. This large enhancement, which is about 7 to 10 times larger than in standard WSMs without tilt, is the focal point of recent experimental debates concerning electronic transport in WSMs.[148, 149, 165] In order to demonstrate the validity of our approach in terms of the covariant Boltzmann equation, we perform conductivity calculations using the Kubo formula. As a result, we find that, apart from quantum corrections at energies close to the band-contact points, both approaches show a high quantitative agreement. The quantum corrections happen to be due to the interband coupling which is neglected in the Boltzmann equation;

The chapter is organized as follows. In Sec. 4.2 we discuss the basic construction of the manifestly covariant Boltzmann equation to study transport in the electron's co-moving frame of reference which is an inertial frame moving with a velocity equal to the electron's drift velocity relative to the laboratory frame of reference. In Sec. 4.3 we compute the conductivity of a two-dimensional anisotropic and tilted Dirac cone using the covariant Boltzmann equation as well as Kubo formula and compare the two results. In Sec. 4.4 we repeat the same calculation for a three-dimensional system of type I WSM having tilt in k_z -direction and compute the longitudinal and perpendicular (to the direction of the tilt) bulk conductivities using covariant Boltzmann formula as well as Kubo formula and then compare them. Furthermore, we provide a qualitative understanding of our findings for the conductivities by computing the tilt-induced renormalization of Fermi velocity, the density of states and Einstein's diffusion relation.

4.2. Covariant Boltzmann equation

Tilted Dirac cones in a magnetic field, in both 2D and 3D materials, can be elegantly described within a covariant formulation,[138, 160, 164] in which the tilt parameter is associated with an effective electric field.

In order to see this, consider first the minimal Dirac Hamiltonian, in which we omit the valley degree of freedom. Let us first consider the manifestly covariant situation with a non-tilted isotropic Dirac cone in three spatial dimensions. In this case, the covariant Dirac equation can be cast into the Schrödinger-type equation, in terms of the Pauli matrices $\sigma = (\sigma_x, \sigma_y, \sigma_z)$ and the 2×2 identity matrix $\mathbf{1}$,

$$(H - i\frac{\partial}{\partial t})|\psi\rangle = 0, \quad (4.1)$$

in terms of the Hamiltonian

$$H = v_F(\mathbf{k} - e \mathbf{A}) \cdot \boldsymbol{\sigma} + e\Phi_{\text{bias}}(\mathbf{r})\mathbf{1}, \quad (4.2)$$

where $\Phi_{\text{bias}}(\mathbf{r}) = -Ey$ is a static potential that we choose (arbitrarily) to give rise to an electric field in the y -direction, while \mathbf{A} is the vector potential that generates a homogeneous (and static) magnetic field in the z -direction, and $|\psi\rangle = \psi(v_F t, x, y, z)$. The Fermi velocity v_F plays the role of the speed of light and here, and in the remainder of this chapter, we use a system of units with $\hbar = 1$. For convenience, we consider the Landau gauge $\mathbf{A} = -yB \hat{x}$ with a vector potential to be oriented in the x -direction although the general arguments do not depend on this choice. While the Dirac equation is invariant under Lorentz transformations, it happens that it is convenient, for a quantum-mechanical solution, to use a Lorentz boost (in the x -direction) to a frame of reference, where the electric field vanishes, in which case we simply need to solve the Hamiltonian for a (charged) Weyl particle in a magnetic field and then transform the solution $\psi'(v_F t', x', y', z')$ in the co-moving frame of reference back to the lab frame, with $\psi'(v_F t', x', y', z') = S(\Lambda)\psi(v_F t, x, y, z)$. Notice that this transformation is only possible in the so-called *magnetic* regime, where the drift velocity $v_D = E/B$ is smaller than the Fermi velocity. It has been shown, both in the case of 2D [162] and 3D [160], that the convenient Lorentz transformations allow for a simple solution of the Hamiltonian (4.2), which agrees with the more cumbersome algebraic solution [163] in an arbitrary frame of reference, where the electric field does not vanish.

Interestingly, the same covariant trick can be used for a tilted Dirac or Weyl cone in the presence of a magnetic field. In this case, we need to add the term

$$v_0(k_x - eA_x)\mathbf{1}, \quad (4.3)$$

to our Hamiltonian (4.2), where we have considered the tilt to be in the x -direction, characterized by the velocity v_0 , which we choose to be smaller than v_F in order to remain in the regime of a type-I WSM. One immediately notices that the additional term conspires with the electric field in the y -direction, and one can indeed define a Hamiltonian

$$H - v_0 k_x \mathbf{1} = v_F(\mathbf{k} - e \mathbf{A}) \cdot \boldsymbol{\sigma} + e(\Phi_{\text{bias}} - \Phi_{\text{eff}})\mathbf{1}, \quad (4.4)$$

which has the same form as (4.2) in terms of the *effective* electric field $E_0 \stackrel{\text{def}}{=} v_0 B$ and thus $\Phi_{\text{eff}} = v_0 A_x = -E_0 y$. The new Hamiltonian is therefore also of covariant form and amenable to a Lorentz transformation, while the extra term $v_0 k_x \mathbf{1}$ remains diagonal in any frame of reference since k_x is a good quantum number in the Landau gauge. We,

therefore, use, for a convenient diagonalization of the Hamiltonian of tilted Dirac and Weyl cones, a Lorentz transformation to the co-moving frame of reference, with velocity v_0 in the x -direction, where $S(\Lambda) = \exp(\vartheta \sigma_x/2)$ and rapidity as $\eta = \tanh \vartheta = E_0/v_F B$, to make the effective electric field E_0 vanish.[136–138, 162, 164] In the new frame the Dirac equation reads

$$(H' - \varepsilon') e^{-\vartheta \sigma_x/2} |\psi\rangle = 0, \quad (4.5)$$

such that

$$\begin{aligned} H' &= S(\Lambda) (H - v_0 k_x \mathbf{1}) S(\Lambda) \\ &= v_F (\mathbf{k}' - e \mathbf{A}') \cdot \boldsymbol{\sigma} + e \Phi'_{\text{bias}}(\mathbf{r}) \mathbf{1}, \end{aligned} \quad (4.6)$$

where \mathbf{A}' and \mathbf{k}' are the corresponding vector potential and momentum vector in the co-moving frame and $\varepsilon' = \gamma \varepsilon$ (for more details, see the appendix).[138, 160] One notices that the spectrum in both the frames are related, i.e. $\varepsilon(E_0, B) - v_0 k_x \equiv \sqrt{1 - \eta^2} [\varepsilon'(B', E'_0 = 0)]$. [138, 160] This, finally, indicates that the spectrum of a tilted system equivalently can be obtained by first solving the system in a simplified boosted frame and then restoring into the original frame by applying an appropriate representation of the inverse Lorentz transformation.

The tilt term $v_0 k_x \mathbf{1}$ in the Hamiltonian (4.4) renormalizes the scattering time of the carriers, $\tau^{-1} = \sum_{\mathbf{k}} |V_{\text{imp}}|^2 \delta(H - \varepsilon_F)$. The anisotropy of the spectrum redefines the Fermi velocity[136] (see Sec. 4.4.3 for more details) such that the Fermi's golden rule gives $\tau = \tau_0(1 + O(\eta^2))$, where τ_0 is the momentum relaxation time when tilt is zero. This recommends that as long as the tilt is moderate, the relaxation time is mainly dominated by impurity scattering.

Furthermore, in the framework of the Liouville equation, the quantum mechanical phase-space distribution function of the carriers of the system (4.4) satisfies the equation $\partial \rho / \partial t + i[H, \rho] = 0$ where ρ is the single-particle density matrix. We next project this equation into the momentum basis $\{|k\rangle\}$ where the Hamiltonian is diagonal and the matrix elements of the density matrix can be written as diagonal and offdiagonal parts, i.e, $\rho_{kk'} = \langle k | \rho | k' \rangle = f_k \delta_{kk'} + g_{kk'}$. Consequently, the Liouville equation will be decomposed into two coupled equations in terms of f_k and $g_{kk'}$ which must be solved simultaneously to obtain the quantum kinetic equation written in terms of the diagonal distribution matrix f_k . [122?] Next, we convert this equation into an effective semiclassical transport equation by taking the Wigner transform of the density matrix f_k and obtain

$$\partial_t f + i\{H(\mathbf{k}), f\}_{P.B} + i[H(\mathbf{k}), f] = 0. \quad (4.7)$$

Here $f \equiv f(\mathbf{r}, \mathbf{k})$ indicates Wigner's (matrix) distribution function, $\{X, Y\}_{P.B} = \partial_{k_\mu} X \partial_{x_\mu} Y - \partial_{x_\mu} X \partial_{k_\mu} Y$ stands for the Poisson's bracket with μ and ν run through the space and momentum dimensions and we adopt Einstein's summation convention. [26, 27, 166, 167] The commutator $[H(\mathbf{k}), f]$ is the quantum coherence correction to the semiclassical transport equation of two band model. In this study, we assume that the perturbations are weak such that the transition between the bands are negligible, therefore all the band coherence effects, such as the Berry curvature correction to the carriers band velocity, are ignored and we consider the transport regime where the conduction limits only within a single band.[122–124] Note that the additional term to the energy, $v_0 k_x \mathbf{1}$, in general changes the kinetic equation, however for the spatially homogeneous distribution function which we consider here its effect vanishes as the Poisson bracket $\{H(\mathbf{k}), f\}_{P.B}$ becomes itself zero in the absence of external fields. However, by introducing the electromagnetic field through minimal coupling in Landau gauge, the Poisson bracket will produce two drift terms illustrating the Lorentz force driving the motion of electrons and written as, $\{H(\mathbf{k} - e\mathbf{A}, \Phi(\mathbf{r})), f\}_{P.B} = -e (\mathbf{E} + \mathbf{E}_0) \cdot \nabla_{\mathbf{k}} f - e \nabla_{\mathbf{k}} \varepsilon(k) \times \mathbf{B} \cdot \nabla_{\mathbf{k}} f$, [122?] where $\nabla_{\mathbf{k}} \varepsilon(k)$ is the group velocity of the carriers in (4.4). Therefore, applying the relaxation time approximation, the resulting kinetic equation of the tilted system reads

$$\partial_t f + (\mathbf{F}_{\mathbf{E}} + \mathbf{F}_{\mathbf{B}}) \cdot \nabla_{\mathbf{k}} f = -\frac{f - f^0}{\tau}, \quad (4.8)$$

where f^0 is the equilibrium distribution of the carriers and \mathbf{k} is the crystal wave vector of the carrier inside the lattice. For simplicity we separate the Lorentz force into two terms, i.e, $\dot{\mathbf{k}} = \mathbf{F}_{\mathbf{E}} + \mathbf{F}_{\mathbf{B}}$, where $\dot{\mathbf{k}}$ represents the time derivative of the crystal momentum, such that

$$\mathbf{F}_{\mathbf{E}} = -e (\mathbf{E} + \mathbf{E}_0), \quad (4.9)$$

$$\mathbf{F}_{\mathbf{B}} = -e \nabla_{\mathbf{k}} \varepsilon(k) \times \mathbf{B}.$$

While the second expression is the force caused by the magnetic field, the first drift term is due to the electric fields (bias and effective), and notice that the tilt term (tilt velocity) in the presence of external fields, only enters, through the drift term, into the kinetic part and has no effect on the collision part of the transport equation for the tilted Dirac system. The covariance of the Boltzmann equation indicates that (4.8) is valid in any frame of reference as long as one prescribes it the transformed fields. The equation takes a relatively simple form in a frame of reference where $\mathbf{E}_0 = 0$.

This, in turn, proves that Hamiltonian (4.4) and its boosted equivalent (4.6) yield the same kinetic equation up to the Lorentz symmetry. We then utilize this similarity and

compute the physical quantity of interest in an appropriate inertial frame by implementing the coordinate-independent Boltzmann transport equation and then restore to the original frame of reference via the Lorentz transformation law. [166–168]

The rest of this section is therefore devoted to the covariant formulation of Boltzmann's transport equation. The distribution function is a Lorentz scalar since it relates to the number of particles, $dN = f(x^\mu, k^\mu) dx^\mu dk_\mu$, through the phase space volume.[26, 166, 169] Lorentz covariance, as a basic structural property of the Dirac equation, can be implemented in investigating the statistical kinetics of the carriers in Dirac (2D) and Weyl (3D) systems. Additionally, we throughout our calculations ignore the spin degree of freedom, as the spin component affected by the Lorentz boost undergoes a precession due to the Wigner rotation[170] whereas our main concern is the study of electronic transport of a tilted system. If the electromagnetic fields are present, the ratio between the two fields yields a new velocity that determines the drift of the charged particle, and its modulus v_{drift} needs to be compared to the effective speed of light v_F . If $\eta = v_{\text{drift}}/v_F < 1$, there exists a Lorentz transformation to a frame of reference that allows us to get rid of the electric field (*magnetic regime*), while the *electric regime* is associated with a drift velocity that is larger than the speed of light ($\eta > 1$), in which case one can get rid of the magnetic field by an appropriate Lorentz boost. In the remainder of this chapter, we concentrate on the magnetic regime, which happens to be relevant for the covariant description of type-I Weyl semimetals with moderately tilted cones.

The covariant Boltzmann equation with electromagnetic fields in manifest covariant form is [26, 166, 168]

$$k^\mu \partial_\mu f + e \mathcal{F}^{\mu\nu} k_\nu \frac{\partial f}{\partial k^\mu} = -\frac{k^\mu u_\mu}{v_F^2} \frac{\delta f}{\tau}, \quad (4.10)$$

where $\delta f = f - f^0$, is the deviation from the equilibrium distribution. The collision kernel is approximated by a suitable relaxation time ansatz where u_μ is the 4-velocity for carrier flow,[166, 168] which in the electron's local rest frame takes the form $u_\mu = (v_F, 0, 0, 0)$. Using relativistic notations, the 4-momentum is $k^\mu = (\varepsilon/v_F, \mathbf{k})$ where ε and v_F are the energy and the Fermi velocity of the carriers, respectively. Note that for the massless carriers with Dirac dispersion we have $k = \varepsilon v/v_F^2$, in terms of the 4-velocity $v_\mu = \dot{x}_\mu = (v_F, \mathbf{v})$, and τ is the carriers scattering time as the time interval between two successive collisions. Writing the electromagnetic tensor $\mathcal{F}^{\mu\nu}$ explicitly in terms of the fields $\mathcal{F}^{0i} = -\mathcal{F}^{i0} = E_i/v_F$, and $\mathcal{F}^{ij} = -\varepsilon_{ij\ell} B_\ell$, the equations of motion read

$$k^\mu \partial_\mu = \frac{\varepsilon}{v_F^2} (\partial_t + \mathbf{v} \cdot \nabla_{\mathbf{k}}), \quad (4.11)$$

$$e \mathcal{F}^{\mu\nu} k_\nu \frac{\partial}{\partial k^\mu} = \frac{\varepsilon}{v_F^2} e \left(\mathbf{E} \cdot \mathbf{v} \frac{\partial}{\partial \varepsilon} + \mathbf{E} \cdot \nabla_{\mathbf{k}} + \mathbf{v} \times \mathbf{B} \cdot \nabla_{\mathbf{k}} \right). \quad (4.12)$$

The drift velocity determines the appropriate Lorentz boost defined as (for instance in the x -direction of space)

$$\Lambda_\nu^\mu = \begin{pmatrix} \gamma & -\gamma\eta & 0 & 0 \\ -\gamma\eta & \gamma & 0 & 0 \\ 0 & 0 & 1 & 0 \\ 0 & 0 & 0 & 1 \end{pmatrix}, \quad (4.13)$$

to the frame of reference where \mathbf{E}_0 vanishes as long as we remain in the magnetic regime, while the small bias field $\mathbf{E} = \delta\mathbf{E}$ is transformed to $\mathbf{E}' = \delta\mathbf{E}' = \gamma\delta\mathbf{E}_\perp + \delta\mathbf{E}_\parallel$ as well as the magnetic field $B'_z = \gamma^{-1} B_z$, ($B'_{x,y} = 0$), in terms of the Lorentz factor

$$\gamma^{-1} = \sqrt{1 - \eta^2}, \quad \eta = v_{\text{drift}}/v_F. \quad (4.14)$$

We thus obtain the solution of the covariant Boltzmann equation for a stationary and homogeneous system, the nonequilibrium distribution, as[86]

$$\delta f = \frac{-e\tau}{1 + \omega'^2\tau^2} \left(\delta\mathbf{E}' + \tau\omega' \frac{\mathbf{B}'}{|\mathbf{B}'|} \times \delta\mathbf{E}' \right) \cdot \nabla_{\mathbf{k}'\varepsilon'} \left(\frac{f^{(0)}}{\partial\varepsilon'} \right), \quad (4.15)$$

where, in the co-moving frame, the cyclotron frequency of Dirac fermions is given by

$$\omega' = e \frac{v_F^2}{\varepsilon'} B'. \quad (4.16)$$

The first term inside the parenthesis in Eq. (4.15) contributes to the longitudinal conductivity whereas the second term gives rise to the Hall current. Throughout this chapter we are only interested in the longitudinal conductivity and hence will neglect the effect of the second term in the conductivity calculations.

The nonequilibrium current due to an infinitesimal bias is defined through the formula

$$\mathbf{J} = -e \text{Tr}(\mathbf{v} \delta f), \quad (4.17)$$

where the trace (Tr) represents the summation over the momentum and other degrees of freedom. While computing the current in the lab frame, we use the Lorentz-invariant distribution function as calculated in Eq. (4.15) prescribed with the transformed fields, namely,

$$\delta\mathbf{E}'_\parallel = \delta\mathbf{E}_\parallel, \quad \delta\mathbf{E}'_\perp = \gamma\delta\mathbf{E}_\perp, \quad (4.18)$$

and then perform the trace by taking into account that the components of the velocity of

the particle in the lab frame should transform according to the relativistic velocity addition formula, in directions parallel and perpendicular to the boost, as

$$v_{\parallel} = \frac{v'_{\parallel} + v_{\text{drift}}}{1 + \frac{v_{\text{drift}}}{v_F^2} v'_{\parallel}}, \quad v_{\perp} = \frac{\sqrt{1 - \frac{v_{\text{drift}}^2}{v_F^2}}}{1 + \frac{v_{\text{drift}}}{v_F^2} v'_{\parallel}} v'_{\perp}. \quad (4.19)$$

Ultimately, one uses the formula $\sigma_{\mu\nu} = \delta J_{\mu} / \delta E_{\nu}$ for the infinitesimal bias fields[171] to restore the longitudinal conductivity parallel and perpendicular to the boost direction and compare them with the result obtained from the Kubo formula and semiclassical Boltzmann calculations.

4.3. Hamiltonian for 2D anisotropic tilted Dirac cones

The emergence of Dirac physics in condensed matter makes it possible to probe relativistic effects in materials. In addition, Dirac physics in materials comprises electronic properties that are generically described by more general Hamiltonians taking into account the anisotropy and the tilt of the energy dispersion. Restricted to two dimensions, the general form of a Dirac Hamiltonian with two bands intersecting linearly in a conical shape reads[134, 136]

$$H_{\text{Dirac}} = v_0^{\mu} k_{\mu} \mathbf{1} + v^{\mu} k_{\mu} \sigma_{\mu}. \quad (4.20)$$

where the indices μ and ν run over the spatial dimensions x, y . In addition to the anisotropic Fermi velocity described by the parameter v^{μ} , this Hamiltonian is specified by two parameters, v_0^x and v_0^y , that characterize the tilt of the Dirac cones. This type of Hamiltonian describes the dispersion of a strained graphene sheet and organic conductors of the α -(BEDT-TTF)₂I₃ family.[134] The additional term $v_0^{\mu} k_{\mu} \mathbf{1}$ can be understood on the basis of tight-binding models for graphene-like systems. Indeed, second-nearest-neighbor hopping induces the tilt of the Dirac cones if the latter are dragged away from the K and K' points of the first Brillouin zone (e.g. by strain) and breaks the particle-hole symmetry of the system.[172, 173]

This sufficiently general form of the Hamiltonian (4.20) can be simplified by rescaling and rotating in momentum and pseudospin spaces,[137, 174] to get

$$e^{i \frac{\xi_{\text{tilt}}}{2} \sigma_z} H_{\text{Dirac}}(\mathcal{R}^{-1} \mathbf{k}) e^{-i \frac{\xi_{\text{tilt}}}{2} \sigma_z} \longmapsto H_{\text{Dirac}}(\mathbf{k}), \quad (4.21)$$

These transformations remove the anisotropy and bring the tilt into the x -direction such

that one obtains the minimal Hamiltonian

$$H_{\text{Dirac}} = v_F \mathbf{k} \cdot \boldsymbol{\sigma} + v_0 k_x \mathbf{1}. \quad (4.22)$$

where, for simplicity, we set the new Fermi and tilt velocities as $v_F = v_x = v_y$ and $v_0 = v_0^x = \eta v_F$, respectively. The transformation \mathcal{R} is given by

$$\mathcal{R}(\xi_{\text{tilt}}) = \begin{pmatrix} \cos \xi_{\text{tilt}} & \frac{v_y}{v_x} \sin \xi_{\text{tilt}} \\ -\sin \xi_{\text{tilt}} & \frac{v_y}{v_x} \cos \xi_{\text{tilt}} \end{pmatrix}, \quad (4.23)$$

where $\xi_{\text{tilt}} = \cos^{-1} \left(\eta^{-1} v_0^x / v_x \right)$, and $0 < \eta < 1$ is the tilt parameter defined as

$$\eta = \sqrt{(v_0^x / v_x)^2 + (v_0^y / v_y)^2}. \quad (4.24)$$

Note that the transformation \mathcal{R} in real space is the combination of a coordinate rescaling followed by a pure SO(2) rotation that maps the original coordinates into modified coordinates in order to remove the anisotropy in $x - y$ plane and bring the tilt into a specific direction, namely, $(x, y)^t \longrightarrow (\cos \xi_{\text{tilt}} + i \sigma_y \sin \xi_{\text{tilt}})(x, \frac{v_x}{v_y} y)^t$, and t stands for matrix transposition.[137, 138]

Now that we obtained the minimal Hamiltonian model for a general 2D Dirac system, next, we address the transport theory of the system under the influence of electromagnetic fields. Under external fields and in the Landau gauge, as we stated in Sec. 4.2, we restore the Hamiltonian (4.4) for 2D. Additionally, in our gauge choice the term $v_0 k_x$ on the left hand side is diagonal in pseudospin and momentum space – it only shifts the spectrum in energy and can thus be absorbed into the Hamiltonian. This indicates that upon minimal coupling the Hamiltonian, $H_{\text{Dirac}} - v_0 k_x \mathbf{1}$, has the same covariant form as that of massless particles in a magnetic field $B \hat{\mathbf{z}}$ and an *effective* electric field E_0 in the y -direction. In the following, we proceed to compute the transport quantities, i.e, longitudinal electric conductivity, by first transforming the system into another inertial frame to remove this effective field.

4.3.1. Conductivity from the Boltzmann equation

The above reasoning allows us to find the Lorentz boost to the appropriate frame of reference, where we can easily calculate the transport coefficients. Notice also that the separation between a strong electric field E_0 and a bias field δE , which was somewhat artificial in the Sec. 4.2, is now much more natural – while δE describes a true electric field used to drive a current through the system, E_0 simply represents the tilt of the Dirac cones and not a physical electric field. Now assuming that the electric field is oriented in the y -direction

as in Eq. (4.4), the bias and magnetic fields under the Lorentz boost in the x -direction transform as

$$E'_x = \delta E_x, \quad E'_y = \gamma \delta E_y, \quad B' \simeq \gamma^{-1} B, \quad (4.25)$$

where we have neglected a small correction $\eta \delta E_x / v_F \ll B$ to the magnetic field in the last expression. Additionally, the components of the velocity of the electron in the lab frame, using Eq. (4.19), relate to those in the co-moving frame via

$$v_x = v_F \frac{\cos \phi' + \eta}{1 + \eta \cos \phi'}, \quad v_y = v_F \frac{\sin \phi'}{\gamma(1 + \eta \cos \phi')}. \quad (4.26)$$

In lights of these relations, due to the relativistic aberration of angles under a boost, the polar angle transforms as

$$d\phi = \frac{d\phi'}{\gamma(1 + \eta \cos \phi')}, \quad (4.27)$$

which resembles the relativistic Doppler factor in *relativistic beaming*. This alternatively indicates the Jacobian of the transformation from the lab into the co-moving frame of reference. Using the transformed form of the velocities v_μ in Eq. (4.26), the Lorentz-invariant distribution function (4.15) in the co-moving frame and that $\nabla_{\mathbf{k}'} \varepsilon' = v_F (\cos \phi', \sin \phi')$, one can easily compute the magnetoconductivity tensor in the lab frame,

$$J_x = \frac{-e^2 \tau}{2\pi} \int \frac{\varepsilon' d\varepsilon'}{\gamma} \left(\frac{\partial f^{(0)}}{\partial \varepsilon'} \right) \int_0^{2\pi} \frac{d\phi'}{2\pi} \frac{(\cos \phi' + \eta) \cos \phi'}{(1 + \eta \cos \phi')^2} \delta E'_x, \quad (4.28)$$

$$J_y = \frac{-e^2 \tau}{2\pi} \int \frac{\varepsilon' d\varepsilon'}{\gamma^2} \left(\frac{\partial f^{(0)}}{\partial \varepsilon'} \right) \int_0^{2\pi} \frac{d\phi'}{2\pi} \frac{(\sin \phi')^2}{(1 + \eta \cos \phi')^2} \delta E'_y. \quad (4.29)$$

Here and in the following parts, we limit our discussion to the diagonal conductivities. Formally, this amounts to considering the limit $\omega' \tau \rightarrow 0$ in Eq. (4.15), i.e. the limit where the scattering time is much smaller than the inverse cyclotron frequency ω' and where Landau quantization does not need to be considered. In computing the nonequilibrium current in the lab frame we, furthermore, need to consider the transformation of the bias fields as given in (4.25). Now noting the Lorentz transformation of the energy and that at zero temperature the Dirac distribution gives $(\partial f^{(0)} / \partial \varepsilon') = -\gamma^{-1} \delta(\varepsilon - \varepsilon_F)$, the current and consequently the conductivity perpendicular to the boost direction (which is identified

with the tilt direction) in the lab frame reads

$$\sigma_{\text{perp}} (= \sigma_{yy}) = \sigma_0 \left(\frac{\gamma - 1}{\eta^2} \right) \varepsilon \tau, \quad (4.30)$$

where $\sigma_0 = e^2/h$ is a fundamental constant such that $h/e^2 = 25.8 \text{ k}\Omega$. Similarly, we find for the conductivity in the direction of the boost (tilt direction)

$$\sigma_{\text{tilt}} (= \sigma_{xx}) = \sigma_0 \left(\frac{\gamma - 1}{\eta^2 \gamma} \right) \varepsilon \tau, \quad (4.31)$$

and one thus realizes that the ratio

$$\frac{\sigma_{\text{perp}}}{\sigma_{\text{tilt}}} = \gamma = (1 - \eta^2)^{-1/2}, \quad (4.32)$$

is a direct measure of the relativistic factor and thus of the tilt strength η .

Notice that the above expressions for the conductivity calculated in the framework of the covariant Boltzmann equation coincide, in the limit $\gamma = 1$, with those obtained previously within semiclassical non-relativistic Boltzmann calculations.[175] We emphasize that both the relativistic and the non-relativistic Boltzmann approaches do not account for quantum corrections in the close vicinity of the band contact points that are responsible, e.g., for the minimal conductivity of graphene.[176] These are better taken into account within the Kubo formalism, which is discussed in the following subsection.

4.3.2. Kubo formula

To verify the validity of the covariant approach, we compute the conductivity using the Kubo formula and check the agreement of both methods. Noting that $v_0 = \eta v_F$, the unitary transformation $U = \exp(-i\pi\sigma \cdot \hat{\mathbf{n}}/4)$, where $\hat{\mathbf{n}} = \hat{\mathbf{z}} \times \mathbf{k} / \sqrt{k_x^2 + k_y^2} = (\sin \phi, -\cos \phi)$, diagonalize the Hamiltonian (4.22), and the spectrum of a general 2D Dirac system thus reads

$$\varepsilon_\alpha = v_F k (\eta \cos \phi + \alpha), \quad (4.33)$$

where ϕ is the momentum vector polar angle and $\alpha = \pm 1$ is the band index. The corresponding Fermi surface is an ellipse. As in the sections above, we consider a system with a moderate tilt $\eta < 1$, such that we remain in the magnetic regime, where we can get rid of the tilt by the appropriate Lorentz boost. In the limit of zero temperature ($T = 0$) for noninteracting systems, the Kubo-Streda formula for the diagonal conductivity gives[177]

$$\sigma_{\mu\mu} = \frac{e^2}{\pi} \sum_{\mathbf{k}} \int d\varepsilon \left(-\frac{\partial f^{(0)}}{\partial \varepsilon} \right) \Pi_{\mu\mu}, \quad (4.34)$$

where the polarization tensor reads

$$\Pi_{\mu\mu} = \text{Tr} (v_\mu \text{Im} G^R v_\mu \text{Im} G^R), \quad (4.35)$$

$\text{Im} G^R = (G^R - G^A)/2i$ and the Heisenberg equation gives the velocity operator as $v_\mu = i[\hat{\mathbf{r}}_\mu, H_{\text{Dirac}}]$ where $\hat{\mathbf{r}}_\mu$ is the position operator. In the self-consistent Born approximation, the first contribution to the advanced (A) and retarded (R) Green's function of graphene in the energy eigenbasis reads

$$G^{R/A}(\varepsilon) = \sum_{\alpha=\pm} \frac{(1 + \alpha \sigma_z)/2}{\varepsilon - v k(\eta \cos \phi + \alpha) \pm i\Gamma}, \quad (4.36)$$

where the decay term is proportional to the scattering (relaxation) time τ via $\Gamma^{-1} = 2\tau$. Using the above definition, the spectral function is a diagonal matrix in energy basis and may be written as

$$\text{Im} G^R = \frac{1}{\Gamma} \begin{pmatrix} \mathfrak{A}_+ & 0 \\ 0 & \mathfrak{A}_- \end{pmatrix}, \quad (4.37)$$

where

$$\mathfrak{A}_\pm = \frac{1}{[z - y(\eta \cos \phi \pm 1)]^2 + 1}, \quad (4.38)$$

in which we defined the dimensionless variables $z = \varepsilon/\Gamma$ and $y = v_F k/\Gamma$. Now to compute conductivity, we first express the velocity matrix in the helicity basis as

$$v_\mu = ev_F \begin{pmatrix} v_\mu^\alpha & v_\mu^{\alpha\alpha'} \\ [v_\mu^{\alpha\alpha'}]^* & v_\mu^{\alpha'} \end{pmatrix}, \quad (4.39)$$

where the band velocities are given by

$$v_\mu^\alpha = (\eta + \alpha \cos \phi, \sin \phi), \quad (4.40)$$

while the off-diagonal velocities read

$$v_\mu^{\alpha\alpha'} = (i \sin \phi e^{-i\phi}, -i \cos \phi e^{-i\phi}). \quad (4.41)$$

We then obtain the polarization as

$$\begin{aligned} \Pi_{\mu\mu} &= \sum_{\alpha} |\mathfrak{A}_\alpha v^\alpha|^2 + \sum_{\alpha \neq \alpha'} \mathfrak{A}_\alpha v_\mu^{\alpha\alpha'} \mathfrak{A}_{\alpha'} v_\mu^{\alpha'\alpha} \\ &= \mathfrak{A}_+^2 (v_\mu^+)^2 + \mathfrak{A}_-^2 (v_\mu^-)^2 + 2 \mathfrak{A}_+ \mathfrak{A}_- |v_\mu^{+-}|^2, \end{aligned} \quad (4.42)$$

where the second term in the first lines shows the quantum coherent mixing of the bands, whereas the first term gives the intraband contribution and we remind that α and α' are the band indices. Now writing the momentum summation in terms of the momentum and angular integrals as $\sum_{\mathbf{k}} \rightarrow (2\pi)^{-2} \int_0^\infty y dy \int_0^{2\pi} d\phi$ and performing the integrals we finally obtain

$$\sigma_{yy} = \frac{\sigma_0}{\pi} \left[\frac{\gamma - 1}{\eta^2} (1 + z \tan^{-1} z) + \frac{2z(\tan^{-1} z - z)(1 - z/\sqrt{z^2 + \eta^2}) + \eta^2}{2\eta^2} \right], \quad (4.43)$$

$$\sigma_{xx} = \frac{\sigma_0}{\pi} \left[\frac{\gamma - 1}{\eta^2 \gamma} (1 + z \tan^{-1} z) + \frac{\eta^2 + 2(z - \tan^{-1} z)(z - \sqrt{z^2 + \eta^2})}{2\eta^2} \right], \quad (4.44)$$

for the diagonal conductivities in the x - and y -directions.

Equations (4.43) and (4.44) are the main result of this section and merit a detailed discussion. First, let us investigate the zero-tilt case, $\eta \rightarrow 0$, in which we obtain

$$\sigma_{xx} = \sigma_{yy} = \sigma_0 \left[\frac{1}{2\pi} (1 + z \tan^{-1} z) + \frac{\tan^{-1} z}{2\pi z} \right]. \quad (4.45)$$

In the high-energy (diffusive) limit $z \gg 1$, we then retrieve the standard result, in agreement with the semiclassical Boltzmann approach, namely[176]

$$\sigma_{xx} = \sigma_{yy} = \sigma_0 \varepsilon \tau / 2, \quad (4.46)$$

which coincides with Eqs. (4.30) and (4.31) in the static limit ($\omega = 0$). We emphasize that in the opposite limit of $z \ll 1$, i.e. at energies close to the Dirac point, band mixing yields quantum corrections that are beyond the reach of the semiclassical Boltzmann approach, within the first Born and relaxation time approximation, and therefore a full quantum treatment is needed. Indeed, the Kubo and Boltzmann approaches yield different results then, as we will show below.

Before comparing both approaches, let us discuss in detail some aspects of the conductivities calculated from the Kubo formula. For the case of non-zero tilt in the diffusive limit, $z = \varepsilon/\Gamma = 2\varepsilon\tau \gg 1$, the conductivities (4.43) and (4.44) can be rewritten as

$$\sigma_{\text{tilt}} (= \sigma_{xx}) = \sigma_0 \left(\frac{\gamma - 1}{\eta^2 \gamma} \frac{z}{2} + \frac{1}{4z} \right), \quad (4.47)$$

$$\sigma_{\text{perp}} (= \sigma_{yy}) = \sigma_0 \left(\frac{\gamma - 1}{\eta^2} \frac{z}{2} + \frac{1}{4z} \right), \quad (4.48)$$

where the last term takes into account the first (quantum) correction in $1/z$. The conduc-

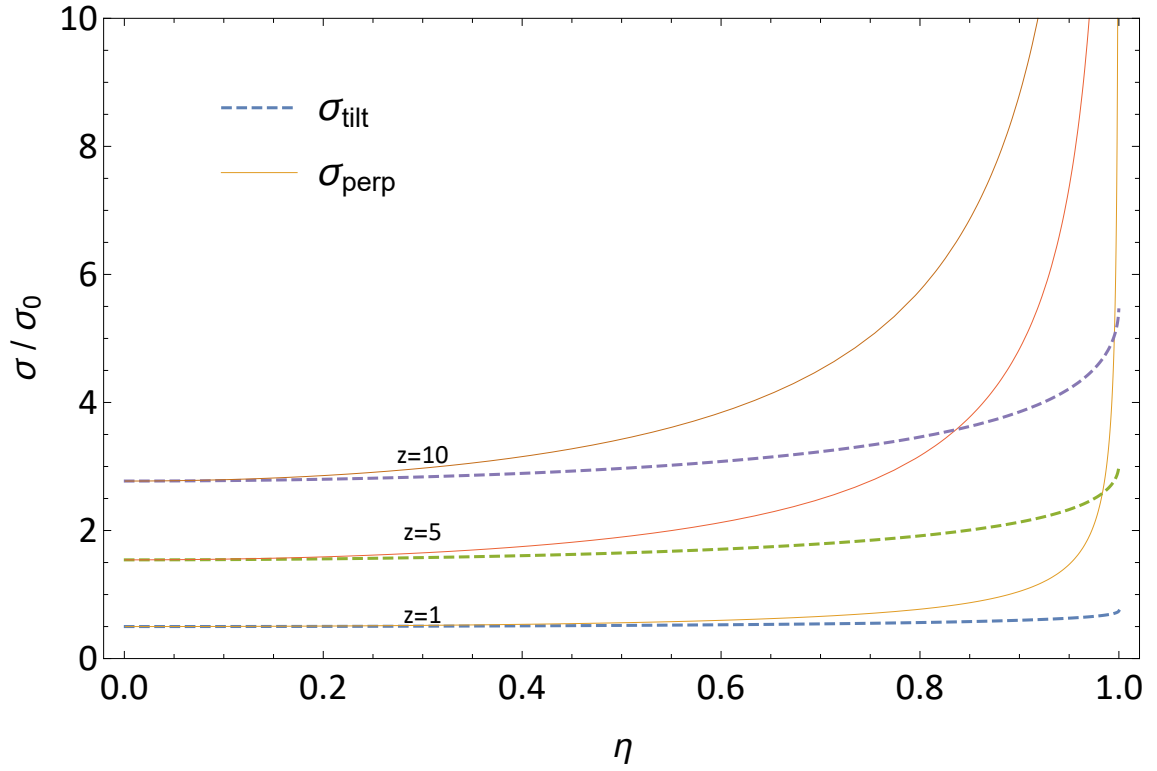


Figure 4.1: (Color online) Comparison between the conductivity of the tilted Graphene in directions perpendicular and parallel to the tilt as a function of the tilt parameter η for values of the normalized energy as $z = 1, 5$ and 10 . Around zero tilt both the parallel and perpendicular conductivities, calculated from the Kubo formula, correspond to the isotropic value; while increasing the tilt develops an anisotropy such that the perpendicular conductivity diverges, while the parallel one continues to grow up to a finite value.

tivities (4.47) and (4.48) are plotted in Fig. 4.1 as a function of the tilt parameter η , for different values of z . First, notice that the result coincides with that in Eq. (4.46) for zero tilt, i.e. in the limit $\eta \rightarrow 0$, where we retrieve also $\sigma_{xx} = \sigma_{yy}$. Figure 4.2 shows a comparison between the conductivities (4.47) and (4.48) obtained from the Kubo approach (dashed lines) and those from the covariant Boltzmann formula, Eqs. (4.31) and (4.30). The only difference resides in the offset of $\delta\sigma = \sigma_0/4z = \sigma_0/8\varepsilon\tau$, which is due to the quantum corrections that are neglected in the latter approach. This offset becomes less relevant at larger values of the tilt where the conductivities are enhanced. This enhancement can globally be understood from the density of states that increases with the tilt parameter. However, this argument in terms of the density of states does not explain the strong anisotropy in the conductivities. While the conductivity σ_{tilt} along the tilt direction remains finite and saturates at a value of

$$\sigma_{\text{tilt}}(\eta \rightarrow 1) = \sigma_0 \left(\varepsilon\tau + \frac{1}{8\varepsilon\tau} \right), \quad (4.49)$$

i.e. the Boltzmann contribution is doubled with respect to the $\eta \rightarrow 0$ limit (4.46), and the conductivity in the perpendicular direction diverges[178] as

$$\sigma_{\text{perp}}(\eta \rightarrow 1) \sim \sigma_0\varepsilon\tau/\sqrt{1-\eta^2}. \quad (4.50)$$

One thus obtains the same behavior (4.32) for the ratio between the conductivities as in the Boltzmann analysis.

This difference in the conductivities stems from the anisotropy of the velocities and mobilities in two directions. Experimentally observed results show that when applying strain to the graphene crystal, the group velocity of the carriers along the strain drops by increasing the strain whereas the group velocity along the perpendicular direction to the strain increases.[179] The tilt affects the carrier density by increasing the number of available states,[136] but ultimately in the surge of scattering events in a tilted (elliptic) isoenergy surface, carrier scattering into a state along the perpendicular direction (ellipse shorter axis) is much more probable than along the tilt (the larger axes) due to the smaller momentum difference. Hence, the mobility of the carriers is largely influenced by the direction of the tilt.[180] This result is inline with another empirical finding showing that the magnetoresistance takes its maximum measure along the tilt direction in α -(BEDT-TTF)₂I₃ organic conductors.[174]

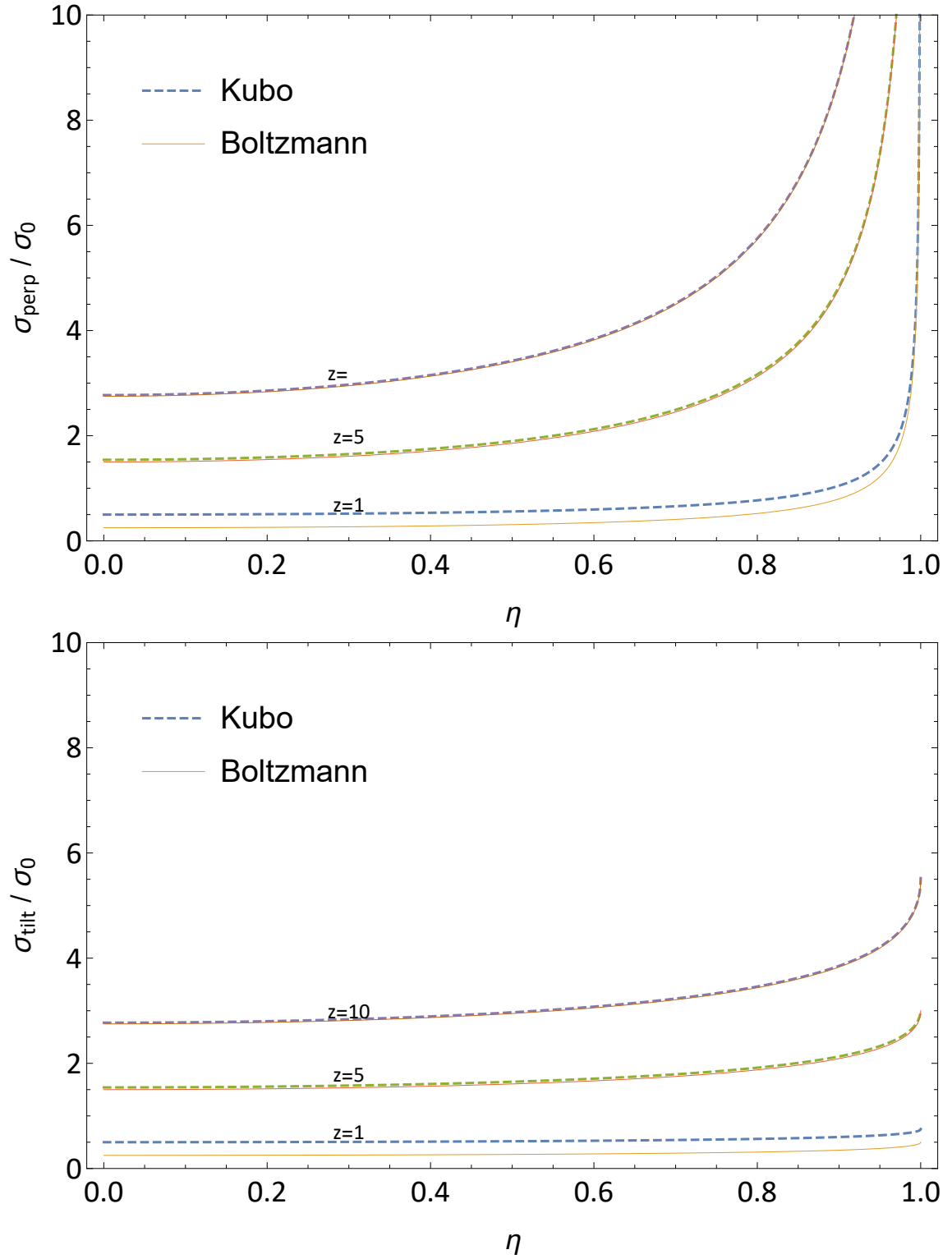


Figure 4.2: (Color online) Comparison between the conductivities $\sigma_{\text{tilt}}/\sigma_0$ and $\sigma_{\text{perp}}/\sigma_0$ of the tilted Graphene in terms of the tilt parameter for energies at $z = 1, 5$ and 10 . Conductivity Calculated from the Kubo formula (dashed) agree with the covariant Boltzmann approach (solid) in (4.31), (4.30). While the perpendicular conductivity diverges in critical limit; the conductivity parallel to tilt direction saturates at finite value.

4.4. Type-I Weyl Semimetal

4.4.1. Boltzmann equation

In this section, we present the core result of this chapter and investigate the magnetoconductivity of type-I Weyl semimetals based on the covariant formalism introduced in Sec. 4.2. Consider a Weyl material in the presence of perpendicular electric and magnetic fields – again, we choose the magnetic field to be oriented in the z -direction and a tilt in the x -direction, i.e. the associated electric field is oriented in the y -direction. The essential part of the 3D Hamiltonian of this system, according to (4.4), can be cast into the form $\tilde{H}_{\text{Weyl}} - v_0 k_x \mathbf{1}$, and, similar to the discussion in 4.2, has a Lorentz symmetric equivalent.

We apply a Lorentz boost in the x -direction with drift velocity $v_0 = E_0/B$ to work in a frame where the electric field vanishes. Noting the representation of the Lorentz boost, the bias fields transform along the boost direction as $\delta E'_{y(z)} = \gamma \delta E_{y(z)}$, $\delta E'_x = \delta E_x$ and the magnetic field as $B'_z = \gamma^{-1} B_z$. Taking the axis of the polar coordinate, $\theta = 0$, along the boost direction, simplifies the expressions and using this parametrization in the co-moving frame we obtain $\nabla_{\mathbf{k}'} \varepsilon' = v_F (\cos \theta', \sin \theta' \cos \phi', \sin \theta' \sin \phi')$. Next, implementing the relativistic addition formula, the velocities transform accordingly as

$$v_x = v_F \frac{\eta + \cos \theta'}{1 + \eta \cos \theta'}, \quad (4.51)$$

$$v_y = v_F \frac{\sin \theta' \cos \phi'}{\gamma(1 + \eta \cos \theta')}, \quad (4.52)$$

$$v_z = v_F \frac{\sin \theta' \sin \phi'}{\gamma(1 + \eta \cos \theta')}. \quad (4.53)$$

Considering the relativistic aberration of the polar angle θ under the Lorentz boost, (4.27), then the solid angle and consequently, the conic cross section transforms as $d\Omega = \gamma^{-2} d\Omega' / (1 + \eta \cos \theta')^2$ where $d\Omega' = d(\cos \theta') d\phi' / (4\pi)$ and the azimuthal angle as $d\phi = d\phi'$. Thus, the nonequilibrium current in the lab frame for each spatial direction will give

$$J_x = \frac{-e^2 \tau}{2\pi^2} \int \frac{\varepsilon'^2 d\varepsilon'}{v_F} \left(\frac{\partial f^{(0)}}{\partial \varepsilon'} \right) \int \frac{d\Omega'}{\gamma^2} \frac{(\cos \theta' + \eta) \cos \theta'}{(1 + \eta \cos \theta')^3} \delta E'_x, \quad (4.54)$$

$$J_y = \frac{-e^2 \tau}{2\pi^2} \int \frac{\varepsilon'^2 d\varepsilon'}{v_F} \left(\frac{\partial f^{(0)}}{\partial \varepsilon'} \right) \int \frac{d\Omega'}{\gamma^3} \frac{\sin^2 \theta' \cos^2 \phi'}{(1 + \eta \cos \theta')^3} \delta E'_y, \quad (4.55)$$

$$J_z = \frac{-e^2 \tau}{2\pi^2} \int \frac{\varepsilon'^2 d\varepsilon'}{v_F} \left(\frac{\partial f^{(0)}}{\partial \varepsilon'} \right)$$

$$\int \frac{d\Omega'}{\gamma^3} \frac{\sin^2 \theta' \sin^2 \phi'}{(1 + \eta \cos \theta')^3} \delta E'_z. \quad (4.56)$$

As a result, we obtain in the lab frame for the conductivity parallel to the boost

$$\sigma_{\text{tilt}} = \sigma_0 \frac{\varepsilon^2 \tau}{\pi v_F} \left(\frac{\tanh^{-1} \eta - \eta}{\eta^3} \right). \quad (4.57)$$

Similarly for the conductivity in the direction perpendicular to the boost we get

$$\sigma_{\text{perp}} = \sigma_0 \frac{\varepsilon^2 \tau}{\pi v_F} \left(\frac{\gamma^2 \eta - \tanh^{-1} \eta}{2\eta^3} \right). \quad (4.58)$$

In the zero-tilt limit, $\gamma \rightarrow 1$, we obtain the isotropic conductivity as $\sigma_{\text{tilt}} = \sigma_{\text{perp}} = \sigma_0 \varepsilon^2 \tau / (3\pi v_F)$, recovering the same result as obtained using semiclassical Boltzmann equation in zero temperature reported elsewhere in the literature. [181–183]

4.4.2. Kubo formalism

Again, we compare the result obtained from the covariant Boltzmann equation to the conductivity calculated within linear response theory. We write a minimal type-I Weyl semimetal Hamiltonian with a tilt in the z -direction (Fig.4.3), parametrized by $\eta = v_0/v < 1$ as

$$H = v_F \mathbf{k} \cdot \boldsymbol{\sigma} + \eta v_F k_z. \quad (4.59)$$

Similar to the case of graphene, the unitary transformation $U = e^{-i\frac{\theta}{2}\boldsymbol{\sigma} \cdot \hat{\mathbf{n}}}$, where $\hat{\mathbf{n}} = \hat{\mathbf{z}} \times \mathbf{k} / \sqrt{k_x^2 + k_y^2}$, brings the Weyl Hamiltonian into the diagonal form. In this basis, the Green's function through the polar parametrization reads

$$G^{R/A}(\varepsilon) = \sum_{\alpha=\pm} \frac{(1 + \alpha \sigma_z)/2}{\varepsilon - v k(\eta \cos \theta + \alpha) \pm i\Gamma}, \quad (4.60)$$

and the spectral function, in terms of the dimensionless variables give similar diagonal form as defined in Eq. (4.37) with

$$\mathfrak{A}_{\pm} = \frac{1}{[z - y(\eta \cos \theta \pm 1)]^2 + 1}. \quad (4.61)$$

Writing the velocity operators in energy basis, as given in Eq. (4.39), we obtain the band diagonal velocities (using spherical coordinates)

$$v_{\mu}^{\alpha} = (\alpha \sin \theta \cos \phi, \alpha \sin \theta \sin \phi, \eta + \alpha \cos \theta), \quad (4.62)$$

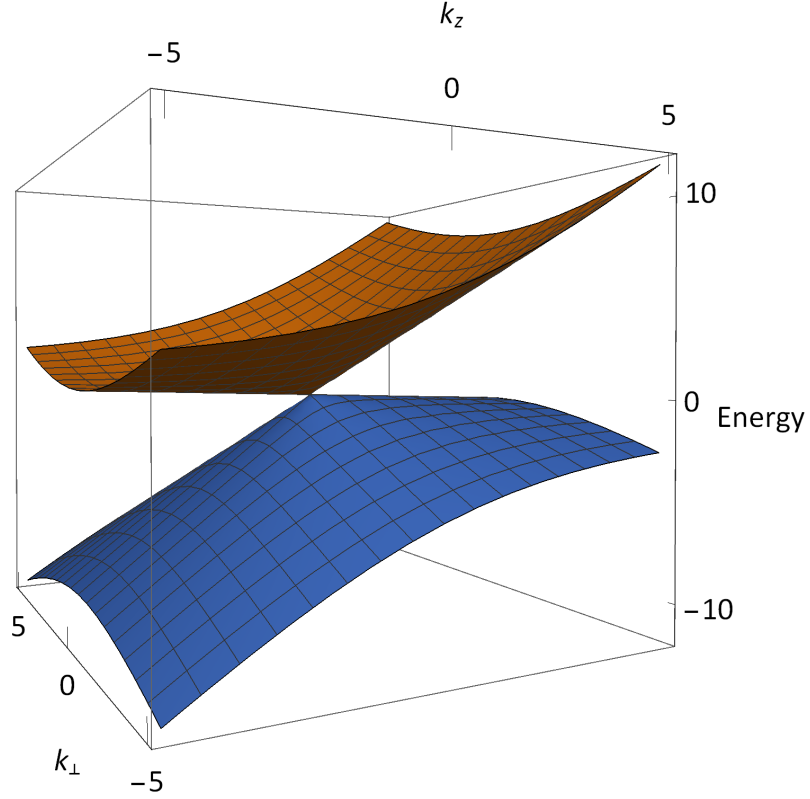


Figure 4.3: The conical spectrum of a tilted Weyl crossing.

and the off-diagonal velocities are

$$v_x^{\alpha\alpha'} = e^{-i\phi}(\cos\theta \cos\phi + i \sin\phi), \quad (4.63)$$

$$v_y^{\alpha\alpha'} = e^{-i\phi}(\cos\theta \sin\phi - i \cos\phi), \quad (4.64)$$

$$v_z^{\alpha\alpha'} = -e^{-i\phi} \sin\theta. \quad (4.65)$$

To compute the conductivity using Eq. (4.34), we write accordingly the conductivity as

$$\sigma_{\mu\mu} = \frac{e^2 \Gamma}{\pi v_F} \langle \Pi_{\mu\mu} \rangle, \quad (4.66)$$

where the polarization tensor is defined as before in Eq. (4.42) with the velocities given in Eqs. (4.62)-(4.65). Moreover, we define the three-dimensional momentum and angular integrals now as $\langle \dots \rangle = (2\pi)^{-3} \int_0^\infty y^2 dy \int_0^\pi \sin\theta d\theta \int_0^{2\pi} d\phi$. One thus finds the conductivity

$$\sigma_{\text{perp}} (= \sigma_{xx} = \sigma_{yy}) = \sigma_0 \frac{\Gamma}{2\pi v_F} (a_1 z^2 + a_2), \quad (4.67)$$

$$\sigma_{\text{tilt}} (= \sigma_{zz}) = \sigma_0 \frac{\Gamma}{2\pi v_F} (a_3 z^2 + a_4), \quad (4.68)$$

where the second term yields the (intrinsic) quantum correction to the conductivity due to the band mixing effects,[184] and the first term is the Drude conductivity which coin-

cides with the result of the Boltzmann equation in the diffusive limit $z \gg 1$. The other parameters are defined as

$$a_1 = \frac{\eta - (1 - \eta^2) \tanh^{-1} \eta}{2\eta^3(1 - \eta^2)}, \quad (4.69)$$

$$a_2 = \frac{\eta + (1 - \eta^2) \tanh^{-1} \eta}{2\eta(1 - \eta^2)}, \quad (4.70)$$

$$a_3 = \frac{\tanh^{-1} \eta - \eta}{\eta^3}, \quad (4.71)$$

$$a_4 = \frac{\tanh^{-1} \eta}{\eta}, \quad (4.72)$$

and we have restored σ_0 by noting that $h = 2\pi$. In the limit of zero tilt ($\eta \rightarrow 0$), we obtain the isotropic conductivity

$$\sigma_{xx}(= \sigma_{yy} = \sigma_{zz}) = \sigma_0 \frac{\Gamma}{4\pi v_F} (z^2/3 + 1), \quad (4.73)$$

recovering the results obtained in previous works using linear response calculations.[132, 133, 185] In figure 4.4, we compare the conductivity of a type-I WSM for zero tilt with Fermi velocity $v \approx c/300$, where c is the speed of light, and constant relaxation time $\tau = 10^{-7}$ s using the Boltzmann approach and Kubo formalism. As in the 2D case, we

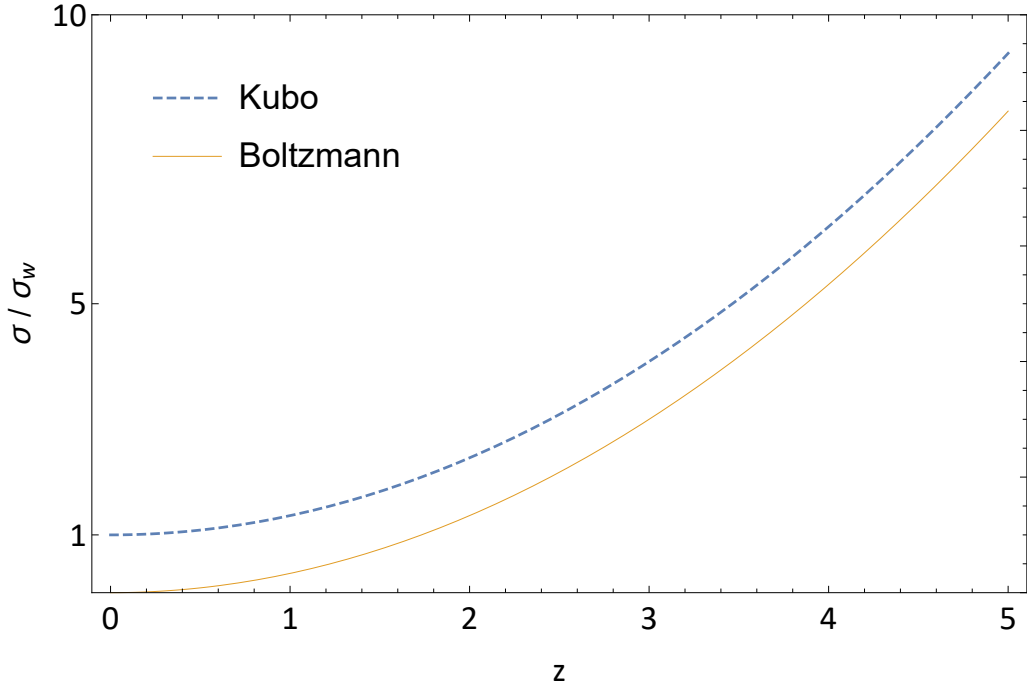


Figure 4.4: (Color online) Isotropic conductivity $\sigma_w = \sigma_0 \frac{\Gamma}{4\pi v_F}$ of Weyl semimetals with zero tilt ($\eta = 0$) as a function of the normalized energy z . The results calculated from the Boltzmann and Kubo approaches agree except for a small offset. This nonzero residual conductivity is due to the band coherence contributions.

notice a significant increase in the conductivities with the tilt in the case of moderate tilt. The discrepancy between the Kubo and Boltzmann conductivities is inherited from the zero-tilt case, where we have already noticed that the Kubo formula systematically yields a larger conductivity. In the same manner as in the 2D case discussed above, the main sources of this discrepancy are quantum interference effects between the two bands that are correctly taken into account via the Kubo formula whereas they are not treated yet in the first order linear approximation of the Boltzmann equation and thus are not present in its results. In the zero-tilt limit, the (isotropic) conductivity shows a parabolic behavior in energy that can be understood qualitatively from the behavior of the density of states for Weyl semimetal, which is quadratic in energy.

In the nonzero tilt limit, we find again, from our calculations based on the Kubo formula, that the conductivity σ_{perp} in the direction perpendicular to the tilt increases and diverges for $\eta \rightarrow 1$ and that the conductivity σ_{tilt} in the tilt direction is smaller than σ_{perp} . However, contrary to the 2D case, σ_{tilt} now also diverges upon increasing tilt (Fig.4.5). The parallel conductivity can be linked to the longitudinal magnetoresistivity if we set the magnetic field in z -direction. Therefore the finite value of conductivity in the direction parallel to the tilt is a theoretical evidence of the enhanced longitudinal magnetoresistance observed in WSM having tilted Weyl points.[165]

This anisotropy in the conductivity can be understood from the covariant point of view where the tilt velocity is identified with an effective electric field normal to its direction, $\mathbf{v}_0 = \mathbf{E}_0 \times \mathbf{B}/B^2$. Thus in effect, the auxiliary field enhances the conductivity along the field (perpendicular the tilt direction).

To further corroborate our approach in terms of the covariant Boltzmann equation, we further inspect the anisotropy and the directional features in the conductivity in the framework of a semiclassical *non-covariant* Boltzmann equation. In this case, we take into account the tilt-induced anisotropy directly in the expression for the averaged velocities, without appealing to Lorentz boosts to a frame of reference, where the dispersion becomes effectively isotropic. We can then write the conductivity as

$$\sigma_{\mu\nu} = \frac{e^2\tau}{2\pi^2v_F^3} \left\langle \frac{v_\mu v_\nu}{(1 + \eta \cos \theta)^3} \right\rangle_\Omega, \quad (4.74)$$

in terms of the band velocities given in Eq. (4.62) where $\langle \cdots \rangle_\Omega$ denotes the averaging over the random solid angles. In performing the angular integrals, the velocity v_z compensates partially for the diverging behavior of the density of states and, as a result, yields a less divergent expression for σ_{zz} . In contrast, the v_x and v_y velocities produce a more singular result and thus yield a strongly divergent behavior of σ_{xx} and σ_{yy} . The calculated

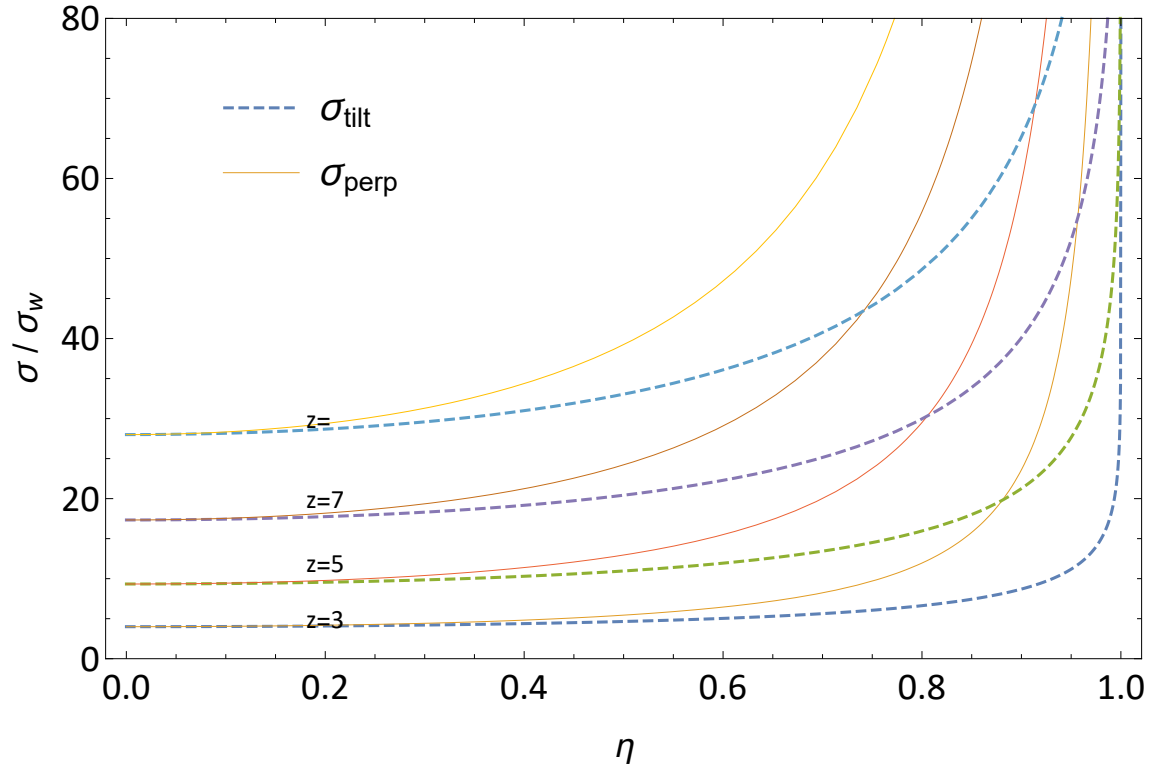


Figure 4.5: (Color online) Comparison between the parallel-perpendicular conductivity of type-I WSM computed from the Kubo formula in terms of the tilt parameter, for different values of the normalized energies. The conductivity in both directions diverge for $\eta \rightarrow 1$, but the divergence is more pronounced in the direction perpendicular to the tilt. In the zero-tilt limit, both conductivities match restoring the isotropic value.

conductivity using the non-covariant Boltzmann equation then gives the expressions

$$\sigma_{xx} = \sigma_{yy} = \sigma_0 \frac{\varepsilon^2 \tau}{\pi v_F} \frac{\eta - (1 - \eta^2) \tanh^{-1} \eta}{2\eta^3(1 - \eta^2)}, \quad (4.75)$$

$$\sigma_{zz} = \sigma_0 \frac{\varepsilon^2 \tau}{\pi v_F} \frac{\tanh^{-1} \eta - \eta}{\eta^3}, \quad (4.76)$$

which agree with (4.58) and (4.57) obtained from the covariant Boltzmann approach. This further confirms the accuracy of the results obtained from the Kubo formula and covariant Boltzmann approach.

As in the 2D case and the above-mentioned zero-tilt limit for Weyl semimetals, we, therefore, find a high degree of accuracy between the Kubo-formula approach and the results from the covariant Boltzmann equation over the whole range of tilt parameters η . This is summarized in Fig. 4.6. Again, the main difference stems from the conductivity offset due to interband contributions that are neglected in the Boltzmann approach. Overall, we find that the increase in the conductivities with the tilt parameter is more pronounced at larger energies, i.e. upon increasing z . This is also represented in the form of a color plot in Fig. 4.7, where we plot the conductivity σ_{perp} in the plane spanned by the tilt parameter and the energy.

4.4.3. Density of states as a function of the tilt parameter

The increase of the conductivity with the tilt of the Weyl cones can be understood qualitatively from an analysis of the density of states (DOS), $g(\varepsilon)$, which enters into the expression of the conductivity in the Einstein relation for a system of d -dimension

$$\sigma_E = \frac{e^2 \bar{v}^2 \tau}{d} g(\varepsilon) \propto g(\varepsilon), \quad (4.77)$$

that we use here for qualitative analysis. The parameter \bar{v} represents an average velocity since the Einstein relation does not make a difference between the directions contrary to the more appropriate Boltzmann or Kubo formulas. The tilt of the Weyl cones enlarges the Fermi surface and thus increases the DOS. This yields eventually an enhanced conductivity in the type-I WSM. The hike of the DOS can be justified using both Lorentz covariance and Sommerfeld expansion. From the covariance point of view and due to the length contraction in lab frame in the direction of boost, it is easy to see that the particle density scales as $dn = \gamma dn'$. Furthermore, since $n = \int d\varepsilon g(\varepsilon) f(T \approx 0)$, and noting the transformation of energy, the DOS in lab frame, by applying the inverse Lorentz boost, then gives $g(\varepsilon) = \gamma^2 g'(\varepsilon')$. Therefore the expression for the DOS of Weyl semimetals in

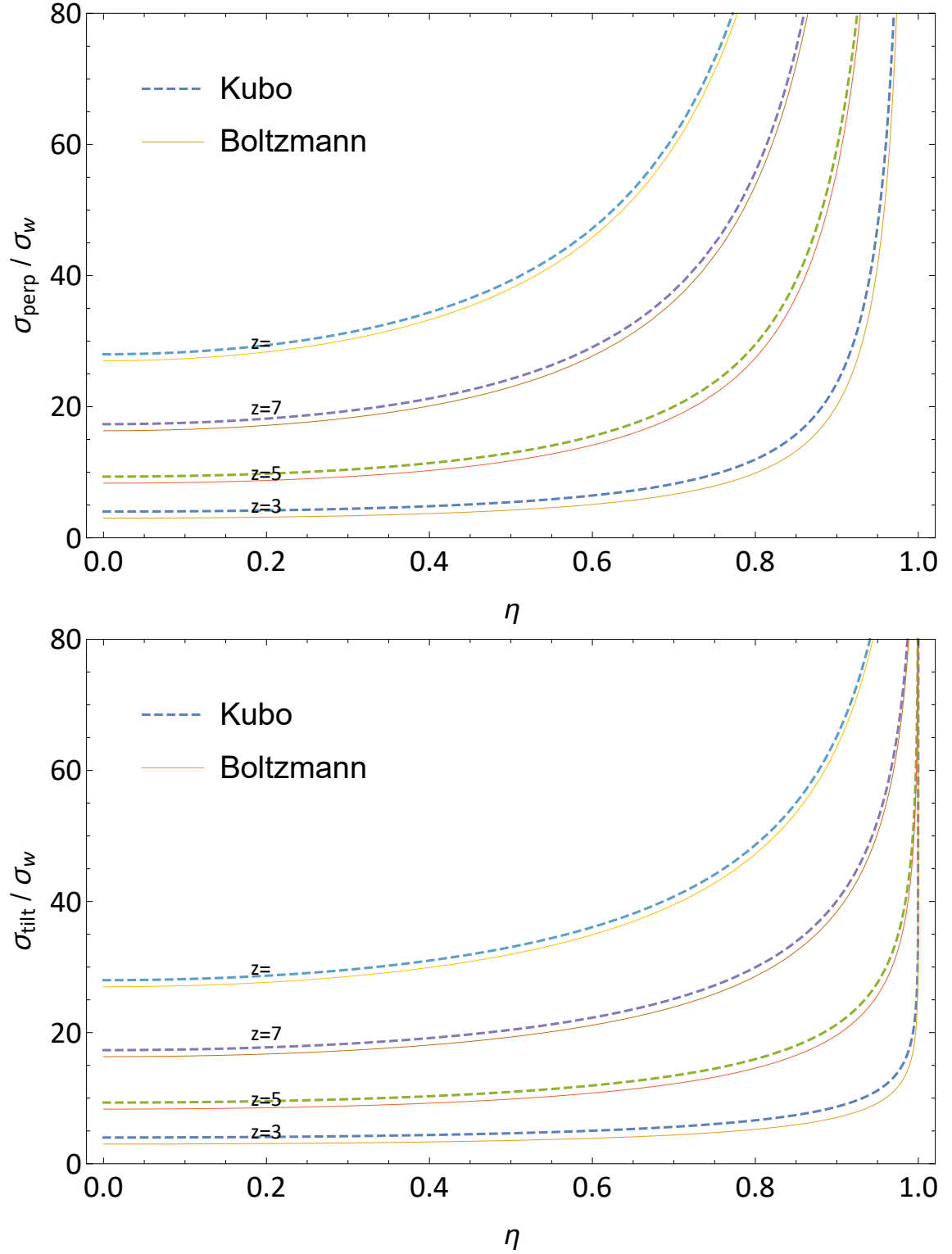


Figure 4.6: (Color online) Conductivity of the tilted type-I WSM perpendicular and parallel to the tilt direction computed from the covariant Boltzmann equation (solid) and Kubo formula (dashed). The conductivities are expressed as a function of the tilt parameter for different values of the normalized energy z . The perpendicular conductivity enhances and diverges at critical value $\eta = 1$ while the parallel increases but stays finite in the critical limit.

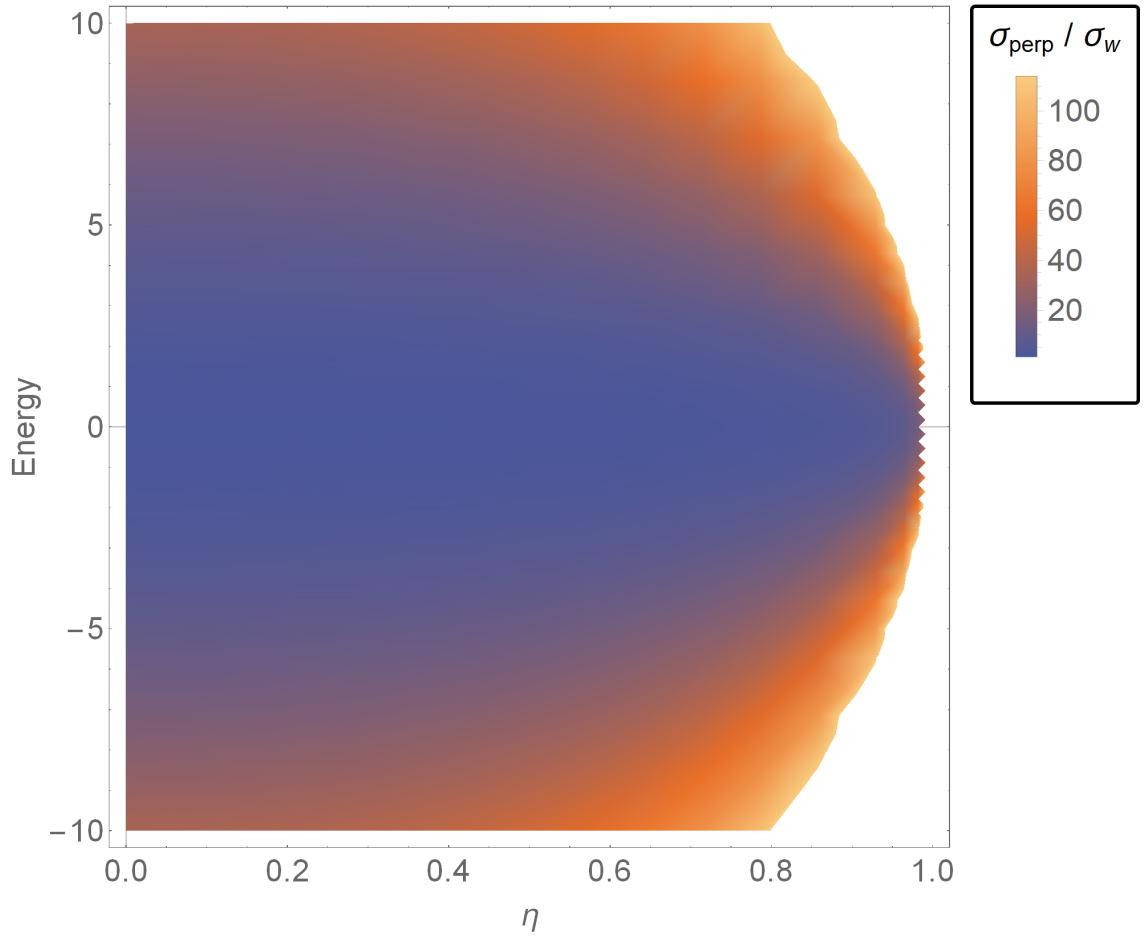


Figure 4.7: (Color online) Density plot of the normalized perpendicular conductivity in terms of the tilt degree and chemical energy.

the lab frame reads

$$g(\varepsilon, \eta) = \frac{\gamma^4}{2\pi^2} \frac{\varepsilon^2}{v_F^3}, \quad (4.78)$$

which is plotted in Fig. 4.8. One notices that the behavior of the DOS reflects indeed, as expected, that of the conductivities. However, we insist that our argument in terms of the DOS is qualitative and not sufficient to explain the anisotropy in the conductivities σ_{tilt} and σ_{perp} . Notice that the increase of the DOS as a function of the tilt parameter can be absorbed into a renormalized Fermi velocity (see Fig. 4.9), with

$$\frac{v_F^*}{v_F} = (1 - \eta^2)^{2/3}. \quad (4.79)$$

In general, the DOS can be calculated by counting the number of occupied states below an energy level. For the WSM having the dispersion (4.59) we obtain

$$\begin{aligned} g(\varepsilon) &= \sum_{\mathbf{k}}^{|k| < k_F} \delta(v_F k (\eta \cos \theta + \alpha) - \varepsilon_F) \\ &= \frac{\varepsilon^2}{4\pi^2 v_F^3} \int_0^\pi \frac{\sin \theta d\theta}{(\eta \cos \theta + \alpha)^3}. \end{aligned} \quad (4.80)$$

In the limit of $0 < \eta < 1$ this integral yields the same result (4.78) as that obtained from the covariance point of view.

4.5. Conclusion

In conclusion, we have studied the influence of the tilt in the dispersion of graphene (or two-dimensional graphene-like systems) and type-I WSM on the magneto-conductivity. The tilt can be described elegantly within a covariant framework of the Dirac equation since it can be viewed as an effective electric field that conspires with the magnetic field. In the case of type-I WSM with moderate tilts, $\eta < 1$, a Lorentz boost into the co-moving frame of reference characterized precisely by the tilt velocity v_0 allows one to get rid of the electric field – this is the co-called magnetic regime in electrodynamics. This relativistic effect, accompanied by a Lorentz transformation back to the lab frame, yields an increased conductivity that we have studied here within the covariant form of the Boltzmann transport equation both in two and three spatial dimensions. We have systematically compared the results of the conductivity from the covariant Boltzmann equation to calculations within the Kubo formula of linear response theory. Furthermore, the conductivities perpendicular to the tilt direction, calculated within the Boltzmann and Kubo approach, are enhanced by an extra factor, both in two- and in three-dimensional

cases, as compared to the direction parallel to the tilt. This demonstrates that transport in a tilted system becomes directional where $\sigma_{\text{tilt}} < \sigma_{\text{perp}}$. This smaller conductivity along the field direction (z -direction) agrees with the experimental evidence on the extremely large and nonsaturating longitudinal (z -direction) magnetoresistance reported on type-I WSM.

Our findings can qualitatively be understood with the help of the DOS, to which the conductivities are roughly proportional, within the simplified picture provided by Einstein's relation. The tilt enhances the DOS by some power of the relativistic Lorentz factor $\gamma = 1/\sqrt{1 - \eta^2}$, which generally enters the expressions, for the conductivities on the one hand and for the DOS, scattering time and effective Fermi velocity on the other hand. We further observe that the power of the Lorentz factor that enters in the expressions of the (surface) conductivities, depends on the orientation of the tilt with respect to that of the conductivity as well as on the system's spatial dimension. For the renormalization of the effective Fermi velocity, for example, we find $v_F^* = v_F \gamma^{-\beta}$ with $\beta_{2D} = 3/4$ and $\beta_{3D} = 2/3$. Thus measuring the ratio v_F^*/v_F experimentally would allow for an experimental determination of the tilt and its magnitude in a type-I WSM.

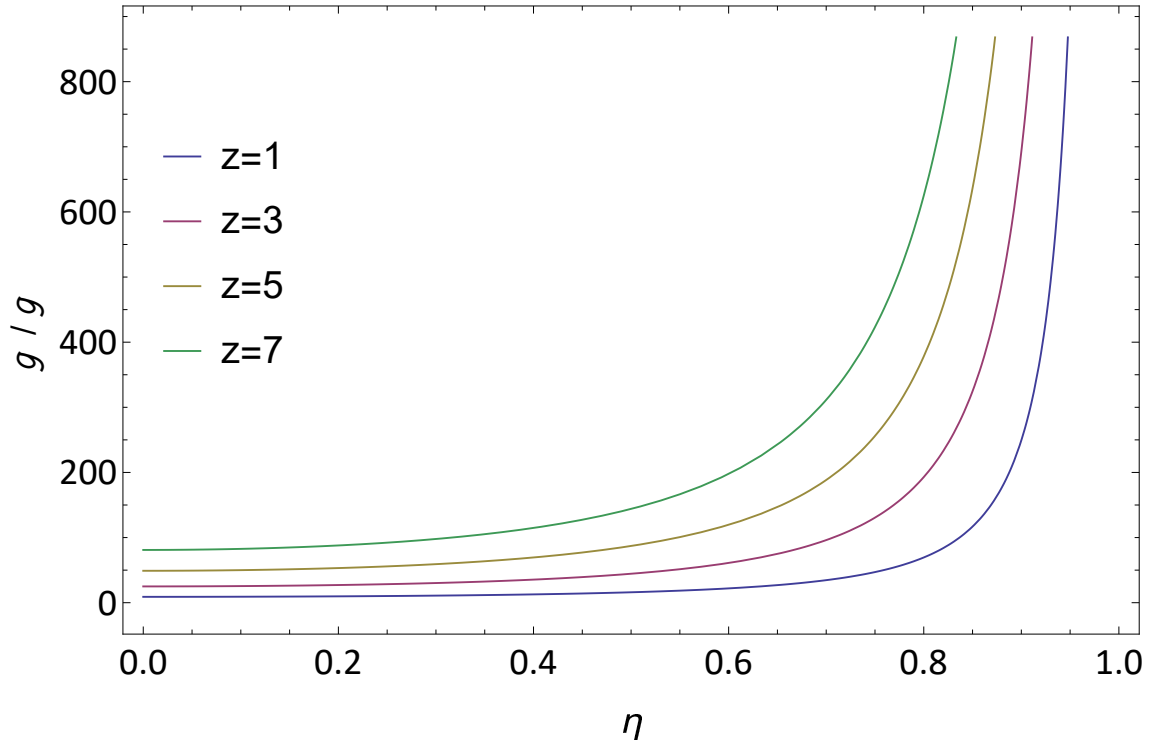


Figure 4.8: Increasing pattern of the normalized Density of states $g(z)/g_0$ of type-I WSM by the degree of tilting, $g_0 = \frac{\Gamma^2}{2\pi^2 v_F^3}$.

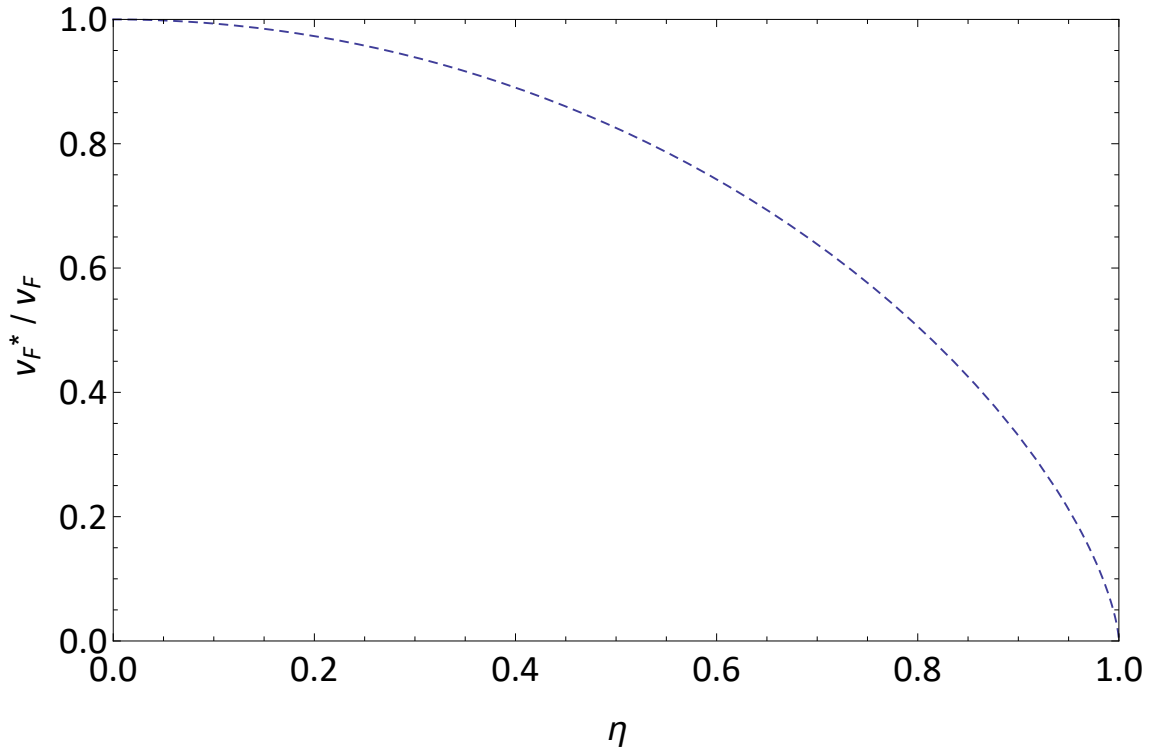


Figure 4.9: Renormalization of the Fermi velocity of type-I WSM with the tilted cone is a clear indication of the Lorentz violation.

Bibliography

- [1] B. Trauzettel, D. V. Bulaev, D. Loss, and G. Burkard, “Spin qubits in graphene quantum dots,” *Nature Physics*, vol. 3, no. 3, p. 192, 2007.
- [2] Z. Gong, G.-B. Liu, H. Yu, D. Xiao, X. Cui, X. Xu, and W. Yao, “Magnetoelectric effects and valley-controlled spin quantum gates in transition metal dichalcogenide bilayers,” *Nature communications*, vol. 4, p. 2053, 2013.
- [3] Y. Ye, J. Xiao, H. Wang, Z. Ye, H. Zhu, M. Zhao, Y. Wang, J. Zhao, X. Yin, and X. Zhang, “Electrical generation and control of the valley carriers in a monolayer transition metal dichalcogenide,” *Nature nanotechnology*, vol. 11, no. 7, p. 598, 2016.
- [4] X. Xu, W. Yao, D. Xiao, and T. F. Heinz, “Spin and pseudospins in layered transition metal dichalcogenides,” *Nature Physics*, vol. 10, no. 5, p. 343, 2014.
- [5] M. Gmitra and J. Fabian, “Graphene on transition-metal dichalcogenides: A platform for proximity spin-orbit physics and optospintronics,” *Phys. Rev. B*, vol. 92, p. 155403, Oct 2015.
- [6] D. Xiao, G.-B. Liu, W. Feng, X. Xu, and W. Yao, “Coupled spin and valley physics in monolayers of mos_2 and other group-vi dichalcogenides,” *Phys. Rev. Lett.*, vol. 108, p. 196802, May 2012.
- [7] J. Fabian, A. Matos-Abiague, C. Ertler, P. Stano, and I. Žutić, “Semiconductor spintronics,” *Acta Physica Slovaca. Reviews and Tutorials*, vol. 57, no. 4-5, pp. 565–907, 2007.
- [8] I. Žutić, J. Fabian, and S. Das Sarma, “Spintronics: Fundamentals and applications,” *Rev. Mod. Phys.*, vol. 76, pp. 323–410, Apr 2004.
- [9] A. H. Castro Neto and F. Guinea, “Impurity-induced spin-orbit coupling in graphene,” *Phys. Rev. Lett.*, vol. 103, p. 026804, Jul 2009.

- [10] L. Chico, M. P. López-Sancho, and M. C. Muñoz, “Curvature-induced anisotropic spin-orbit splitting in carbon nanotubes,” *Phys. Rev. B*, vol. 79, p. 235423, Jun 2009.
- [11] D. Gosálbez-Martínez, J. J. Palacios, and J. Fernández-Rossier, “Spin-orbit interaction in curved graphene ribbons,” *Phys. Rev. B*, vol. 83, p. 115436, Mar 2011.
- [12] A. Avsar, J. Y. Tan, T. Taychatanapat, J. Balakrishnan, G. Koon, Y. Yeo, J. Lahiri, A. Carvalho, A. Rodin, E. O’Farrell, *et al.*, “Spin–orbit proximity effect in graphene,” *Nature communications*, vol. 5, p. 4875, 2014.
- [13] M. Gmitra, D. Kochan, and J. Fabian, “Spin-orbit coupling in hydrogenated graphene,” *Phys. Rev. Lett.*, vol. 110, p. 246602, Jun 2013.
- [14] J. R. Schaibley, H. Yu, G. Clark, P. Rivera, J. S. Ross, K. L. Seyler, W. Yao, and X. Xu, “Valleytronics in 2d materials,” *Nature Reviews Materials*, vol. 1, no. 11, p. 16055, 2016.
- [15] D. Xiao, W. Yao, and Q. Niu, “Valley-contrasting physics in graphene: Magnetic moment and topological transport,” *Phys. Rev. Lett.*, vol. 99, p. 236809, Dec 2007.
- [16] J.-H. Chen, G. Autès, N. Alem, F. Gargiulo, A. Gautam, M. Linck, C. Kisielowski, O. V. Yazyev, S. G. Louie, and A. Zettl, “Controlled growth of a line defect in graphene and implications for gate-tunable valley filtering,” *Phys. Rev. B*, vol. 89, p. 121407, Mar 2014.
- [17] D. Gunlycke and C. T. White, “Graphene valley filter using a line defect,” *Phys. Rev. Lett.*, vol. 106, p. 136806, Mar 2011.
- [18] C. Weeks, J. Hu, J. Alicea, M. Franz, and R. Wu, “Engineering a robust quantum spin hall state in graphene via adatom deposition,” *Phys. Rev. X*, vol. 1, p. 021001, Oct 2011.
- [19] A. Pachoud, A. Ferreira, B. Özyilmaz, and A. H. Castro Neto, “Scattering theory of spin-orbit active adatoms on graphene,” *Phys. Rev. B*, vol. 90, p. 035444, Jul 2014.
- [20] S. Abdelouahed, A. Ernst, J. Henk, I. V. Maznichenko, and I. Mertig, “Spin-split electronic states in graphene: Effects due to lattice deformation, rashba effect, and adatoms by first principles,” *Phys. Rev. B*, vol. 82, p. 125424, Sep 2010.

- [21] J. Ding, Z. Qiao, W. Feng, Y. Yao, and Q. Niu, “Engineering quantum anomalous/valley hall states in graphene via metal-atom adsorption: An ab-initio study,” *Phys. Rev. B*, vol. 84, p. 195444, Nov 2011.
- [22] Y. Ren, X. Deng, Z. Qiao, C. Li, J. Jung, C. Zeng, Z. Zhang, and Q. Niu, “Single-valley engineering in graphene superlattices,” *Phys. Rev. B*, vol. 91, p. 245415, Jun 2015.
- [23] V. Cheianov, V. Fal’ko, O. Syljuåsen, and B. Altshuler, “Hidden kekulé ordering of adatoms on graphene,” *Solid State Communications*, vol. 149, no. 37-38, pp. 1499–1501, 2009.
- [24] S. Datta, *Electronic transport in mesoscopic systems*. Cambridge university press, 1997.
- [25] F. A. Buot, “Mesoscopic physics and nanoelectronics: nanoscience and nanotechnology,” *Physics Reports*, vol. 234, no. 2-3, pp. 73–174, 1993.
- [26] R. L. Liboff, *Kinetic theory: classical, quantum, and relativistic descriptions*. Springer Science & Business Media, 2003.
- [27] F. T. Vasko and O. E. Raichev, *Quantum Kinetic Theory and Applications: Electrons, Photons, Phonons*. Springer Science & Business Media, 2006.
- [28] M. Bonitz, *Quantum kinetic theory*. Springer, 2016.
- [29] W. Lu and C. M. Lieber, “Nanoelectronics from the bottom up,” in *Nanoscience And Technology: A Collection of Reviews from Nature Journals*, pp. 137–146, World Scientific, 2010.
- [30] R. Waser *et al.*, *Nanoelectronics and information technology*. Wiley Online Library, 2003.
- [31] Y. Tokura, M. Kawasaki, and N. Nagaosa, “Emergent functions of quantum materials,” *Nature Physics*, vol. 13, no. 11, p. 1056, 2017.
- [32] A. Soumyanarayanan, N. Reyren, A. Fert, and C. Panagopoulos, “Emergent phenomena induced by spin–orbit coupling at surfaces and interfaces,” *Nature*, vol. 539, no. 7630, p. 509, 2016.
- [33] W. A. Harrison, *Elementary Electronic Structure: Revised*. World Scientific Publishing Company, 2004.

- [34] O. K. Andersen and O. Jepsen, “Explicit, first-principles tight-binding theory,” *Phys. Rev. Lett.*, vol. 53, pp. 2571–2574, Dec 1984.
- [35] D. Sanchez-Portal, E. Artacho, and J. M. Soler, “Projection of plane-wave calculations into atomic orbitals,” *Solid State Communications*, vol. 95, no. 10, pp. 685–690, 1995.
- [36] N. Marzari, A. A. Mostofi, J. R. Yates, I. Souza, and D. Vanderbilt, “Maximally localized wannier functions: Theory and applications,” *Rev. Mod. Phys.*, vol. 84, pp. 1419–1475, Oct 2012.
- [37] I. Paul and G. Kotliar, “Thermal transport for many-body tight-binding models,” *Phys. Rev. B*, vol. 67, p. 115131, Mar 2003.
- [38] C. Bena and G. Montambaux, “Remarks on the tight-binding model of graphene,” *New Journal of Physics*, vol. 11, no. 9, p. 095003, 2009.
- [39] G. M. Maksimova, V. Y. Demikhovskii, and E. V. Frolova, “Wave packet dynamics in a monolayer graphene,” *Phys. Rev. B*, vol. 78, p. 235321, Dec 2008.
- [40] J. Jung and A. H. MacDonald, “Tight-binding model for graphene π -bands from maximally localized wannier functions,” *Phys. Rev. B*, vol. 87, p. 195450, May 2013.
- [41] S. Konschuh, M. Gmitra, and J. Fabian, “Tight-binding theory of the spin-orbit coupling in graphene,” *Phys. Rev. B*, vol. 82, p. 245412, Dec 2010.
- [42] V. Gusynin, S. Sharapov, and J. Carbotte, “Ac conductivity of graphene: from tight-binding model to 2+ 1-dimensional quantum electrodynamics,” *International Journal of Modern Physics B*, vol. 21, no. 27, pp. 4611–4658, 2007.
- [43] V. M. Pereira, A. H. Castro Neto, and N. M. R. Peres, “Tight-binding approach to uniaxial strain in graphene,” *Phys. Rev. B*, vol. 80, p. 045401, Jul 2009.
- [44] S. Reich, J. Maultzsch, C. Thomsen, and P. Ordejón, “Tight-binding description of graphene,” *Phys. Rev. B*, vol. 66, p. 035412, Jul 2002.
- [45] A. C. Neto, F. Guinea, N. M. Peres, K. S. Novoselov, and A. K. Geim, “The electronic properties of graphene,” *Reviews of modern physics*, vol. 81, no. 1, p. 109, 2009.

- [46] A. R. Akhmerov and C. W. J. Beenakker, “Detection of valley polarization in graphene by a superconducting contact,” *Phys. Rev. Lett.*, vol. 98, p. 157003, Apr 2007.
- [47] D. Huertas-Hernando, F. Guinea, and A. Brataas, “Spin-orbit-mediated spin relaxation in graphene,” *Phys. Rev. Lett.*, vol. 103, p. 146801, Sep 2009.
- [48] C. Ertler, S. Konschuh, M. Gmitra, and J. Fabian, “Electron spin relaxation in graphene: The role of the substrate,” *Phys. Rev. B*, vol. 80, p. 041405, Jul 2009.
- [49] N. Tombros, C. Jozsa, M. Popinciuc, H. T. Jonkman, and B. J. Van Wees, “Electronic spin transport and spin precession in single graphene layers at room temperature,” *Nature*, vol. 448, no. 7153, p. 571, 2007.
- [50] N. Tombros, S. Tanabe, A. Veligura, C. Jozsa, M. Popinciuc, H. Jonkman, and B. Van Wees, “Anisotropic spin relaxation in graphene,” *Physical review letters*, vol. 101, no. 4, p. 046601, 2008.
- [51] D. Kochan, M. Gmitra, and J. Fabian, “Spin relaxation mechanism in graphene: Resonant scattering by magnetic impurities,” *Phys. Rev. Lett.*, vol. 112, p. 116602, Mar 2014.
- [52] R. G. Mani, J. Hankinson, C. Berger, and W. A. De Heer, “Observation of resistively detected hole spin resonance and zero-field pseudo-spin splitting in epitaxial graphene,” *Nature communications*, vol. 3, p. 996, 2012.
- [53] K. Pi, W. Han, K. McCreary, A. Swartz, Y. Li, and R. Kawakami, “Manipulation of spin transport in graphene by surface chemical doping,” *Physical review letters*, vol. 104, no. 18, p. 187201, 2010.
- [54] H. Min, J. E. Hill, N. A. Sinitsyn, B. R. Sahu, L. Kleinman, and A. H. MacDonald, “Intrinsic and rashba spin-orbit interactions in graphene sheets,” *Phys. Rev. B*, vol. 74, p. 165310, Oct 2006.
- [55] H. Ochoa, A. H. Castro Neto, and F. Guinea, “Elliot-yafet mechanism in graphene,” *Phys. Rev. Lett.*, vol. 108, p. 206808, May 2012.
- [56] C. L. Kane and E. J. Mele, “Quantum spin hall effect in graphene,” *Phys. Rev. Lett.*, vol. 95, p. 226801, Nov 2005.
- [57] D. Ma, Z. Li, and Z. Yang, “Strong spin–orbit splitting in graphene with adsorbed au atoms,” *Carbon*, vol. 50, no. 1, pp. 297–305, 2012.

- [58] J. Balakrishnan, G. K. W. Koon, M. Jaiswal, A. C. Neto, and B. Özyilmaz, “Colossal enhancement of spin–orbit coupling in weakly hydrogenated graphene,” *Nature Physics*, vol. 9, no. 5, p. 284, 2013.
- [59] L. Brey, “Spin-orbit coupling in graphene induced by adatoms with outer-shell p orbitals,” *Phys. Rev. B*, vol. 92, p. 235444, Dec 2015.
- [60] B. Uchoa, L. Yang, S.-W. Tsai, N. M. R. Peres, and A. H. Castro Neto, “Theory of scanning tunneling spectroscopy of magnetic adatoms in graphene,” *Phys. Rev. Lett.*, vol. 103, p. 206804, Nov 2009.
- [61] A. Cresti, B. K. Nikolić, J. H. García, and S. Roche, “Charge, spin and valley hall effects in disordered graphene,” *arXiv preprint arXiv:1610.09917*, 2016.
- [62] A. W. Cummings, J. H. Garcia, J. Fabian, and S. Roche, “Giant spin lifetime anisotropy in graphene induced by proximity effects,” *Phys. Rev. Lett.*, vol. 119, p. 206601, Nov 2017.
- [63] H. Zeng, G.-B. Liu, J. Dai, Y. Yan, B. Zhu, R. He, L. Xie, S. Xu, X. Chen, W. Yao, *et al.*, “Optical signature of symmetry variations and spin-valley coupling in atomically thin tungsten dichalcogenides,” *Scientific reports*, vol. 3, p. 1608, 2013.
- [64] D. Pesin and A. H. MacDonald, “Spintronics and pseudospintronics in graphene and topological insulators,” *Nature materials*, vol. 11, no. 5, p. 409, 2012.
- [65] A. Rycerz, J. Tworzydło, and C. Beenakker, “Valley filter and valley valve in graphene,” *Nature Physics*, vol. 3, no. 3, p. 172, 2007.
- [66] B. Soodchomshom, “Perfect spin-valley filter controlled by electric field in ferromagnetic silicene,” *Journal of Applied Physics*, vol. 115, no. 2, p. 023706, 2014.
- [67] M. M. Grujić, M. i. c. v. Tadić, and F. m. c. M. Peeters, “Spin-valley filtering in strained graphene structures with artificially induced carrier mass and spin-orbit coupling,” *Phys. Rev. Lett.*, vol. 113, p. 046601, Jul 2014.
- [68] H.-Z. Lu, W. Yao, D. Xiao, and S.-Q. Shen, “Intervalley scattering and localization behaviors of spin-valley coupled dirac fermions,” *Phys. Rev. Lett.*, vol. 110, p. 016806, Jan 2013.
- [69] A. K. Geim and K. S. Novoselov, “The rise of graphene,” in *Nanoscience and Technology: A Collection of Reviews from Nature Journals*, pp. 11–19, World Scientific, 2010.

- [70] M. Katsnelson, “Zitterbewegung, chirality, and minimal conductivity in graphene,” *The European Physical Journal B-Condensed Matter and Complex Systems*, vol. 51, no. 2, pp. 157–160, 2006.
- [71] K. Nomura and A. MacDonald, “Quantum transport of massless dirac fermions,” *Physical review letters*, vol. 98, no. 7, p. 076602, 2007.
- [72] S. V. Morozov, K. S. Novoselov, M. I. Katsnelson, F. Schedin, L. A. Ponomarenko, D. Jiang, and A. K. Geim, “Strong suppression of weak localization in graphene,” *Phys. Rev. Lett.*, vol. 97, p. 016801, Jul 2006.
- [73] E. McCann, K. Kechedzhi, V. I. Fal’ko, H. Suzuura, T. Ando, and B. Altshuler, “Weak-localization magnetoresistance and valley symmetry in graphene,” *Physical Review Letters*, vol. 97, no. 14, p. 146805, 2006.
- [74] H. Suzuura and T. Ando, “Crossover from symplectic to orthogonal class in a two-dimensional honeycomb lattice,” *Physical review letters*, vol. 89, no. 26, p. 266603, 2002.
- [75] P. Ostrovsky, I. Gornyi, and A. Mirlin, “Electron transport in disordered graphene,” *Physical Review B*, vol. 74, no. 23, p. 235443, 2006.
- [76] T. Ando, Y. Zheng, and H. Suzuura, “Dynamical conductivity and zero-mode anomaly in honeycomb lattices,” *Journal of the Physical Society of Japan*, vol. 71, no. 5, pp. 1318–1324, 2002.
- [77] N. Peres, F. Guinea, and A. C. Neto, “Electronic properties of disordered two-dimensional carbon,” *Physical Review B*, vol. 73, no. 12, p. 125411, 2006.
- [78] V. M. Pereira, J. Nilsson, and A. H. Castro Neto, “Coulomb impurity problem in graphene,” *Phys. Rev. Lett.*, vol. 99, p. 166802, Oct 2007.
- [79] Y.-W. Tan, Y. Zhang, K. Bolotin, Y. Zhao, S. Adam, E. H. Hwang, S. Das Sarma, H. L. Stormer, and P. Kim, “Measurement of scattering rate and minimum conductivity in graphene,” *Phys. Rev. Lett.*, vol. 99, p. 246803, Dec 2007.
- [80] C. Jang, S. Adam, J.-H. Chen, E. D. Williams, S. Das Sarma, and M. S. Fuhrer, “Tuning the effective fine structure constant in graphene: Opposing effects of dielectric screening on short- and long-range potential scattering,” *Phys. Rev. Lett.*, vol. 101, p. 146805, Oct 2008.

- [81] A. F. Morpurgo and F. Guinea, “Intervalley scattering, long-range disorder, and effective time-reversal symmetry breaking in graphene,” *Phys. Rev. Lett.*, vol. 97, p. 196804, Nov 2006.
- [82] A. Morpurgo and F. Guinea, “Intervalley scattering, long-range disorder, and effective time-reversal symmetry breaking in graphene,” *Physical review letters*, vol. 97, no. 19, p. 196804, 2006.
- [83] W. Kohn and J. M. Luttinger, “Quantum theory of electrical transport phenomena,” *Phys. Rev.*, vol. 108, pp. 590–611, Nov 1957.
- [84] J. M. Luttinger and W. Kohn, “Quantum theory of electrical transport phenomena. ii,” *Phys. Rev.*, vol. 109, pp. 1892–1909, Mar 1958.
- [85] J. Rammer, *Quantum field theory of non-equilibrium states*. Cambridge University Press, 2007.
- [86] T. Ando, “Screening effect and impurity scattering in monolayer graphene,” *Journal of the Physical Society of Japan*, vol. 75, no. 7, p. 074716, 2006.
- [87] E. G. Mishchenko, A. V. Shytov, and B. I. Halperin, “Spin current and polarization in impure two-dimensional electron systems with spin-orbit coupling,” *Phys. Rev. Lett.*, vol. 93, p. 226602, Nov 2004.
- [88] İ. Adagideli, M. Scheid, M. Wimmer, G. Bauer, and K. Richter, “Extracting current-induced spins: spin boundary conditions at narrow hall contacts,” *New Journal of Physics*, vol. 9, no. 10, p. 382, 2007.
- [89] A. A. Burkov and D. G. Hawthorn, “Spin and charge transport on the surface of a topological insulator,” *Phys. Rev. Lett.*, vol. 105, p. 066802, Aug 2010.
- [90] i. d. I. m. c. Adagideli and G. E. W. Bauer, “Intrinsic spin hall edges,” *Phys. Rev. Lett.*, vol. 95, p. 256602, Dec 2005.
- [91] E. G. Mishchenko and B. I. Halperin, “Transport equations for a two-dimensional electron gas with spin-orbit interaction,” *Phys. Rev. B*, vol. 68, p. 045317, Jul 2003.
- [92] A. A. Burkov, A. S. Núñez, and A. H. MacDonald, “Theory of spin-charge-coupled transport in a two-dimensional electron gas with rashba spin-orbit interactions,” *Phys. Rev. B*, vol. 70, p. 155308, Oct 2004.

- [93] Z. Liu, B. Zhou, Y. Zhang, Z. Wang, H. Weng, D. Prabhakaran, S.-K. Mo, Z. Shen, Z. Fang, X. Dai, *et al.*, “Discovery of a three-dimensional topological dirac semimetal, na₃bi,” *Science*, vol. 343, no. 6173, pp. 864–867, 2014.
- [94] N. P. Armitage, E. J. Mele, and A. Vishwanath, “Weyl and dirac semimetals in three-dimensional solids,” *Rev. Mod. Phys.*, vol. 90, p. 015001, Jan 2018.
- [95] S. M. Young, S. Zaheer, J. C. Y. Teo, C. L. Kane, E. J. Mele, and A. M. Rappe, “Dirac semimetal in three dimensions,” *Phys. Rev. Lett.*, vol. 108, p. 140405, Apr 2012.
- [96] S. Borisenko, Q. Gibson, D. Evtushinsky, V. Zabolotnyy, B. Büchner, and R. J. Cava, “Experimental realization of a three-dimensional dirac semimetal,” *Phys. Rev. Lett.*, vol. 113, p. 027603, Jul 2014.
- [97] A. A. Burkov and L. Balents, “Weyl semimetal in a topological insulator multi-layer,” *Phys. Rev. Lett.*, vol. 107, p. 127205, Sep 2011.
- [98] B. Q. Lv, H. M. Weng, B. B. Fu, X. P. Wang, H. Miao, J. Ma, P. Richard, X. C. Huang, L. X. Zhao, G. F. Chen, Z. Fang, X. Dai, T. Qian, and H. Ding, “Experimental discovery of weyl semimetal taas,” *Phys. Rev. X*, vol. 5, p. 031013, Jul 2015.
- [99] B. Lv, N. Xu, H. Weng, J. Ma, P. Richard, X. Huang, L. Zhao, G. Chen, C. Matt, F. Bisti, *et al.*, “Observation of weyl nodes in taas,” *Nature Physics*, vol. 11, no. 9, p. 724, 2015.
- [100] B. Yan and C. Felser, “Topological materials: Weyl semimetals,” *Annual Review of Condensed Matter Physics*, vol. 8, pp. 337–354, 2017.
- [101] M. Goerbig and G. Montambaux, *Dirac Fermions in Condensed Matter and Beyond*, pp. 25–53. Cham: Springer International Publishing, 2017.
- [102] S. Jia, S.-Y. Xu, and M. Z. Hasan, “Weyl semimetals, fermi arcs and chiral anomalies,” *Nature materials*, vol. 15, no. 11, p. 1140, 2016.
- [103] H. Nielsen and M. Ninomiya, “A no-go theorem for regularizing chiral fermions,” *Physics Letters B*, vol. 105, no. 2, pp. 219 – 223, 1981.
- [104] S.-Y. Xu, I. Belopolski, N. Alidoust, M. Neupane, G. Bian, C. Zhang, R. Sankar, G. Chang, Z. Yuan, C.-C. Lee, *et al.*, “Discovery of a weyl fermion semimetal and topological fermi arcs,” *Science*, vol. 349, no. 6248, pp. 613–617, 2015.

- [105] X. Wan, A. M. Turner, A. Vishwanath, and S. Y. Savrasov, “Topological semimetal and fermi-arc surface states in the electronic structure of pyrochlore iridates,” *Phys. Rev. B*, vol. 83, p. 205101, May 2011.
- [106] K. Deng, G. Wan, P. Deng, K. Zhang, S. Ding, E. Wang, M. Yan, H. Huang, H. Zhang, Z. Xu, J. Denlinger, A. Fedorov, H. Yang, W. Duan, H. Yao, Y. Wu, S. Fan, H. Zhang, X. Chen, and S. Zhou, “Experimental observation of topological fermi arcs in type-II weyl semimetal MoTe₂,” *Nature Physics*, vol. 12, pp. 1105–1110, sep 2016.
- [107] Y. Wu, D. Mou, N. H. Jo, K. Sun, L. Huang, S. L. Bud’ko, P. C. Canfield, and A. Kaminski, “Observation of fermi arcs in the type-ii weyl semimetal candidate wte₂,” *Phys. Rev. B*, vol. 94, p. 121113, Sep 2016.
- [108] C. Wang, Y. Zhang, J. Huang, S. Nie, G. Liu, A. Liang, Y. Zhang, B. Shen, J. Liu, C. Hu, Y. Ding, D. Liu, Y. Hu, S. He, L. Zhao, L. Yu, J. Hu, J. Wei, Z. Mao, Y. Shi, X. Jia, F. Zhang, S. Zhang, F. Yang, Z. Wang, Q. Peng, H. Weng, X. Dai, Z. Fang, Z. Xu, C. Chen, and X. J. Zhou, “Observation of fermi arc and its connection with bulk states in the candidate type-ii weyl semimetal wte₂,” *Phys. Rev. B*, vol. 94, p. 241119, Dec 2016.
- [109] H. Weyl, “Elektron und gravitation. i,” *Zeitschrift fur Physik*, vol. 56, pp. 330–352, May 1929.
- [110] A. A. Zyuzin, S. Wu, and A. A. Burkov, “Weyl semimetal with broken time reversal and inversion symmetries,” *Phys. Rev. B*, vol. 85, p. 165110, Apr 2012.
- [111] S. L. Adler, “Axial-vector vertex in spinor electrodynamics,” *Phys. Rev.*, vol. 177, pp. 2426–2438, Jan 1969.
- [112] X. Huang, L. Zhao, Y. Long, P. Wang, D. Chen, Z. Yang, H. Liang, M. Xue, H. Weng, Z. Fang, X. Dai, and G. Chen, “Observation of the chiral-anomaly-induced negative magnetoresistance in 3d weyl semimetal taas,” *Phys. Rev. X*, vol. 5, p. 031023, Aug 2015.
- [113] A. A. Zyuzin and A. A. Burkov, “Topological response in weyl semimetals and the chiral anomaly,” *Phys. Rev. B*, vol. 86, p. 115133, Sep 2012.
- [114] C.-L. Zhang, S.-Y. Xu, I. Belopolski, Z. Yuan, Z. Lin, B. Tong, G. Bian, N. Ali-doust, C.-C. Lee, S.-M. Huang, *et al.*, “Signatures of the adler–bell–jackiw chiral

- anomaly in a weyl fermion semimetal,” *Nature communications*, vol. 7, p. 10735, 2016.
- [115] D. T. Son and B. Z. Spivak, “Chiral anomaly and classical negative magnetoresistance of weyl metals,” *Phys. Rev. B*, vol. 88, p. 104412, Sep 2013.
 - [116] Q. Li, D. E. Kharzeev, C. Zhang, Y. Huang, I. Pletikosić, A. Fedorov, R. Zhong, J. Schneeloch, G. Gu, and T. Valla, “Chiral magnetic effect in zrt 5,” *Nature Physics*, vol. 12, no. 6, p. 550, 2016.
 - [117] J. Xiong, S. K. Kushwaha, T. Liang, J. W. Krizan, W. Wang, R. Cava, and N. Ong, “Signature of the chiral anomaly in a dirac semimetal: a current plume steered by a magnetic field,” *arXiv preprint arXiv:1503.08179*, 2015.
 - [118] M. A. Stephanov and Y. Yin, “Chiral kinetic theory,” *Phys. Rev. Lett.*, vol. 109, p. 162001, Oct 2012.
 - [119] N. Yamamoto, “Generalized bloch theorem and chiral transport phenomena,” *Phys. Rev. D*, vol. 92, p. 085011, Oct 2015.
 - [120] G. m. c. Başar, D. E. Kharzeev, and H.-U. Yee, “Triangle anomaly in weyl semimetals,” *Phys. Rev. B*, vol. 89, p. 035142, Jan 2014.
 - [121] D. Culcer, E. H. Hwang, T. D. Stanescu, and S. Das Sarma, “Two-dimensional surface charge transport in topological insulators,” *Phys. Rev. B*, vol. 82, p. 155457, Oct 2010.
 - [122] D. Culcer, A. Sekine, and A. H. MacDonald, “Interband coherence response to electric fields in crystals: Berry-phase contributions and disorder effects,” *Phys. Rev. B*, vol. 96, p. 035106, Jul 2017.
 - [123] R. Shindou and L. Balents, “Gradient expansion approach to multiple-band fermi liquids,” *Phys. Rev. B*, vol. 77, p. 035110, Jan 2008.
 - [124] C. H. Wong and Y. Tserkovnyak, “Quantum kinetic equation in phase-space textured multiband systems,” *Phys. Rev. B*, vol. 84, p. 115209, Sep 2011.
 - [125] G. Sundaram and Q. Niu, “Wave-packet dynamics in slowly perturbed crystals: Gradient corrections and berry-phase effects,” *Phys. Rev. B*, vol. 59, pp. 14915–14925, Jun 1999.

- [126] J. Ma and D. A. Pesin, “Chiral magnetic effect and natural optical activity in metals with or without weyl points,” *Phys. Rev. B*, vol. 92, p. 235205, Dec 2015.
- [127] M.-C. Chang and M.-F. Yang, “Chiral magnetic effect in a two-band lattice model of weyl semimetal,” *Phys. Rev. B*, vol. 91, p. 115203, Mar 2015.
- [128] M. Nakahara, *Geometry, topology and physics*. CRC Press, 2003.
- [129] A. Bohm, A. Mostafazadeh, H. Koizumi, Q. Niu, and J. Zwanziger, *The geometric phase in quantum systems: foundations, mathematical concepts, and applications in molecular and condensed matter physics*. Springer Science & Business Media, 2013.
- [130] D. T. Son and N. Yamamoto, “Berry curvature, triangle anomalies, and the chiral magnetic effect in fermi liquids,” *Phys. Rev. Lett.*, vol. 109, p. 181602, Nov 2012.
- [131] X. Huang, L. Zhao, Y. Long, P. Wang, D. Chen, Z. Yang, H. Liang, M. Xue, H. Weng, Z. Fang, X. Dai, and G. Chen, “Observation of the chiral-anomaly-induced negative magnetoresistance in 3d weyl semimetal taas,” *Phys. Rev. X*, vol. 5, p. 031023, Aug 2015.
- [132] P. E. C. Ashby and J. P. Carbotte, “Chiral anomaly and optical absorption in weyl semimetals,” *Phys. Rev. B*, vol. 89, p. 245121, Jun 2014.
- [133] E. V. Gorbar, V. A. Miransky, and I. A. Shovkovy, “Chiral anomaly, dimensional reduction, and magnetoresistivity of weyl and dirac semimetals,” *Phys. Rev. B*, vol. 89, p. 085126, Feb 2014.
- [134] A. Kobayashi, S. Katayama, Y. Suzumura, and H. Fukuyama, “Massless fermions in organic conductor,” *Journal of the Physical Society of Japan*, vol. 76, no. 3, p. 034711, 2007.
- [135] H. Fukuyama, “Anomalous orbital magnetism and hall effect of massless fermions in two dimension,” *Journal of the Physical Society of Japan*, vol. 76, no. 4, p. 043711, 2007.
- [136] M. O. Goerbig, J.-N. Fuchs, G. Montambaux, and F. Piéchon, “Tilted anisotropic dirac cones in quinoid-type graphene and α -(BEDT-TTF)₂I₃,” *Phys. Rev. B*, vol. 78, p. 045415, Jul 2008.

- [137] J. Sári, C. Tóke, and M. O. Goerbig, “Magnetoplasmons of the tilted anisotropic dirac cone material $\alpha - (\text{bedt} - \text{ttf})_2\text{i}_3$,” *Phys. Rev. B*, vol. 90, p. 155446, Oct 2014.
- [138] J. Sári, M. O. Goerbig, and C. Tóke, “Magneto-optics of quasirelativistic electrons in graphene with an inplane electric field and in tilted dirac cones in $\alpha - (\text{BEDT TTF})_2\text{i}_3$,” *Phys. Rev. B*, vol. 92, p. 035306, Jul 2015.
- [139] A. A. Soluyanov, D. Gresch, Z. Wang, Q. Wu, M. Troyer, X. Dai, and B. A. Bernevig, “Type-II weyl semimetals,” *Nature*, vol. 527, pp. 495–498, nov 2015.
- [140] L. Huang, T. M. McCormick, M. Ochi, Z. Zhao, M.-T. Suzuki, R. Arita, Y. Wu, D. Mou, H. Cao, J. Yan, N. Trivedi, and A. Kaminski, “Spectroscopic evidence for a type II weyl semimetallic state in MoTe₂,” *Nature Materials*, vol. 15, pp. 1155–1160, jul 2016.
- [141] S.-Y. Xu, N. Alidoust, G. Chang, H. Lu, B. Singh, I. Belopolski, D. S. Sanchez, X. Zhang, G. Bian, H. Zheng, M.-A. Hsuan, Y. Bian, S.-M. Huang, C.-H. Hsu, T.-R. Chang, H.-T. Jeng, A. Bansil, T. Neupert, V. N. Strocov, H. Lin, S. Jia, and M. Z. Hasan, “Discovery of lorentz-violating type ii weyl fermions in laalge,” *Science Advances*, vol. 3, no. 6, 2017.
- [142] N. Xu, Z. Wang, A. Weber, A. Magrez, P. Bugnon, H. Berger, C. Matt, J. Ma, B. Fu, B. Lv, *et al.*, “Discovery of weyl semimetal state violating lorentz invariance in mote₂,” *arXiv preprint arXiv:1604.02116*, 2016.
- [143] A. Liang, J. Huang, S. Nie, Y. Ding, Q. Gao, C. Hu, S. He, Y. Zhang, C. Wang, B. Shen, *et al.*, “Electronic evidence for type ii weyl semimetal state in mote₂,” *arXiv preprint arXiv:1604.01706*, 2016.
- [144] K. Koepnik, D. Kasinathan, D. V. Efremov, S. Khim, S. Borisenko, B. Büchner, and J. van den Brink, “ TaIrTe_4 : A ternary type-ii weyl semimetal,” *Phys. Rev. B*, vol. 93, p. 201101, May 2016.
- [145] G. Autes, D. Gresch, M. Troyer, A. A. Soluyanov, and O. V. Yazyev, “Robust type-ii weyl semimetal phase in transition metal diphosphides x p_2 ($\text{x} = \text{mo}, \text{w}$),” *Physical review letters*, vol. 117, no. 6, p. 066402, 2016.
- [146] L. Muechler, A. Alexandradinata, T. Neupert, and R. Car, “Topological nonsymmorphic metals from band inversion,” *Physical Review X*, vol. 6, no. 4, p. 041069, 2016.

- [147] T. M. McCormick, I. Kimchi, and N. Trivedi, “Minimal models for topological weyl semimetals,” *Physical Review B*, vol. 95, no. 7, p. 075133, 2017.
- [148] M. N. Ali, J. Xiong, S. Flynn, J. Tao, Q. D. Gibson, L. M. Schoop, T. Liang, N. Hal-dolaarachchige, M. Hirschberger, N. Ong, *et al.*, “Large, non-saturating magnetore-sistance in wte 2,” *Nature*, vol. 514, no. 7521, p. 205, 2014.
- [149] N. Kumar, Y. Sun, N. Xu, K. Manna, M. Yao, V. Süß, I. Leermakers, O. Young, T. Förster, M. Schmidt, *et al.*, “Extremely high magnetoresistance and conductivity in the type-ii weyl semimetals wp 2 and mop 2,” *Nature Communications*, vol. 8, no. 1, p. 1642, 2017.
- [150] Y. Wang, E. Liu, H. Liu, Y. Pan, L. Zhang, J. Zeng, Y. Fu, M. Wang, K. Xu, Z. Huang, *et al.*, “Gate-tunable negative longitudinal magnetoresistance in the pre-dicted type-ii weyl semimetal wte 2,” *Nature communications*, vol. 7, p. 13142, 2016.
- [151] Y.-Y. Lv, X. Li, B.-B. Zhang, W. Y. Deng, S.-H. Yao, Y. B. Chen, J. Zhou, S.-T. Zhang, M.-H. Lu, L. Zhang, M. Tian, L. Sheng, and Y.-F. Chen, “Experimen-tal observation of anisotropic adler-bell-jackiw anomaly in type-ii weyl semimetal wte_{1.98} crystals at the quasiclassical regime,” *Phys. Rev. Lett.*, vol. 118, p. 096603, Mar 2017.
- [152] A. A. Zyuzin and R. P. Tiwari, “Intrinsic anomalous hall effect in type-ii weyl semimetals,” *JETP letters*, vol. 103, no. 11, pp. 717–722, 2016.
- [153] T. M. McCormick, R. C. McKay, and N. Trivedi, “Semiclassical theory of anoma-lous transport in type-ii topological weyl semimetals,” *Physical Review B*, vol. 96, no. 23, p. 235116, 2017.
- [154] S. Saha and S. Tewari, “Anomalous nernst effect in type-ii weyl semimetals,” *The European Physical Journal B*, vol. 91, no. 1, p. 4, 2018.
- [155] Y. Ferreiros, A. A. Zyuzin, and J. H. Bardarson, “Anomalous nernst and thermal hall effects in tilted weyl semimetals,” *Phys. Rev. B*, vol. 96, p. 115202, Sep 2017.
- [156] S. P. Mukherjee and J. P. Carbotte, “Absorption of circular polarized light in tilted type-i and type-ii weyl semimetals,” *Phys. Rev. B*, vol. 96, p. 085114, Aug 2017.
- [157] Z.-M. Yu, Y. Yao, and S. A. Yang, “Predicted unusual magnetoresponse in type-ii weyl semimetals,” *Physical review letters*, vol. 117, no. 7, p. 077202, 2016.

- [158] T. E. O'Brien, M. Diez, and C. W. J. Beenakker, "Magnetic breakdown and klein tunneling in a type-ii weyl semimetal," *Phys. Rev. Lett.*, vol. 116, p. 236401, Jun 2016.
- [159] V. Arjona, E. V. Castro, and M. A. H. Vozmediano, "Collapse of landau levels in weyl semimetals," *Phys. Rev. B*, vol. 96, p. 081110(R), Aug 2017.
- [160] S. Tchoumakov, M. Civelli, and M. O. Goerbig, "Magnetic-field-induced relativistic properties in type-i and type-ii weyl semimetals," *Physical review letters*, vol. 117, no. 8, p. 086402, 2016.
- [161] S. Tchoumakov, M. Civelli, and M. O. Goerbig, "Magnetic description of the fermi arc in type-i and type-ii weyl semimetals," *Physical Review B*, vol. 95, no. 12, p. 125306, 2017.
- [162] V. Lukose, R. Shankar, and G. Baskaran, "Novel electric field effects on landau levels in graphene," *Physical review letters*, vol. 98, no. 11, p. 116802, 2007.
- [163] N. Peres and E. V. Castro, "Algebraic solution of a graphene layer in transverse electric and perpendicular magnetic fields," *Journal of Physics: Condensed Matter*, vol. 19, no. 40, p. 406231, 2007.
- [164] M. O. Goerbig, J.-N. Fuchs, G. Montambaux, and F. Piéchon, "Electric-field-induced lifting of the valley degeneracy in α -(BEDT-TTF)₂I₃ dirac-like landau levels," *EPL (Europhysics Letters)*, vol. 85, p. 57005, mar 2009.
- [165] C. Shekhar, A. K. Nayak, Y. Sun, M. Schmidt, M. Nicklas, I. Leermakers, U. Zeitler, Y. Skourski, J. Wosnitza, Z. Liu, *et al.*, "Extremely large magnetoresistance and ultrahigh mobility in the topological weyl semimetal candidate nbp," *Nature Physics*, vol. 11, no. 8, p. 645, 2015.
- [166] C. Cercignani and G. M. Kremer, "Relativistic boltzmann equation," in *The Relativistic Boltzmann Equation: Theory and Applications*, pp. 31–63, Springer, 2002.
- [167] S. R. De Groot, "On relativistic kinetic theory," in *Fundamental problems in statistical mechanics. Volume 5*, 1980.
- [168] J. Anderson and H. Witting, "A relativistic relaxation-time model for the boltzmann equation," *Physica*, vol. 74, no. 3, pp. 466–488, 1974.
- [169] F. Jüttner, "Das maxwellsche gesetz der geschwindigkeitsverteilung in der relativtheorie," *Annalen der Physik*, vol. 339, no. 5, pp. 856–882, 1911.

- [170] S. Weinberg, *The quantum theory of fields. Vol. 1: Foundations*. Cambridge University Press, 1995.
- [171] A. Puglisi, S. Plumari, and V. Greco, “Electric conductivity from the solution of the relativistic boltzmann equation,” *Phys. Rev. D*, vol. 90, p. 114009, Dec 2014.
- [172] M. O. Goerbig, “Electronic properties of graphene in a strong magnetic field,” *Rev. Mod. Phys.*, vol. 83, pp. 1193–1243, Nov 2011.
- [173] A. Kretinin, G. L. Yu, R. Jalil, Y. Cao, F. Withers, A. Mishchenko, M. I. Katsnelson, K. S. Novoselov, A. K. Geim, and F. Guinea, “Quantum capacitance measurements of electron-hole asymmetry and next-nearest-neighbor hopping in graphene,” *Phys. Rev. B*, vol. 88, p. 165427, Oct 2013.
- [174] T. Morinari, T. Himura, and T. Tohyama, “Possible verification of tilted anisotropic dirac cone in α -(bedt-ttf) $2i3$ using interlayer magnetoresistance,” *Journal of the Physical Society of Japan*, vol. 78, no. 2, pp. 023704–023704, 2009.
- [175] T. Stauber, N. M. R. Peres, and F. Guinea, “Electronic transport in graphene: A semiclassical approach including midgap states,” *Phys. Rev. B*, vol. 76, p. 205423, Nov 2007.
- [176] K. Ziegler, “Minimal conductivity of graphene: Nonuniversal values from the kubo formula,” *Physical Review B*, vol. 75, no. 23, p. 233407, 2007.
- [177] E. Akkermans and G. Montambaux, *Mesoscopic physics of electrons and photons*. Cambridge university press, 2007.
- [178] Y. Suzumura, I. Proskurin, and M. Ogata, “Effect of tilting on the in-plane conductivity of dirac electrons in organic conductor,” *Journal of the Physical Society of Japan*, vol. 83, no. 2, p. 023701, 2013.
- [179] S.-M. Choi, S.-H. Jhi, and Y.-W. Son, “Effects of strain on electronic properties of graphene,” *Phys. Rev. B*, vol. 81, p. 081407, Feb 2010.
- [180] T. Cheng, H. Lang, Z. Li, Z. Liu, and Z. Liu, “Anisotropic carrier mobility in two-dimensional materials with tilted dirac cones: theory and application,” *Physical Chemistry Chemical Physics*, vol. 19, no. 35, pp. 23942–23950, 2017.
- [181] K.-S. Kim, H.-J. Kim, and M. Sasaki, “Boltzmann equation approach to anomalous transport in a weyl metal,” *Physical Review B*, vol. 89, no. 19, p. 195137, 2014.

- [182] A. A. Burkov, M. D. Hook, and L. Balents, “Topological nodal semimetals,” *Phys. Rev. B*, vol. 84, p. 235126, Dec 2011.
- [183] R. Lundgren, P. Laurell, and G. A. Fiete, “Thermoelectric properties of weyl and dirac semimetals,” *Physical Review B*, vol. 90, no. 16, p. 165115, 2014.
- [184] P. Hosur, S. A. Parameswaran, and A. Vishwanath, “Charge transport in weyl semimetals,” *Phys. Rev. Lett.*, vol. 108, p. 046602, Jan 2012.
- [185] C. J. Tabert, J. P. Carbotte, and E. J. Nicol, “Optical and transport properties in three-dimensional dirac and weyl semimetals,” *Phys. Rev. B*, vol. 93, p. 085426, Feb 2016.
- [186] R. B. Dingle and R. Dingle, *Asymptotic expansions: their derivation and interpretation*, vol. 48. Academic Press London, 1973.

Appendix A

COHERENT DYNAMICS OF DIRAC PARTICLES IN GRAPHENE

A.1. Tightbinding of the Dirac Hamiltonian

The orbital motion of an electron in the honeycomb lattice of graphene is approximated by the bare hopping Hamiltonian (where we use the units $\hbar = 1$)

$$H_0 = t \sum_{\mathbf{r}_i, \boldsymbol{\delta}_j} (|\mathbf{r}_i\rangle\langle\mathbf{r}_i + \boldsymbol{\delta}_j| + \text{h.c.}), \quad (\text{A.1})$$

where $|\mathbf{r}_i\rangle$ and $|\mathbf{r}_i + \boldsymbol{\delta}_j\rangle$ represent the orthogonal basis comprised of the single electronic π -orbitals in sites A and B, respectively, and $\boldsymbol{\delta}_j$ represents the infinitesimal displacement between the two nearest atomic sites. The tight binding Hamiltonian in the second quantized form reads

$$H_0 = t \sum_{\mathbf{r}_i, \boldsymbol{\delta}_j} \left(\psi_A^\dagger(\mathbf{r}_i) \psi_B(\mathbf{r}_i + \boldsymbol{\delta}_j) + \text{h.c.} \right), \quad (\text{A.2})$$

where $\psi_{A/B}^\dagger$ ($\psi_{A/B}$) are the operators creating (annihilating) particles at the corresponding position of the atomic sites A and B. The parameter t is the nearest neighbor hopping which for graphene is about $t = 3 \text{ eV}$ [45]. The carbon atoms are localized in graphene lattice around $\mathbf{r}_i = n_1 \mathbf{a}_1 + n_2 \mathbf{a}_2$ where \mathbf{a}_1 and \mathbf{a}_2 are the primitive cell vectors. Furthermore, the unit vectors connecting the triangular lattice points are given by, Fig.2.1,

$$\boldsymbol{\delta}_1 = a \left(0, \frac{1}{\sqrt{3}} \right), \quad \boldsymbol{\delta}_2 = \frac{a}{2} \left(1, -\frac{1}{\sqrt{3}} \right), \quad \boldsymbol{\delta}_3 = \frac{a}{2} \left(-1, -\frac{1}{\sqrt{3}} \right), \quad (\text{A.3})$$

where the lattice spacing is about $a = 1.42 \text{ \AA}$. By mapping the local electronic basis into the Bloch basis via a Fourier transform

$$|\mathbf{k}\rangle = \frac{1}{\sqrt{N}} \sum_{\mathbf{r}_i} e^{i\mathbf{r}_i \cdot \mathbf{k}} |\mathbf{r}_i\rangle, \quad (\text{A.4})$$

where N is the number of unit cells, we can cast the orbital Hamiltonian into the Bloch form $H_0 = \sum_{\mathbf{k}} H_0(\mathbf{k})$ and extract the linear dispersion relation. The conduction and valence bands cross at two time reversal momenta $\mathbf{K}_\tau = \tau(\frac{4\pi}{3a}, 0)$, so-called valleys in graphene, where $\tau = \pm$ is the valley index and $\mathbf{K}_\pm = \pm\mathbf{K}$.

Next we turn into the second quantized form and use the field operators (localized basis) consisting of an extended envelope functions around the each valley momenta and attempt to obtain the electronic structure and effective Hamiltonian. The field operator then reads

$$\psi(\mathbf{r}_i) = \sum_{\tau=\pm} \psi_\tau(\mathbf{r}_i) e^{-i\mathbf{K}_\tau \cdot \mathbf{r}_i}. \quad (\text{A.5})$$

It is straightforward to show that the tight binding model in Eq. (A.1) reproduces the standard Dirac Hamiltonian for graphene

$$\begin{aligned} H_0 &= t \sum_{\mathbf{r}_i, \delta_j} \left(\left[\psi_{+A}^\dagger(\mathbf{r}_i) e^{i\mathbf{K} \cdot \mathbf{r}_i} + \psi_{-A}^\dagger(\mathbf{r}_i) e^{-i\mathbf{K} \cdot \mathbf{r}_i} \right] \times \right. \\ &\quad \left. \left[\psi_{+B}(\mathbf{r}_i + \delta_j) e^{-i\mathbf{K} \cdot (\mathbf{r}_i + \delta_j)} + \psi_{-B}(\mathbf{r}_i + \delta_j) e^{i\mathbf{K} \cdot (\mathbf{r}_i + \delta_j)} \right] + \text{h.c.} \right), \\ &= t \sum_{\mathbf{r}_i, \delta_j} \left(\psi_{+A}^\dagger(\mathbf{r}_i) \psi_{+B}(\mathbf{r}_i + \delta_j) e^{-i\mathbf{K} \cdot \delta_j} + \psi_{-A}^\dagger(\mathbf{r}_i) \psi_{-B}(\mathbf{r}_i + \delta_j) e^{i\mathbf{K} \cdot \delta_j} + \text{h.c.} \right), \end{aligned} \quad (\text{A.6})$$

where $\psi_{\tau,\sigma} = \psi_\tau \otimes \psi_\sigma$ with τ and σ being the valley and sublattice degrees of freedom. On writing this representation we neglected the intervalley scattering terms. Next, since $\delta \ll 1$, we use the Taylor expansion for the field operator for the sublattice B as

$$\psi_{\pm B}(\mathbf{r}_i + \delta_j) = \psi_{\pm B}(\mathbf{r}_i) + \delta_j \cdot \nabla \psi_{\pm B}(\mathbf{r}_i) + O(|\delta|^2), \quad (\text{A.7})$$

and in light of the relations

$$\sum_{j=1}^3 e^{\pm i\mathbf{K} \cdot \delta_j} = 0, \quad \sum_{j=1}^3 \delta_j e^{\pm i\mathbf{K} \cdot \delta_j} = \frac{a\sqrt{3}}{2} (\pm i, 1), \quad (\text{A.8})$$

and, furthermore, applying the integration by parts by noting that $(\nabla \psi_B) \psi_A = \nabla(\psi_B \psi_A) + \psi_B \nabla \psi_A$, we arrive at

$$\begin{aligned} H_0 &= \frac{ta\sqrt{3}}{2} \sum_{\mathbf{r}_i} \left(\psi_{+A}^\dagger(\mathbf{r}_i) \partial \psi_{+B}(\mathbf{r}_i) + \psi_{-A}^\dagger(\mathbf{r}_i) \partial^* \psi_{-B}(\mathbf{r}_i) \right. \\ &\quad \left. - \psi_{+B}^\dagger(\mathbf{r}_i) \partial^* \psi_{+A}(\mathbf{r}_i) + \psi_{-B}^\dagger(\mathbf{r}_i) \partial \psi_{-A}(\mathbf{r}_i) \right). \end{aligned} \quad (\text{A.9})$$

where for simplicity we defined $\partial = i\partial_x + \partial_y$ and its complex conjugate. Noting that the momentum operator in real space gives $\mathbf{k} = -i\nabla$, the continuum representation of the

Hamiltonian will give

$$H_0 = - \int d^2\mathbf{r} \Psi^\dagger h \Psi, \quad (\text{A.10})$$

where the orbital Hamiltonian is

$$h = v_F \tau_0 \otimes (-i\partial_x \sigma_x - i\partial_y \sigma_y), \quad (\text{A.11})$$

and the effective Fermi velocity is $v_F = \sqrt{3}at/2\hbar \approx 0.9 \times 10^6 \text{ m/s}$, and the valley isotropic basis is, [46],

$$\Psi^\dagger = \begin{pmatrix} \psi_{+A}^\dagger & \psi_{+B}^\dagger & -\psi_{-B}^\dagger & \psi_{-A}^\dagger \end{pmatrix}. \quad (\text{A.12})$$

This concludes that the two valley tightbinding representation, also, yields the standard Dirac Hamiltonian for graphene.

A.2. Keldysh formalism

In this section, we rederive the quantum Boltzmann equation from the Keldysh formalism by supplementing the Dyson equations. The two point Green's functions in the notation where $x = (t, r)$ satisfy the left and right Dyson's equations

$$(G_0^{-1} - \Sigma) \circ \mathbb{G} = 1, \quad \mathbb{G} \circ (G_0^{-1} - \Sigma) = 1, \quad (\text{A.13})$$

or their compact form

$$[G_0^{-1} - \Sigma \circ \mathbb{G}]_- = 0, \quad (\text{A.14})$$

where the notation \circ stands for the convolution of two operators. The nonequilibrium Green's functions, here, are matrices in the Keldysh space and defined as

$$\mathbb{G} = \begin{pmatrix} G^R & G^K \\ 0 & G^A \end{pmatrix}, \quad \text{and} \quad \Sigma = \begin{pmatrix} \Sigma^R & \Sigma^K \\ 0 & \Sigma^A \end{pmatrix}. \quad (\text{A.15})$$

Now substituting these matrices back into Dyson's equation yields a matrix equations, whose diagonal component reads

$$(G_0^{-1} - \Sigma^{R(A)}) \circ G^{R(A)} = 1, \quad (\text{A.16})$$

and the same equation can be written for its Hermitian conjugate. Likewise, for the off-diagonal component we get

$$(G_0^{-1} - \Sigma^R) \circ G^K = \Sigma^K \circ G^A. \quad (\text{A.17})$$

Subtracting last relations from its conjugate would relate the Keldysh, retarded and advanced Green's functions, i.e,

$$[G^R]^{-1} \circ G^K - G^K \circ [G^A]^{-1} = \Sigma^K \circ G^A - G^R \circ \Sigma^K. \quad (\text{A.18})$$

We, next, parameterize the Keldysh function with the help of a “generalized distribution function” f as

$$G^K = G^R \circ f - f \circ G^A, \quad (\text{A.19})$$

such that Wigner transformation of this will give back the general distribution function up to zeroth order as $\mathfrak{g} = G^R f - f G^A$. This parameterisation allows us to derive an equation of motion for the distribution function from the equation of motion for the Green's function. We put the equation (A.17) into the form

$$(G_0^{-1} - \Sigma^R) \circ G^K \circ (G_0^{-1} - \Sigma^A) = \Sigma^K, \quad (\text{A.20})$$

now using the parametrization of the Keldysh function (A.19), we obtain

$$\underbrace{-[G_0^{-1} \circ f]_-}_{\text{kinetic term}} = \underbrace{\Sigma^K - (\Sigma^R \circ f - f \circ \Sigma^A)}_{\text{collision term}}. \quad (\text{A.21})$$

Noting that the bare Green's function is given by $G_0^{-1}(x_1) = i\partial_{t_1} + iv_F \sigma \cdot \nabla_{r_1} - V_{\text{cl}}(r_1, t_1)$, next, setting $V_{\text{cl}} = 0$, then the left-hand side commutator up on Wigner transform may be written as

$$\begin{aligned} & -[i\partial_{t_1} + iv_F \vec{\sigma} \cdot \nabla_{r_1} - V_{\text{cl}}(r_1, t_1) \circ f]_- \xrightarrow{\text{WT}} \\ & -i[\varepsilon, f]_{PB} + v_F \left([\sigma_{\mathbf{k}}, f]_- + \frac{i}{2} ([\sigma_{\mathbf{k}}, f]_{PB} - [h, \sigma_{\mathbf{k}}]_{PB}) \right) \\ & = -i\partial_t f + v_F [\sigma_{\mathbf{k}}, f]_- - \frac{iv_F}{2} [\vec{\sigma}, \nabla_r f]_+. \end{aligned} \quad (\text{A.22})$$

To compute the collision terms we first need to specify the approximate form of the self-energies. In the self-consistent Born approximation the lowest order self-energy after averaging over impurity configurations according to Dyson equation is

$$\Sigma(x_1, x_2) = \langle V(x_1) G(x_1, x_2) V(x_2) \rangle. \quad (\text{A.23})$$

Assuming the random Gaussian disorder where

$$\langle V(x_1) V(x_2) \rangle = \gamma \delta(x_1 - x_2), \quad \langle V(x_1) \rangle = 0, \quad (\text{A.24})$$

the Wigner transform (WT) of the self-energy term becomes

$$\Sigma(\mathbf{r}_1 - \mathbf{r}_2; t_1 - t_2) = \gamma \delta(\mathbf{r}_1 - \mathbf{r}_2) G(\mathbf{r}_1, \mathbf{r}_2; t_1 - t_2) \xrightarrow{\text{WT}} \Sigma(\mathbf{k}, \varepsilon) = \gamma \sum_{\mathbf{k}'} G(\mathbf{k} - \mathbf{k}', \varepsilon) \quad (\text{A.25})$$

on the other hand we have

$$\text{Im}\Sigma(\mathbf{r}_1, \mathbf{r}_2; \varepsilon) \delta(\mathbf{r}_1 - \mathbf{r}_2) = \gamma \text{Im}G(\mathbf{r}_1, \mathbf{r}_1; \varepsilon) \quad (\text{A.26})$$

after integration and noting the space-resolved density of states, $\text{DOS} = -\int \frac{dx}{\pi} \text{Im}G(x, x; \varepsilon)$, and the decay time, $\text{Im}\Sigma = -\frac{1}{2\tau}$, one gets $\gamma = \frac{1}{2\pi\tau \text{DOS}}$ and therefore

$$\Sigma(\mathbf{k}, \varepsilon) = \frac{1}{2\pi\tau \text{DOS}} \sum_{\mathbf{k}'} G(\mathbf{k} - \mathbf{k}', \varepsilon). \quad (\text{A.27})$$

Now the Wigner transform of the collision term becomes

$$\begin{aligned} \Sigma^k - (\Sigma^R \circ f - f \circ \Sigma^A) &\xrightarrow{\text{WT}} \frac{1}{2\pi\tau \text{DOS}} \sum_{\mathbf{k}'} \mathfrak{g}_{\mathbf{k}'} \\ &\quad - \frac{1}{2\pi\tau \text{DOS}} \sum_{\mathbf{k}'} \left(G^R(\mathbf{k}', \varepsilon) f_{\mathbf{k}} - f_{\mathbf{k}} G^A(\mathbf{k}', \varepsilon) \right), \\ &= \frac{1}{\tau} \rho + \frac{i}{\tau} f_{\mathbf{k}}, \end{aligned} \quad (\text{A.28})$$

where we have defined $\rho = \frac{1}{2\pi \text{DOS}} \sum_{\mathbf{k}} \mathfrak{g}$, and the sum over the momentum is performed via integrating out the band structure energy ξ and averaging over the momentum direction, i.e.,

$$\sum_{\mathbf{k}'} \longrightarrow \text{DOS} \int d\xi \sum_{\hat{\mathbf{k}}'}, \quad \xi = \varepsilon(k') - \mu. \quad (\text{A.29})$$

Overall combining the kinetic and collision terms we finally obtain

$$\partial_t f_{\mathbf{k}} + i v_F [\sigma_{\mathbf{k}}, f_{\mathbf{k}}]_- + \frac{v_F}{2} [\vec{\sigma}, \nabla_r f_{\mathbf{k}}]_+ = i \frac{\rho}{\tau} - \frac{f_{\mathbf{k}}}{\tau}, \quad (\text{A.30})$$

where multiplying this relation from the left with G^R and from the right with G^A and subtracting two relations yields

$$\partial_t \mathfrak{g}_{\mathbf{k}} + i v_F [\sigma_{\mathbf{k}}, \mathfrak{g}_{\mathbf{k}}]_- + \frac{v_F}{2} [\vec{\sigma}, \nabla_r \mathfrak{g}_{\mathbf{k}}]_+ = \frac{i}{\tau} \left(G^R(\mathbf{k}, \varepsilon) \rho - \rho G^A(\mathbf{k}, \varepsilon) \right) - \frac{\mathfrak{g}_{\mathbf{k}}}{\tau}. \quad (\text{A.31})$$

A.3. Derivation of the diffusion equations

In this appendix, we establish the set of diffusion equations from the transport equation to study the real space kinetics Dirac particles in graphene. The stationary source term in

Eq.2.89 reads

$$\begin{aligned} \mathfrak{L}_{\mathbf{k}z}^{(0)}(\rho) = \pi\tau^{-1} \left\{ \left((1 + \sigma_{\hat{\mathbf{k}}})\rho_0 + \hat{\mathbf{k}} \cdot \mathbf{s} + \mathbf{s} \cdot \boldsymbol{\sigma} \right) \delta(z - \xi_k^+) \right. \\ \left. + \left((1 - \sigma_{\hat{\mathbf{k}}})\rho_0 - \hat{\mathbf{k}} \cdot \mathbf{s} + \mathbf{s} \cdot \boldsymbol{\sigma} \right) \delta(z - \xi_k^-) \right\}, \end{aligned} \quad (\text{A.32})$$

where to derive this relation we reexpressed the density matrix in a vector form, i.e,

$$\rho = n + \boldsymbol{\sigma} \cdot \mathbf{s}, \quad \mathbf{s} = (s_1, s_2, s_3). \quad (\text{A.33})$$

We have vividly made use of the following relations

$$\sigma_{\mathbf{k}}\sigma_{\mathbf{k}'} = (\mathbf{k} \cdot \mathbf{k}') + i\boldsymbol{\sigma} \cdot (\mathbf{k} \times \mathbf{k}'), \quad (\text{A.34})$$

$$[\sigma_{\mathbf{k}}, \sigma_{\mathbf{k}'}]_- = 2i(\mathbf{k} \times \mathbf{k}') \cdot \boldsymbol{\sigma}, \quad (\text{A.35})$$

$$\sigma_{\mathbf{k}}\boldsymbol{\sigma} = \mathbf{k} - i\mathbf{k} \times \boldsymbol{\sigma}, \quad (\text{A.36})$$

$$\boldsymbol{\sigma}\sigma_{\mathbf{k}} = \mathbf{k} + i\mathbf{k} \times \boldsymbol{\sigma}, \quad (\text{A.37})$$

$$\sigma_i\sigma_j\sigma_\ell = \delta_{ij}\sigma_\ell + i\varepsilon_{ijr}\sigma_r\sigma_\ell = \delta_{ij}\sigma_\ell + \delta_{\ell j}\sigma_i - \delta_{i\ell}\sigma_j + i\varepsilon_{ij\ell}, \quad (\text{A.38})$$

$$\sigma_{\mathbf{k}}\boldsymbol{\sigma}\sigma_{\mathbf{k}} = 2(\boldsymbol{\sigma} \cdot \mathbf{k})\mathbf{k} - \boldsymbol{\sigma}, \quad (\text{A.39})$$

$$\overline{\sigma_{\hat{\mathbf{k}}}\boldsymbol{\sigma}\sigma_{\hat{\mathbf{k}}}} = 0. \quad (\text{A.40})$$

The different corrections to the solution of the equation Eq.2.89 then give

$$\mathfrak{g}_{\mathbf{k},\varepsilon^\pm}^{(0)} = a_1(\rho_0 \pm \hat{\mathbf{k}} \cdot \mathbf{s}) + \left(a_1 n \hat{\mathbf{k}} + a_2 \mathbf{s} + a_3 \hat{\mathbf{k}} \times \mathbf{s} + a_4 (\mathbf{s} \cdot \hat{\mathbf{k}}) \hat{\mathbf{k}} \right) \cdot \boldsymbol{\sigma}, \quad (\text{A.41})$$

$$\mathfrak{g}_{\mathbf{k},\varepsilon^\pm}^{(1)} = \mathcal{B}_0 + \mathcal{B}_i\sigma_i, \quad (\text{A.42})$$

$$\mathfrak{g}_{\mathbf{k},\varepsilon^\pm}^{(2)} = -v_F \left\{ ((\xi_1 - \xi_3)\sigma_i + 2i\xi_2 \varepsilon_{jil}k_j\sigma_\ell + 2\xi_3 k_i k_j \sigma_j) \partial_i \mathcal{B}_0 + (\xi_1 + \xi_3) \nabla \cdot \mathcal{B} \right\} \quad (\text{A.43})$$

$$(\text{A.44})$$

where

$$\mathcal{B}_0 = b_1 \partial_i s_i + b_2 k_i \partial_i n + b_3 \varepsilon_{ij\ell} k_j \partial_i s_\ell + b_4 k_i k_j \partial_i s_j \quad (\text{A.45})$$

$$\begin{aligned} \mathcal{B}_i = b_1 \partial_i n + (\pm b_1 k_j \partial_i s_j + b_3 k_j \varepsilon_{ij\ell} \partial_\ell \rho_0) \\ + (b_4 k_i k_j \partial_j n \mp b_3 k_j k_m \varepsilon_{i\ell m} \partial_\ell s_j) \pm b_4 k_i k_j k_\ell \partial_\ell s_j. \end{aligned} \quad (\text{A.46})$$

We iteratively derive the above relations using

$$\begin{aligned} \mathfrak{L}_{\mathbf{k}\varepsilon}^{(1)}(\mathfrak{g}_{\mathbf{k},\varepsilon^\pm}^{(0)}) = -v_F \left\{ a_1 (\partial_i n \pm k_j \partial_i s_j) \sigma_i + (a_2 \partial_i s_i + a_1 k_i \partial_i n + a_3 \varepsilon_{ij\ell} k_j \partial_i s_\ell \right. \\ \left. + a_4 k_i k_j \partial_i s_j) \right\}, \end{aligned} \quad (\text{A.47})$$

$$\mathfrak{L}_{\mathbf{k},\varepsilon^\pm}^{(1)}(\mathfrak{g}_{\mathbf{k}\varepsilon}^{(1)}) = -v_F(\boldsymbol{\sigma} \cdot \nabla \mathcal{B}_0 + \nabla \cdot \mathcal{B}), \quad (\text{A.48})$$

where the coefficients in the limit of $\alpha\tau \ll 1$, and defining $\gamma = \varepsilon\tau$, are given as

$$\begin{aligned} a_1 &= \pi, & a_2 &= \pi \frac{1}{1+4\gamma^2}, & a_3 &= 2\pi \frac{\gamma}{1+4\gamma^2}, & a_4 &= 4\pi \frac{\gamma^2}{1+4\gamma^2}, \\ b_1 &= -\pi \frac{v_F\tau}{1+4\gamma^2}, & b_2 &= -v_F\tau \pi, & b_3 &= -2\pi \frac{v_F\tau\gamma}{1+4\gamma^2}, & b_4 &= -4\pi \frac{v_F\tau\gamma^2}{1+4\gamma^2}. \end{aligned} \quad (\text{A.49})$$

We, next, reduce the transport equation that we established here into a diffusion model. To study transport phenomena in realistic physical systems it is essential to formulate a kinetic equation written in macroscopic variables. The general distribution matrix $\mathfrak{g}_{\mathbf{k},z}$ depends on $\mathbf{k}, \mathbf{x}, t$, whereas if one integrates out the momentum dependency \mathbf{k} it would result the bare classical distribution matrix depending only on macroscopic variables \mathbf{x}, t . To establish the drift-diffusion equation we integrate over the momentum dependency of the perturbative solution:

$$\mathfrak{g}_{\mathbf{k}\varepsilon} = \mathfrak{g}_{\mathbf{k}\varepsilon}^{(0)} + \mathfrak{g}_{\mathbf{k}\varepsilon}^{(1)} + \mathfrak{g}_{\mathbf{k}\varepsilon}^{(2)}. \quad (\text{A.50})$$

The following averages will be useful in deriving the drift diffusion equation, i.e.,

$$\overline{\mathfrak{g}_{\mathbf{k}\varepsilon}^{(0)}} = a_1 n + (a_2 + \frac{a_4}{2}) \boldsymbol{\sigma} \cdot \mathbf{s}, \quad (\text{A.51})$$

$$\overline{\mathfrak{g}_{\mathbf{k}\varepsilon}^{(1)}} = (b_1 + \frac{b_4}{2}) \nabla \cdot \mathbf{s} + (b_1 + \frac{b_4}{2}) \nabla n \cdot \boldsymbol{\sigma} + \frac{b_3}{2} (\nabla \times \mathbf{s}) \cdot \boldsymbol{\sigma}, \quad (\text{A.52})$$

$$\overline{\mathfrak{g}_{\mathbf{k}\varepsilon}^{(2)}} = d_1 \nabla^2 n + d_2 \nabla(\nabla \cdot \mathbf{s}) \cdot \boldsymbol{\sigma} + d_3 \nabla^2 \mathbf{s} \cdot \boldsymbol{\sigma}, \quad (\text{A.53})$$

where the average means the momentum integration $\overline{\mathfrak{g}(\mathbf{k})} = \int \frac{d\mathbf{k}}{(2\pi)^2} \mathfrak{g}(\mathbf{k})$ where the components of the momentum vector in two dimensions read $\mathbf{k} = k(\cos \phi, \sin \phi)$. Note that while averaging over the momentum directions we have used the relations

$$\begin{aligned} \overline{k_{i_1} k_{i_2}} &= \frac{1}{2} \delta_{i_1 i_2}, & \overline{k_{i_1} k_{i_2} k_{i_3}} &= 0, & \overline{k_{i_1}^4} &= \frac{3}{8}, & \overline{k_{i_1}^2 k_{i_2}^2} &= \frac{1}{8}, \\ \overline{k_{i_1} k_{i_2} k_{i_3} k_{i_4}} &= \frac{3}{8} \underbrace{\delta_{i_1 i_2} \delta_{i_2 i_3} \delta_{i_3 i_4}}_{\text{identical indices}} + \frac{1}{8} (\delta_{i_1 i_2} \delta_{i_3 i_4} + \delta_{i_1 i_3} \delta_{i_2 i_4} + \delta_{i_1 i_4} \delta_{i_2 i_3}), \end{aligned} \quad (\text{A.54})$$

$$\begin{aligned} \partial_{ij} \overline{k_i k_j k_t k_\ell} \sigma_t s_\ell &= \frac{3}{8} \partial_i^2 s_i \sigma_i + \frac{1}{8} (\partial_i^2 s_j \sigma_j + 2\partial_{ij} s_j \sigma_j), \\ &= \frac{1}{8} \sigma_i \partial_j^2 s_i + \frac{1}{4} \sigma_i \partial_{ij} s_j = \frac{1}{8} \boldsymbol{\sigma} \cdot \left(\nabla^2 \mathbf{s}_\perp + 2\nabla(\nabla \cdot \mathbf{s}_\perp) \right), \end{aligned} \quad (\text{A.55})$$

where $\mathbf{s}_\perp = (s_1, s_2)$. We furthermore defined the coefficients as

$$d_1 = -v_F(\xi_1 + \xi_3)(b_1 + \frac{b_4}{2}) = \pi v_F^2 \tau^2 \frac{1 + 2\gamma^2}{1 + 4\gamma^2}, \quad (\text{A.56})$$

$$d_2 = -v_F(-i\xi_2 b_3 + \frac{\xi_3 b_4}{4}) = 2\pi v_F^2 \tau^2 \frac{\gamma^2 - \gamma^4}{(1 + 4\gamma^2)^2}, \quad (\text{A.57})$$

$$d_3 = -v_F(\xi_1(b_1 + \frac{b_4}{2}) + i\xi_2 b_3) = \pi v_F^2 \tau^2 \frac{(1 + 2\gamma^2)^2 + 2\gamma^2}{(1 + 4\gamma^2)^2}. \quad (\text{A.58})$$

Substituting these results back into the kinetic equation one obtain the set of diffusion equations which will be used to study the coupled dynamics of charge carriers in graphene, namely,

$$D \nabla^2 n - v_F \nabla \cdot \mathbf{s}_\perp = 0, \quad (\text{A.59})$$

$$F_1 D \nabla^2 \mathbf{s}_\perp + F_2 D \nabla(\nabla \cdot \mathbf{s}_\perp) - F_3 \frac{v_F}{2} \nabla n = \frac{\gamma^2}{(1 + 4\gamma^2)} \frac{\mathbf{s}_\perp}{\tau}, \quad (\text{A.60})$$

$$F_4 D \nabla^2 s_3 - F_5 \frac{v_F}{2} (\hat{\mathbf{z}} \times \nabla) \cdot \mathbf{s}_\perp = \frac{\gamma^2}{1 + 4\gamma^2} \frac{s_3}{\tau}, \quad (\text{A.61})$$

where we defined

$$F_1 = \frac{(1 + 2\gamma^2)^2 + 2\gamma^2}{(1 + 4\gamma^2)^2}, \quad (\text{A.62})$$

$$F_2 = \frac{2(\gamma^2 - \gamma^4)}{(1 + 4\gamma^2)^2}, \quad (\text{A.63})$$

$$F_3 = \frac{1 + 2\gamma^2}{2(1 + 4\gamma^2)}, \quad (\text{A.64})$$

$$F_4 = \frac{(1 + 2\gamma^2)^2 + 2\gamma^2}{(1 + 4\gamma^2)^2}, \quad (\text{A.65})$$

$$F_5 = \frac{\gamma}{1 + 4\gamma^2}. \quad (\text{A.66})$$

A.4. Charge-spin coupling

In this part, we derive the microscopic model of charge-spin coupling for graphene's Dirac particles in a transport regime where the SOC strength is strong. The (pseudo)spin current can be defined as

$$\mathbf{J} = ev_F \text{tr}(\sigma \sum_{\mathbf{k}} f_{\mathbf{k}}). \quad (\text{A.67})$$

Note that the general distribution matrix was given by (2.86), hence, using the matrix form of the Green's functions and integrating over the energy variable we obtain

$$f_{\mathbf{k}} = \frac{1}{2} \int dz \mathbf{g}_{\mathbf{k}z}. \quad (\text{A.68})$$

Now, using the above relation we express the current as

$$\mathbf{J} = \frac{ev_F}{2} \int dz \sum_{\mathbf{k}} \text{tr}(\sigma \mathbf{g}_{\mathbf{k}z}), \quad (\text{A.69})$$

and using the perturbative expressions of $\mathbf{g}_{\mathbf{k}z}$ as it is given in A.50 then we find that

$$\mathbf{J}_{\text{charge}} = \frac{e}{2} \int dz (v_F \mathbf{s} + D \nabla n). \quad (\text{A.70})$$

The charge density and charge current on the other hand is defined in the second quantization language as

$$\rho_e(\mathbf{r}) = e \psi^\dagger(\mathbf{r}) \psi(\mathbf{r}), \quad \mathbf{J}(\mathbf{r}) = e \text{Re}\{\psi^\dagger(\mathbf{r}) \mathbf{v} \psi(\mathbf{r})\}, \quad (\text{A.71})$$

such that one can Analogously define the spin density and spin current

$$\mathbf{s}(\mathbf{r}) = \psi^\dagger(\mathbf{r}) \hat{\mathbf{S}} \psi(\mathbf{r}), \quad \mathbb{J}_s(\mathbf{r}) = \text{Re}\{\psi^\dagger(\mathbf{r}) \hat{\mathbb{J}}_s \psi(\mathbf{r})\}, \quad (\text{A.72})$$

where the spin and spin current operators now give

$$\hat{\mathbf{S}} = \frac{\hbar}{2} \vec{\sigma}, \quad \hat{\mathbb{J}}_s = \frac{1}{2} [\hat{\mathbf{S}}, \mathbf{v}]_+ = \frac{\hbar}{4} [\vec{\sigma}, \mathbf{v}]_+, \quad (\text{A.73})$$

where spin density is a vector while spin current is a tensor of rank 2 having two cartesian components. For the Dirac Hamiltonian given by

$$\mathbf{H} = v_F \boldsymbol{\sigma} \cdot \mathbf{k}, \quad (\text{A.74})$$

the velocity operator is the pseudospin operator which reads

$$\dot{x}_i = \frac{v_F}{i\hbar} [x_i, p_j]_- \sigma_j = v_F \sigma_i, \quad (\text{A.75})$$

and the pseudospin current is

$$\hat{\mathbb{J}}_i^\nu = \frac{\hbar}{4} [\sigma^\nu, \dot{x}_i]_+ = \frac{\hbar v_F}{2} \delta_i^\nu. \quad (\text{A.76})$$

Next averaging over the statistical ensemble gives the pseudospin current gives as

$$\begin{aligned} \mathbb{J}_i^\nu &= \text{tr} \left(\sum_{\mathbf{k}} f_{\mathbf{k}} \hat{\mathbb{J}}_i^\nu \right), \\ &= \frac{v_F}{2} \delta_i^\nu \int dz \text{tr} \left(\sum_{\mathbf{k}} \mathbf{g}_{\mathbf{k}z} \right), \\ &= \frac{v_F}{2} \delta_i^\nu \int dz \left(\text{tr} \overline{\mathbf{g}_{\mathbf{k}\epsilon}^{(0)}} + \text{tr} \overline{\mathbf{g}_{\mathbf{k}\epsilon}^{(1)}} \right), \\ &= \frac{1}{2} \delta_i^\nu \int dz \left(v_F \rho_0 + \frac{4(1+2\gamma^2)}{1+4\gamma^2} D \nabla \cdot \mathbf{s} \right), \end{aligned}$$

$$\begin{aligned}
&= \frac{1}{2} \left(v_F \mathbf{n} + \frac{4(1+2\gamma^2)}{1+4\gamma^2} D \nabla \cdot \mathfrak{s} \right) \delta_i^\nu, \\
&= \frac{1}{2} \left(v_F \mathbf{n} + D \nabla \cdot \mathfrak{s} \right) \delta_i^\nu,
\end{aligned} \tag{A.77}$$

where we have used the perturbative expression for the distribution function and the total charge and the total pseudospin densities are defined through

$$\mathbf{n} = \int dz \rho_0, \quad \mathfrak{s} = \int dz \mathbf{s}. \tag{A.78}$$

The direction of spin orientation (spin polarization) is given by the statistical average of spin operator

$$\mathbf{p} = \langle \hat{\mathbf{S}} \rangle = \text{tr}(\rho \hat{\mathbf{S}}) = \mathbf{S}. \tag{A.79}$$

Appendix B

LORENTZ TRANSFORMATION OF THE DIRAC HAMILTONIAN

In this appendix, we provide details for the Lorentz transformation (LT) of the Hamiltonian (4.4). As mentioned in the main text, we redefine this Hamiltonian as $\tilde{H} = H - v_0 k_x \mathbf{1}$ and, for convenience, set $\Phi = \Phi_{\text{bias}} - \Phi_{\text{eff}}$. Using (4.5) and (4.6), the eigenvalue problem after applying a pure Lorentz boost in x -direction, where $\eta = \tanh \vartheta$, gives

$$\begin{aligned} & \left(e^{\vartheta \sigma_x / 2} \tilde{H} e^{\vartheta \sigma_x / 2} - \varepsilon e^{\vartheta \sigma_x} \right) |\tilde{\psi}\rangle = \\ & \left\{ \gamma \begin{pmatrix} e\Phi + v_F \eta \pi_x - \varepsilon & v_F \pi_x - \eta \varepsilon + e\eta \Phi \\ v_F \pi_x - \eta \varepsilon + e\eta \Phi & e\Phi + v_F \eta \pi_x - \varepsilon \end{pmatrix} + v_F k_y \sigma_y \right\} |\tilde{\psi}\rangle, \\ & = \left(v_F (k'_x - eA'_x) \sigma_x + v_F k'_y \sigma_y + e\Phi' - \varepsilon' \right) |\tilde{\psi}\rangle, \end{aligned}$$

where the kinetic momentum is $\boldsymbol{\pi} = \mathbf{k} - e\mathbf{A}$ and $|\tilde{\psi}\rangle = e^{-\vartheta \sigma_x / 2} |\psi\rangle$. In the last line, we have used the LTs

$$k'_x = \gamma(k_x - \eta \frac{\varepsilon}{v_F}), \quad \varepsilon' = \gamma(\varepsilon - v_0 k_x) = \gamma \varepsilon, \quad (\text{B.1})$$

and note that $v_0 = \eta v_F$. Moreover, the four-potential $A^\mu = (\Phi/v_F, \mathbf{A})$ likewise transforms as

$$\begin{pmatrix} A'^0 \\ A'^1 \\ A'^2 \\ A'^3 \end{pmatrix} = \begin{pmatrix} \gamma & -\gamma\eta & 0 & 0 \\ -\gamma\eta & \gamma & 0 & 0 \\ 0 & 0 & 1 & 0 \\ 0 & 0 & 0 & 1 \end{pmatrix} \begin{pmatrix} A^0 \\ A^1 \\ A^2 \\ A^3 \end{pmatrix}, \quad (\text{B.2})$$

where $\gamma = (1 - \eta^2)^{-1/2}$. We thus obtain

$$\Phi' = \gamma(\Phi - \eta v_F A_x), \quad (\text{B.3})$$

$$A'_x = \gamma(A_x - \eta \frac{\Phi}{v_F}), \quad (\text{B.4})$$

and $A'_{y(z)} = A_{y(z)} = 0$. Furthermore, noting that $\mathbf{v}_{\text{boost}} = \mathbf{v}_{\text{drift}} = \mathbf{E}_0 \times \mathbf{B}/B^2$, for $\mathbf{E}_0 = v_0 B \hat{\mathbf{y}}$ and $\mathbf{B} = B \hat{\mathbf{z}}$, one finds that $\mathbf{v}_{\text{boost}} = \mathbf{v}_{\text{drift}} = v_0 \hat{\mathbf{x}}$. The rapidity of the transformation is also defined as $\eta = \tanh \vartheta = E_0/v_F B$. In magnetic regime $\eta \delta E/v_F \ll \eta E_0/v_F < B$, and in the Landau gauge, we ultimately obtain

$$\Phi'_{\text{eff}} = \gamma(\Phi_{\text{eff}} - \eta v_F A_x) = \gamma(-E_0 + v_0 B)y = 0, \quad (\text{B.5})$$

$$\Phi'_{\text{bias}} = \gamma \Phi_{\text{bias}} = -\gamma \delta E y, \quad (\text{B.6})$$

$$\begin{aligned} A'_x &= \gamma(A_x - \eta \Phi/v_F) \approx -\gamma(B - \eta E_0/v_F)y, \\ &= -\gamma^{-1} B y. \end{aligned} \quad (\text{B.7})$$

This implies that the boost removes the effective field in the Hamiltonian (4.4) such that now in the boosted frame we simply have

$$\tilde{H}' = v_F (\mathbf{k}' - e \mathbf{A}') \cdot \boldsymbol{\sigma} + e \Phi'_{\text{bias}}. \quad (\text{B.8})$$

Appendix C

RENORMALIZATION OF EINSTEIN RELATION

We, here, illustrate how the conductivity is originated from the systems microscopic dynamics according the Einstein's kinetic relation. The number of occupied states according to the Boltzmann distribution function is defined as

$$n = \int dk f(\varepsilon) = \int_{-\infty}^{+\infty} d\varepsilon \text{DOS}(\varepsilon) f(\varepsilon), \quad (\text{C.1})$$

where in low temperature one can adopt the Fermi distribution as the step function or use the Sommerfeld expansion to simplify the integral into

$$n \approx \int_{-\infty}^{\mu} d\varepsilon \text{DOS}(\varepsilon), \quad (T = 0). \quad (\text{C.2})$$

Therefore, integrating the density of states give the carrier density as

$$n = \frac{g_s g_\tau}{4\pi} \left(\frac{\varepsilon_F}{\hbar v_F} \right)^2, \quad (\text{C.3})$$

and one obtains

$$\frac{D}{\mu} = \frac{1}{e} \frac{n}{\frac{\partial n}{\partial \varepsilon_F}} = \frac{1}{2e} \varepsilon_F, \quad (\text{C.4})$$

where the mobility gives

$$\mu = \frac{e}{\hbar} \frac{\ell}{k_F} = e\tau \frac{v_F}{\hbar \sqrt{\pi n}}. \quad (\text{C.5})$$

Noting the spin and valley degrees of freedom $g_S = g_\tau = 2$, $D = 1/2 v_F^2 \tau$ and $\ell = v_F \tau$. Noting the temperature dependence of the carrier density then mobility of graphene decreases by increasing temperature. However in finite temperature the Fermi-Dirac integrals needs to be calculated straightforwardly. In general noting the density of states in graphene as

$$\text{DOS}(\varepsilon) = \frac{g_s g_\tau}{2\pi \hbar^2 v_F^2} |\varepsilon|, \quad (\text{C.6})$$

then the carrier density yields

$$n = \frac{g_s g_\tau}{2\pi} \left(\frac{k_B T}{\hbar v_F} \right)^2 F_1(\beta\eta), \quad (\text{C.7})$$

where the Fermi-Dirac integral is given by

$$F_j(\alpha) = \frac{1}{\Gamma(j+1)} \int_0^\infty dx \frac{x^j}{e^{x-\alpha} + 1}. \quad (\text{C.8})$$

The following asymptotic behavior of Fermi-Dirac integrals, [186], will prove useful in interpreting the temperature dependence of carrier density

$$F_j\left(\frac{\eta}{k_B T}\right) = \begin{cases} e^{\frac{\eta}{k_B T}}, & \mu \ll k_B T, \\ \frac{1}{\Gamma(j+2)} \left(\frac{\eta}{k_B T}\right)^{j+1} \left\{ 1 + \frac{\pi^2}{6} \frac{\Gamma(j+2)}{\Gamma(j)} \left(\frac{k_B T}{\eta}\right)^2 + O(T^4) \right\}, & \mu \gg k_B T. \end{cases} \quad (\text{C.9})$$

Therefor, for linear dispersion at low temperature where $\xi = \eta/k_B T \ll 1$ the carrier density gives

$$n = \frac{g_s g_\tau}{4\pi} \left(\frac{\eta}{\hbar v_F} \right)^2 (1 + \pi^2 \xi^2 / 3). \quad (\text{C.10})$$

Next, noting the properties of Fermi-Dirac integrals as

$$\partial_\alpha F_j(\alpha) = F_{j-1}(\alpha), \quad (\text{C.11})$$

derivative of the carrier density with respect to the chemical potential becomes

$$\frac{\partial n}{\partial \mu} = \frac{g_s g_\tau}{2\pi} \frac{k_B T}{(\hbar v_F)^2} F_0(\beta\eta), \quad (\text{C.12})$$

where

$$F_0(\beta\eta) = \ln(e^{\beta\eta} + 1) = \min\left(\frac{\eta}{k_B T}, \ln 2\right). \quad (\text{C.13})$$

Therefore, in general the mobility is given as

$$\mu = eD \frac{1}{k_B T} \left(\frac{F_0}{F_1} \right). \quad (\text{C.14})$$

The generalized Einstein relation thus read

$$\frac{D}{\mu} = \frac{1}{e} \frac{n}{\frac{\partial n}{\partial \eta}} = \frac{k_B T}{e} \frac{F_1}{F_0} \quad (\text{C.15})$$

$$= \frac{\eta}{2e} \left\{ 1 + \frac{\pi^2}{3} \left(\frac{k_B T}{\eta} \right)^2 \right\}, \quad (\text{C.16})$$

where

$$\frac{F_1}{F_0} = \frac{1}{2} \frac{\eta}{k_B T} \left\{ 1 + \frac{\pi^2}{3} \left(\frac{k_B T}{\eta} \right)^2 \right\}. \quad (\text{C.17})$$

The origin of this deviation from the classical law rests in the factor F_1/F_0 . In the low temperature limit one can neglect the second order term in temperature and set $\eta = \varepsilon_F = \hbar v_F \sqrt{\pi n}$ to obtain

$$\frac{D}{\mu} = \frac{\hbar}{2e} \varepsilon_F = \frac{\hbar}{2e} v_F \sqrt{\pi n}. \quad (\text{C.18})$$

This in turn indicates that the Diffusion-mobility relationship in low temperature is purely quantum mechanical and goes linear in chemical potential (Fermi energy) and does not depend on the thermal energy.

Now nothing the rescaling of the carrier density and the Fermi velocity in lab frame as $n_{\text{lab}} = \gamma n_0$, $v_F^{\text{lab}} = \gamma^{-3/2} v_F$ one can expect the modified form of the Einstein relation as

$$\left(\frac{D}{\mu} \right)_{\text{lab}} = \gamma^{-1} \left(\frac{\hbar}{2e} v_F \sqrt{\pi n} \right). \quad (\text{C.19})$$

The conductivity, furthermore, reads $\sigma = ne\mu$, such that in the low temperature we obtain

$$\sigma = D e^2 \frac{\partial n}{\partial \eta} = g_s g_\tau \frac{e^2}{h} \Lambda, \quad (\text{C.20})$$

where the dimensionless parameter is denied as

$$\Lambda = D \left(\frac{k_F}{v_F} \right). \quad (\text{C.21})$$

The calculations we introduced so far are in the absence of external fields and indicate that that classical Einstein kinetic relation does not hold true in when there is disorder scattering.